QED corrections to DIS cross section with tagged photon

E. A. Kuraev
Bogoliubov Laboratory of Theoretical Physics, JINR, 141980 Dubna, Russia

N. P. Merenkov
Kharkov Institute of Physics and Technology, 310108 Kharkov, Ukraine

(Submitted 28 August 1997)
Pis'ma Zh. Éksp. Teor. Fiz. **66**, No. 6, 367–372 (25 September 1997)

We calculate the QED corrections to the deep inelastic scattering cross section with tagged photon at HERA, taking into account the leading and next-to-leading contributions. Different types of event selection are investigated. © *1997 American Institute of Physics.*
[S0021-3640(97)00118-7]

PACS numbers: 13.60.Hb, 12.20.Ds

1. In order to investigate the proton structure functions $F_2(x,Q^2)$ and $F_L(x,Q^2)$ in a large region of their arguments it is necessary to measure the cross section of the process $e+p\to e+X$ for different values of the center-of-mass energy. For this purpose one can employ a method suggested in Ref. 1, which utilizes radiative events. This method employs a photon detector (PD) in the forward direction along the 3-momentum of the initial electron beam. Such a device is part of the luminosity monitors of the H1 and ZEUS experiments at HERA.

The emission of photons in the forward direction can be interpreted as a reduction of the effective beam energy, which can be determined in every radiative event by means of a tagged photon energy. For a high-precision description of the corresponding cross section one has to consider the radiative corrections. In this letter we calculate the QED radiative corrections to the deep inelastic scattering cross section provided that at least one hard photon is recorded by the PD. Our result includes the leading and next-to-leading contributions for calorimetric and inclusive event selections. Our approach to the calculation of the QED corrections is based on the investigation of all the essential Feynman diagrams which describe the observed cross section within the chosen approximation. The same approach was used recently for corresponding calculations in the case of small angle Bhabha scattering at LEP1.[2]

2. Our aim is to calculate the QED radiative correction to neutral current events with simultaneous detection of a hard photon emitted along the initial electron direction with an energy ε in the process

$$e(p_1)+p(P)\to e(p_2)+\gamma(k)+X+(\gamma),$$

where ($\theta_1=\widehat{p_1k}\lesssim\theta_0\approx 5\cdot 10^{-4}$ rad). The cross section under consideration in the lowest Born approximation has the following form:

$$z\frac{d^3\sigma}{y\ dx\ dy\ dz}=\frac{\alpha}{2\pi}P(z,L_0)\tilde{\Sigma},$$

$$\tilde{\Sigma}=\Sigma(\hat{x},\hat{y},\hat{Q}^2)=\frac{2\pi\alpha^2(-\hat{Q}^2)}{\hat{Q}^2\hat{x}\hat{y}^2}F_2(\hat{x},\hat{Q}^2)\left[2(1-\hat{y})-2\hat{x}^2\hat{y}^2\frac{M^2}{\hat{Q}^2}\right.$$
$$\left.+\left(1+4\hat{x}^2\frac{M^2}{\hat{Q}^2}\right)\frac{\hat{y}^2}{1+R}\right],$$

$$R=\left(1+4\hat{x}^2\frac{M^2}{\hat{Q}^2}\right)\frac{F_2(\hat{x},\hat{Q}^2)}{2\hat{x}F_1(\hat{x},\hat{Q}^2)}-1,\quad P(z,L_0)=\frac{1+z^2}{1-z}L_0-\frac{2z}{1-z},\tag{1}$$

$$\alpha(-\hat{Q}^2)=\frac{\alpha}{1-\Pi(-\hat{Q}^2)},\quad L_0=\ln\left(\frac{\varepsilon^2\theta_0^2}{m^2}\right),\quad z=\frac{\varepsilon-k^0}{\varepsilon}.$$

On the left-hand side of Eq. (1) we use the standard Bjorken variables

$$x=\frac{Q^2}{2P(p_1-p_2)},\quad y=\frac{2P(p_1-p_2)}{V},\quad Q^2=2p_1p_2,\tag{2}$$

and on the right-hand side — the *shifted* ones

$$\hat{Q}^2=zQ^2,\quad \hat{x}=\frac{zxy}{z+y-1},\quad \hat{y}=\frac{z+y-1}{z}.\tag{3}$$

The quantities F_2 and F_1 are the proton structure functions. Here, since we are interested mainly with the events at small Q^2, we neglect Z-boson exchange contribution.

The model-independent QED correction to the Born cross section includes the contributions due to virtual and real (soft, with energy less than $\Delta\varepsilon$, and hard, with energy greater than $\Delta\varepsilon$) photon emission. The virtual and soft photon correction can be derived with the help of the Compton tensor given in Ref. 3. The corresponding contribution to the observed cross section in the framework of our approximation reads

$$z\frac{d^3\sigma^{SV}}{y\ dx\ dy\ dz}=\left(\frac{\alpha}{2\pi}\right)^2[P(z,L_0)\rho-T]\tilde{\Sigma},\tag{4}$$

where

$$\rho=2(L_Q-1)\ln\frac{\Delta^2}{y_0}+3L_Q+3\ln z-\ln^2 y_0-\frac{\pi^2}{3}-\frac{9}{2}+L_{i2}\left(\frac{1+c}{2}\right),$$

$$T=\frac{1+z^2}{1-z}L_0[(2L_0L_Q-L_0-2\ln(1-z))\ln z+\ln^2 z-2L_{i2}(1-z)]$$
$$-\frac{4z\ln z}{1-z}L_Q-\frac{1+2z-z^2}{2(1-z)}L_0,\tag{5}$$

$$L_Q=\ln\frac{Q^2}{m^2},\quad y_0=\frac{\varepsilon_2}{\varepsilon},\quad L_{i2}(x)=-\int_0^x\frac{dt}{t}\ln(1-t),$$

ε_2 is the energy of the scattered electron, and $c=\cos\theta_s$ (θ_s is the electron scattering angle). The quantity y_0 can be expressed in terms of standard Bjorken variables as

$$y_0=1-y+xyE/\varepsilon,$$

where E is the proton energy.

As concerns the contribution due to additional hard photon emission, we will divide it on three parts:

$$z\frac{d^3\sigma^H}{y\,dx\,dy\,dz}=\left(\frac{\alpha}{2\pi}\right)^2(\Sigma_a+\Sigma_b+\Sigma_{sc}). \tag{6}$$

The first term describes the case when the additional photon is intercepted by the PD. The corresponding contribution can be derived using formula (Π.6) of Ref. 4. It reads

$$\Sigma_a=\frac{1}{2}L_0\left[L_0\left(P_\theta^{(2)}(z)+2\frac{1+z^2}{1-z}\left(\ln z-\frac{3}{2}-2\ln\Delta\right)\right)+6(1-z)\right.$$
$$\left.+\left(-1-z+4\frac{1}{1-z}\right)\ln^2 z-4\frac{(1+z)^2}{1-z}\ln\frac{1-z}{\Delta}\right]\widetilde{\Sigma}, \tag{7}$$

where we use the notation $P_\theta^{(2)}(z)$ for the θ-part of the second-order kernel of the expansion of the nonsinglet electron structure function:

$$P_\theta^{(2)}(z)=2\left[\frac{1+z^2}{1-z}\left(2\ln(1-z)-\ln z+\frac{3}{2}\right)+\frac{1}{2}(1+z)\ln z-1+z\right].$$

The second term on the right-hand side of Eq. (6) describes the case when an additional hard photon moves along the final electron direction and falls within a small cone with an opening angle θ_0' centered along the electron momentum. The corresponding contribution depends on the manner of event selection. For inclusive event selection, when only the electron energy is detected in the final state, the result can be derived using formula (Π.8) of Ref. 4:

$$\Sigma_b^{\rm incl}=P(z,L_0)\int_{\Delta/y_0}^{y_2^{\max}}\frac{dy_2}{1+y_2}\left[\frac{1+(1+y_2)^2}{y_2}(\widetilde{L}-1)+y_2\right]\Sigma_s,\quad \Sigma_s=\Sigma(x_b,y_b,Q_b^2), \tag{8}$$

where

$$\widetilde{L}=\ln(\varepsilon\theta_0'/m)^2+2\ln y_0,\quad y_2=\frac{x_2}{y_0},\quad y_2^{\max}=\frac{2z-y_0(1+c)}{y_0(1+c)},$$

$$x_b=\frac{zxy(1+y_2)}{z-(1-y)(1+y_2)},\quad y_b=\frac{z-(1-y)(1+y_2)}{z},\quad Q_b^2=Q^2z(1+y_2).$$

More realistic is calorimetric event selection, in which case the total energy of the scattered electron and photon is detected inside a small cone with opening angle $2\theta_0'$

along the momentum of the final electron. If the photon escapes this cone, then only the energy of the scattered electron is measured. In that case the result can be written as

$$\Sigma_b^{\rm cal}=P(z,L_0)\int_{\Delta/y_0}^{\infty}\frac{dy_2}{(1+y_2)^3}\left[\frac{1+(1+y_2)^2}{y_2}(\tilde{L}-1)+y_2\right]\tilde{\Sigma}. \tag{9}$$

In the last equation we use the relation

$$\Sigma_s=\frac{1}{(1+y_2)^2}\tilde{\Sigma}, \tag{10}$$

which is valid in the calorimetric setup. Note that the quantity Σ_a does not depend on event selection.

The third term on the right-hand side of Eq. (6) describes the contribution due to semicollinear kinematics, when the additional photon escapes both the PD and the narrow cone along the 3-momentum of the scattered electron. We note that in this case the event selection by definition is inclusive. The result can be derived by the help of the quasireal electron method[5] and has the form

$$\Sigma_{sc}=P(z,L_0)\left[\int_{\Delta}^{x_2^t}\frac{dx_2}{x_2}\frac{z^2+(z-x_2)^2}{z(z-x_2)}\ln\frac{2(1-c)}{\theta_0^2}\Sigma_t+\int_{\Delta}^{y_2^{\max}}\frac{dy_2}{y_2}\frac{1+(1+y_2)^2}{1+y_2}\right.$$
$$\left.\times\ln\frac{2(1-c)}{\theta_0'^2}\Sigma_s+Z\right],\quad \Sigma_t=\Sigma(x_t,y_t,Q_t^2), \tag{11}$$

$$x_t=\frac{xy(z-x_2)}{z-x_2+y-1},\quad y_t=\frac{z-x_2+y-1}{z-x_2},\quad Q_t^2=Q^2(z-x_2)\quad x_2^t=z-y_0(1+c)/2,$$

where the quantity Z represents the integral over the whole photon phase space of the function free from collinear and infrared singularities. It reads

$$Z=-\frac{4(1-c)}{Q^2}\int_0^{\infty}\frac{du}{1+u^2}\left[\int_{\eta}^{1}\frac{dt_1}{t_1|t_1-a|}\int_0^{x_m}\frac{dx_2}{x_2}(\Phi(t_1,t(t_1,u)-\Phi(a,0))\right.$$
$$\left.+\int_{\eta}^{a}\frac{dt_1}{t_1 a}\int_0^{x_m}\frac{dx_2}{x_2}(\Phi(a,0)-\Phi(0,a))\right]_{\eta\to 0}, \tag{12}$$

where

$$t(t_1,u)=\frac{(a-t_1)^2(1+u^2)}{y_++u^2y_-}.$$

Here we put in the explicit expression for $\Phi(t_1,t_2)$:

$$\Phi(t_1,t_2)=\alpha^2(Q_{sc}^2)\left[\left(\frac{M^2x_{sc}}{Q_{sc}^2}F_2(x_{sc},Q_{sc}^2)-F_1(x_{sc},Q_{sc}^2)\right)\frac{Q_{sc}^4-2st+z^2Q^4}{Q_{sc}^4}\right.$$

$$+\frac{V^2}{Q_{sc}^4}F_2(x_{sc},Q_{sc}^2)\left[x_{sc}(z^2+(1-y)^2)+xy(1-y)\left(z-\frac{s}{Q^2}\right)\right.$$
$$\left.-xyz\left(z-\frac{t}{Q^2}\right)\right]\Bigg],$$

$$Q_{sc}^2=zQ^2-s-t,\quad s=4\epsilon^2y_0x_2t_2,\quad t=-4\epsilon^2zx_2t_1, \tag{13}$$

and x_m has the form

$$x_m=\frac{z(e+p)-\Delta_m-y_0(e+z)-(p-z)y_0c}{z+e-y_0+(p-z)c_1+y_0c_2},\quad e=\frac{E_p}{\epsilon},$$

$$p=\frac{P_p}{\epsilon},\quad \Delta_m=\frac{(M+m_\pi)^2-M^2}{2\epsilon^2}, \tag{14}$$

where m_π is the pion mass.

3. The final result is the sum of (4) and (6). It is convenient to represent it as a sum of two terms

$$z\,\frac{d\sigma}{y\,dy\,dx}=\left(\frac{\alpha}{2\pi}\right)^2(\Sigma_i+\Sigma_f), \tag{15}$$

where the first one is universal or, in other words, does not depend on the manner of event selection. It can be written as

$$\Sigma_i=\left[\frac{1}{2}L_0^2P_\theta^{(2)}(z)+P(z,L_0)\left[\frac{1-16x-z^2}{2(1+z^2)}+\left(3-2\ln y_0+\frac{4z}{1+z^2}\,\frac{L_Q}{L_0}\right)\right.\right.$$
$$\times\ln z+\ln^2 y_0-2\,\mathrm{Li}_2(z)+2\,\mathrm{Li}_2\left(\frac{1+c}{2}\right)-\frac{2(1+z)^2}{1+z^2}\,\ln(1-z)+\frac{1-z^2}{2(1+z^2)}$$
$$\left.\left.\times\ln^2 z\right]\right]\widetilde{\Sigma}+P(z,L_0)\widetilde{\Sigma}\,\ln\frac{2(1-c)}{\theta_0^2}\left[\int_0^{u_0}\frac{du}{u}(1+(1-u)^2)\left(\frac{\Sigma_t}{(1-u)\widetilde{\Sigma}}-1\right)\right.$$
$$\left.-\int_{u_0}^1\frac{du}{u}(1+(1-u)^2)\right]+Z,\quad u=x_2/z,\quad u_0=x_t/z. \tag{16}$$

Because the quantity θ_0 is a physical parameter which defines the condition for the tagged photon registration, it enters in the final result.

The second term on the right-hand side of Eq. (15) just depends on the event selection. It is defined with final-state radiation only. For inclusive event selection we have

$$\Sigma_f = \Sigma_f^{\rm incl} = P(z,L_0)\int_0^{x_2^s/y_0}\left[\left(\frac{1+(1+y_2)^2}{y_2}L+y_2\right)\frac{1}{1+y_2}\,\theta\left(y_2-\frac{\Delta}{y_0}\right)+L\,\delta(y_2)\right.$$
$$\left.\times\left(2\ln\frac{\Delta}{y_0}+\frac{3}{2}\right)\right]\Sigma_s dy_2, \quad L=L_Q+\ln y_0-1. \tag{17}$$

In this case θ_0' is an auxiliary parameter and does not enter the expression for the cross section.

In the more realistic, calorimetric setup the counter of events does not distinguish the events with a bare electron and events in which the electron is accompanied by a hard photon, both having been emitted within a small cone with opening angle $2\theta_0'$ along the direction of the scattered electron. In this setup

$$\Sigma_f = \Sigma_f^{\rm cal} = P(z,L_0)\left[\frac{1}{2}\widetilde{\Sigma}+\ln\frac{2(1-c)}{\theta_0'^2}\int_0^\infty\frac{dy_2}{y_2}\,\frac{1+(1+y_2)^2}{1+y_2}\right]\theta(y_2^s-y_2)$$
$$\left.\times\Sigma_s-\frac{1}{(1+y_2)^2}\widetilde{\Sigma}\right]\Bigg]. \tag{18}$$

In the calorimetric manner of event selection the parameter θ_0' is the physical one and appears in the final result. However, the mass singularity, which is connected with the emission of the scattered electron, cancels out in accordance with the Lee–Nauenberg theorem.[6]

The numerical calculations for some experimental setups at HERA will be given in subsequent publications.[7]

The authors thank H. Anlauf, A. Arbuzov, and L. Trentadue for fruitful discussions and critical remarks. This work was supported by INTAS Grant 93-1867.

[1] M. W. Krasny, W. Placzek, and H. Spiesberger, Z. Phys. C **53**, 687 (1992).
[2] A. B. Arbuzov *et al.*, Nucl. Phys. B **485**, 457 (1997); N. P. Merenkov *et al.*, Acta Phys. Pol. B **28**, 491 (1997).
[3] E. A. Kuraev, N. P. Merenkov, and V. S. Fadin, Yad. Fiz. **45**, 852 (1987) [Sov. J. Nucl. Phys. **45**, 486 (1987)].
[4] N. P. Merenkov, Yad. Fiz. **48**, 1782 (1988) [Sov. J. Nucl. Phys. **48**, 1073 (1988)].
[5] V. N. Baier, V. S. Fadin, and V. A. Khoze, Nucl. Phys. B **65**, 381 (1973).
[6] T. D. Lee and M. Nauenberg, Phys. Rev. **133**, B1549 (1964).
[7] H. Anlauf, A. B. Arbuzov, E. A. Kuraev, and N. P. Merenkov, in preparation.

Published in English in the original Russian journal. Edited by Steve Torstveit.

A built-in scale in the initial spectrum of density perturbations: evidence from cluster and CMB data

F. Atrio-Barandela[a)]
Física Teórica, Facultad de Ciencias, Universidad de Salamanca, 37008 Spain

J. Einasto[b)]
Tartu Observatory, EE-2444 Tõravere, Estonia

S. Gottlöber[c)] and V. Müller[d)]
Astrophysikalisches Institut Potsdam, D-14482 Potsdam, Germany

A. Starobinsky[e)]
Landau Institute for Theoretical Physics, 117334 Moscow, Russia

(Submitted 7 August 1997)
Pis'ma Zh. Éksp. Teor. Fiz. **66**, No. 6, 373–378 (25 September 1997)

We calculate the temperature anisotropies of the cosmic microwave background (CMB) for several initial power spectra of density perturbations with a built-in scale suggested by recent optical data on the spatial distribution of rich clusters of galaxies. Using cosmological models with different values of the spectral index, baryon fraction, Hubble constant, and cosmological constant, we compare the calculated radiation power spectrum with the CMB temperature anisotropies measured by the Saskatoon experiment. We show that spectra with a spike at 120 h^{-1} Mpc are in agreement with the Saskatoon data. The combined evidence from cluster and CMB data favors the presence of a peak and a subsequent break in the initial matter power spectrum. Such a feature is similar to the prediction of an inflationary model wherein an inflaton field is evolving through a kink in the potential. © *1997 American Institute of Physics.* [S0021-3640(97)00218-1]

PACS numbers: 98.70.Vc, 95.85.Bh, 97.10.Ri

One of the crucial problems in cosmology is to determine the shape and amplitude of the initial (primordial) power spectrum of density perturbations. In the standard Friedman–Robertson–Walker cosmology this spectrum is arbitrary. It is specified as an initial condition at the cosmological singularity (the Big Bang). The only restriction is on the type of perturbations: they should belong to those modes which do not destroy the homogeneity of the Universe at early times — in particular, they should represent the growing mode in the case of adiabatic perturbations. For the scales of interest, the opposite assumption would result in the Universe being highly anisotropic and inhomogeneous at the time of the Big Bang nucleosynthesis (BBN), which would completely spoil its predictions for the primordial abundance of light elements. On the other hand, the simplest inflationary models of the early Universe predict the power spectrum of the growing mode of adiabatic perturbations at present to be approximately scale-invariant,

i.e., Harrison–Zeldovich, characterized by a slope $n \approx 1$ on large scales.[1] In addition to processes during the inflationary era, the current power spectrum is determined by physical processes occurring during the radiation-dominated regime that freeze out and damp the growth of density perturbations within the cosmological horizon. The final spectrum depends on the values of the cosmological parameters and on the exact nature of dark matter present in the Universe.

From the observational point of view, the current (evolved) power spectrum of matter density perturbations can be estimated by measuring the clustering properties of galaxies and clusters of galaxies. Using the distribution of rich Abell clusters, the spectrum has been recently determined on scales from $k \approx 0.03$ up to $k \approx 0.3\, h$ Mpc^{-1} (Ref. 2; h is the Hubble constant in units of 100 km$\cdot$s^{-1}Mpc^{-1}). The observed power spectrum contains a spike at $k \approx 0.05\, h$ Mpc^{-1}. A similar feature on the same scale has been observed in the one-dimensional deep galaxy red-shift survey in the direction of Galactic poles, in the two-dimensional power spectrum obtained from the Las Campanas Redshift Survey of galaxies, and from the deprojected power spectrum of the angular APM galaxy survey.[3]

The purpose of this letter is to confront the power spectrum of matter density perturbations obtained from cluster data with measurements of CMB temperature anisotropies on different angular scales. We shall use the observations made at Saskatoon.[4] By using a synthetic antenna beam, the Saskatoon group was able to measure temperature anisotropies with five different angular resolutions corresponding to multipoles between $l \approx 80$ and $l \approx 400$. This range makes the experiment especially well suited for comparison with the cluster power spectrum,[2] since it roughly corresponds to the wavelengths probed by the cluster data. We used the 4-year COBE data[5] to get the absolute normalization and the shape of the matter power spectrum at scales close to the present cosmological horizon.

We calculate CMB temperature anisotropies for three different initial power spectra: (a) a scale-free initial spectrum with a power-law exponent n, (b) a double power-law approximation to the cluster spectrum, and (c) a spectrum based on the observed cluster spectrum. Outside the measured range, this last was extrapolated assuming a scale-free spectrum. At large wave numbers ($k \geqslant 0.05\, h$ Mpc^{-1}) the shape of the observed cluster spectrum is similar to that of galaxies.[6] For the power spectrum (b) at small scales we used a slope $n = -1.8$, which is a smooth extrapolation of the cluster data. However, since this region of the power spectrum has little influence on multipoles above $l = 400$, this assumption will not affect our conclusions. At large scales the spectrum is poorly determined. Within observational errors, it is compatible with being the Harrison–Zeldovich spectrum. Furthermore, the COBE/DMR data indicate[5] that the power spectrum of matter density perturbations has $n \approx 1$ for $k \approx 0.003\, h$ Mpc^{-1}; more exactly, $n = 1.1 \pm 0.2$. Accordingly, we varied the slope at large scales in that range.

The initial power spectrum is determined as follows:

$$P_0(k) = P(k)/T^2(k), \tag{1}$$

where $P(k)$ is the power spectrum of matter perturbations at the current epoch, and $T(k)$ is the transfer function for a particular CDM model. The transfer function depends only on physical processes taking place within the horizon. In the previous expression we

assumed that the observed cluster power spectrum $P_{cl}(k)$ was proportional to $P(k)$ over the range probed by the cluster data: $P_{cl}(k)=b_{cl}^2 P(k)$, where b_{cl} is the bias factor for clusters of galaxies.

We assume the Universe has a flat geometry. We did not consider mixed dark matter (MDM) models here. They differ from CDM models mainly at small wavelengths, which have little influence on our results. Furthermore, MDM models with one stable neutrino and $h \geqslant 0.5$ have problems in creating small scale structure. In these models galaxy formation occurs too late,[7] and considering scale-free MDM models with $n>1$ does not help.[8] In what follows we shall consider $\Omega_b+\Omega_c+\Omega_\Lambda=1$, with Ω_b, Ω_c, and Ω_Λ being the fraction of the energy density in baryons, cold dark matter, and vacuum energy (cosmological constant), respectively.

To calculate the radiation power spectrum we used the packages COSMICS and CMBFAST.[9] The radiation power spectrum was normalized to the COBE/DMR 4-year data[5] using the multipole $l=10$ as a central value instead of the quadrupole.[10] A comparison with the cluster power spectrum gives $b_{cl} \approx 3$ for $n \approx 1$. We have performed the integration for the three primordial spectra and parameters: $n=1.0,\ldots,1.4$; the Hubble constant from $h=0.3$ to 0.8; the baryon density from $\Omega_b h^2=0.005$ to 0.033, centered on the range suggested by BBN.[11] We also considered models with a cosmological constant. In these models we chose a Hubble constant that makes the Universe 14 Gyr old. It ranged from $h=0.5$ for $\Omega_\Lambda=0.1$ to $h=0.7$ for $\Omega_\Lambda=0.7$, in agreement with the recalibration of the Hubble constant and cosmic ages made in Ref. 12 using the new determination of distances to subdwarfs and Cepheids based on the Hipparcos data. The amplitude of a temperature anisotropy expected on a given angular scale was found using the window function that best models the synthetic beam pattern of the Saskatoon experiment for that scale.[4] Finally, for each model we calculated the χ^2-deviation between the theoretical prediction and the Saskatoon data. In Fig. 1 we plot the intervals in the parameter space at 68% and 95% confidence levels. The dashed lines indicate the range $0.007 \leqslant \Omega_b h^2 \leqslant 0.024$ favored by BBN.[11]

Figure 1 shows that CMB data alone exclude a large range of parameter space for each of our three basic models. The standard CDM model is compatible with the CMB data for values of the Hubble constant and baryon fraction that are almost out of the range of astronomical interest. An increase of the power index n helps, but such models are not viable because they overproduce mass fluctuations on scales of $8\,h^{-1}$ Mpc (σ_8). Actually, it is well known that even the scale-invariant CDM model normalized to the COBE data is excluded for that reason. The best scale-free model has a fairly large cosmological constant, $\Omega_\Lambda \approx 0.6$. A CDM model with a large cosmological constant and a high baryon fraction was suggested in Ref. 13 to explain the presence of large walls and voids in the distribution of galaxies. The fact that the energy densities of the baryon and dark-matter fractions are comparable in this model results in the appearance of noticeable Sakharov oscillations in the transfer function for cold dark matter and baryons after recombination. As for the cluster-based and double power-law spectra, both fit the results of the Saskatoon experiment rather well in the range of parameters of astronomical interest. The best agreement with the CMB data is obtained for a low or vanishing cosmological constant, and for a spectral index $n=1$. The allowed range of the Hubble constant is rather large for a reasonable baryon fraction.

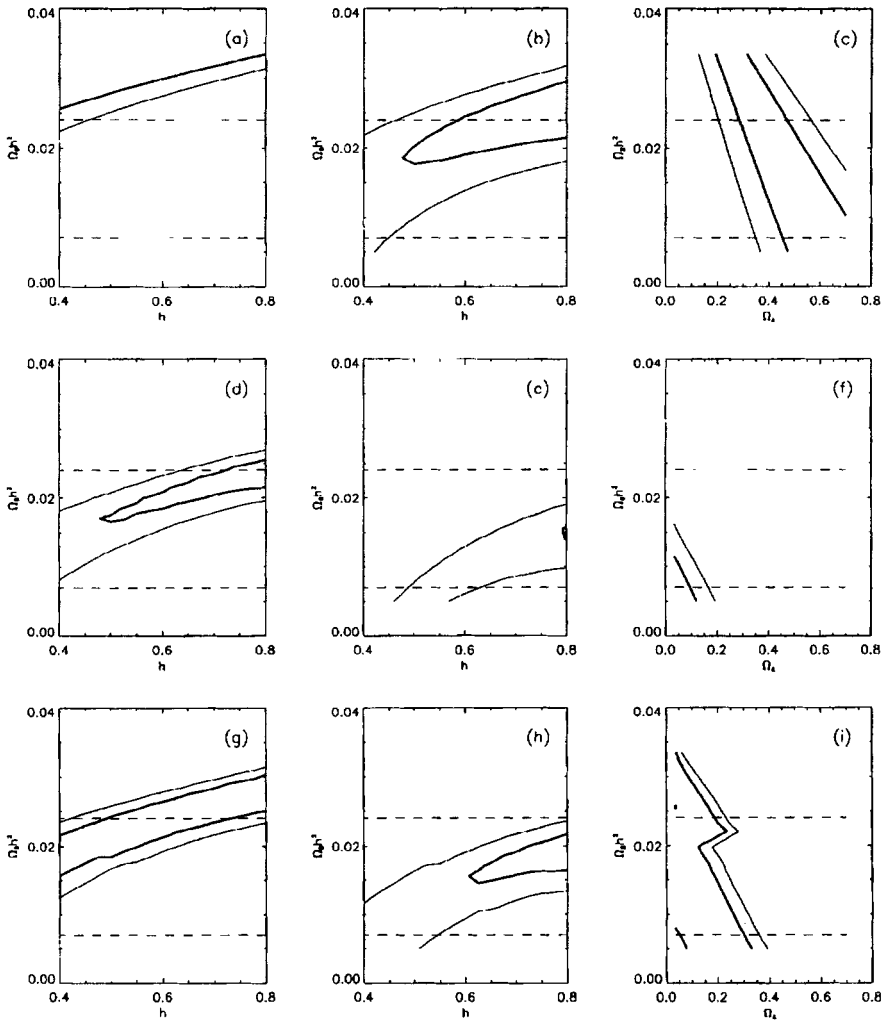

FIG. 1. Goodness-of-fit contours of χ^2 at 68% (thick lines) and 95% (thin lines) confidence levels. The first row displays the results for the scale-free model, the second row for the double power-law model, and the lowest row for the cluster-spectrum-based model. In the first column we plot models with varying Hubble constant and baryon fraction for a spectral index $n=1$ at large scales and zero cosmological constant. In the middle column the same diagrams are repeated for $n=1.2$. The last column displays the results for models with different values of the cosmological constant.

In Fig. 2 we compare the matter power spectra and temperature anisotropy spectra for our three basic models with the data. The cosmological parameters were chosen to reproduce the CMB data within the 68% confidence level. As expected, the temperature anisotropy spectra are very similar. In other words, the present CMB data alone are not sufficient to discriminate between models. In contrast, the matter power spectra are very different. The scale-free model with a large cosmological constant has a broad maximum

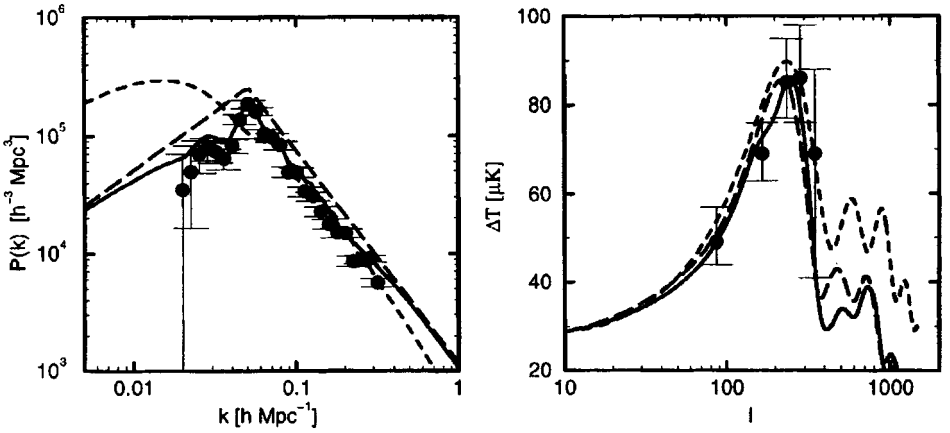

FIG. 2. Comparison of matter power spectra and radiation temperature anisotropies with cluster and CMB data. Dots with 1σ error bars represent the observational data: the measured cluster spectrum is in the left-hand panel and the Saskatoon data on CMB temperature anisotropies are in the right-hand panel. The scale-free model spectra (short-dashed lines) are computed using the following parameters: $h=0.6$, $\Omega_b=0.07$, $\Omega_c=0.23$, and $\Omega_\Lambda=0.7$ (short-dashed lines). The cluster spectrum (solid lines) was calculated using $h=0.6$, $\Omega_b=0.08$, $\Omega_c=0.92$, and $\Omega_\Lambda=0$; and the double power-law models (long-dashed) using $h=0.6$, $\Omega_b=0.05$, $\Omega_c=0.95$, and $\Omega_\Lambda=0$.

at large wave numbers ($k\approx 0.01\ h$ Mpc^{-1}); the maximum of the first acoustic oscillation occurs at $k\approx 0.1\ h$ Mpc^{-1} and is of a rather small relative amplitude. Both scales are well outside the allowed range of the observed spike in the spectrum: $k_0=0.052\pm 0.005\ h$ Mpc^{-1} (Ref. 2). Therefore we conclude that, contrary to the expectation of Ref. 13, this spike is not related to acoustic oscillations in the baryon–photon plasma. The scale-free model spectrum agrees with the observed cluster (and galaxy) spectrum at short wavelengths up to the peak. However, no combination of cosmological parameters reproduces the spike at $k=k_0$. The existence of a broad maximum is an intrinsic property of all scale-free models and such a maximum cannot produce a regular supercluster–void network, as was shown in Ref. 14. On the other hand, the cluster and double power-law spectra fit the observed cluster spectrum by construction and reproduce the CMB data, i.e., they fit both data sets equally well. Therefore the present combined cluster and CMB data favor models with a built-in scale in the *initial* spectrum.

Double inflation models provide a possible scenario in which the formation of a spike could have taken place.[15] The presence of two scalar fields driving the evolution of the Universe has a built-in scale defined by the moment when the inflaton field that initially drove inflation becomes subdominant. Another possibility which does not require a fine tuning of the initial energy density of different scalar fields is when the inflaton field evolves through a kink in the potential. A quick change in the first derivative in the inflaton potential generates a sharp spike in the matter power spectrum followed by a break in amplitude.[16] Note that this effect is beyond the slow-roll approximation to the motion of the inflaton field or any adiabatic correction to it. The initial power spectrum found in Ref. 16 is very similar to the empirical initial power spectrum that follows from

the measured cluster spectrum plotted in the left panel of Fig. 2; the relative amplitudes of the spike and break are also close to the observed values.

The main conclusion we can draw from our study is that, within the accuracy of present measurements, the combined cluster and CMB temperature anisotropy data suggest the existence of a break in the initial power spectrum of matter density perturbations. The spike found earlier in the cluster power spectrum[2] accounts for the observed high amplitude of the first Doppler peak in the CMB spectrum, if the baryon fraction is not too high ($\Omega_b h^2 < 0.024$ for $h \simeq 0.6$). On the other hand, if the cosmological constant is large ($\Omega_\Lambda > 0.4$), then it would be difficult to reconcile a built-in scale in the initial matter power spectrum with the present CMB data. Only new and more-accurate observations of the power spectrum, both optical and CMB, can discriminate between these two alternatives.

We thank Ed Bertschinger, Uros Seljak, and Matias Zaldarriaga for permission to use their software packages COSMICS and CMBFAST for calculating the angular power spectrum of the microwave background radiation, and Alex Szalay for a stimulating discussion. This study was supported by grants from the German Science Foundation, Estonian Science Foundation, Astrophysical Institute Potsdam, and by Spanish German Integrated Actions HA 1995 - 0079. F. A. B. would like to acknowledge the support of the Junta de Castilla y León, Grant SA40/97. A. S. acknowledges the support of the Russian Fund for Fundamental Research, Grant 96-02-17591.

[a)]e-mail: atrio@astro.usal.es
[b)]einasto@max.aai.ee
[c)]sgottloeber@aip.de
[d)]vmueller@aip.de
[e)]alstar@landau.ac.ru

---

[1] S. Hawking, Phys. Lett. B **115**, 295 (1982); A. Starobinsky, Phys. Lett. B **117**, 175 (1982); A. Guth, and S.-Y. Pi, Phys. Rev. Lett. **49**, 1110 (1982); J. M. Bardeen, P. Steinhardt, and M. Turner, Phys. Rev. D **28**, 679 (1983).
[2] J. Einasto, M. Einasto, S. Gottlöber *et al.*, Nature **385**, 139 (1997).
[3] T. J. Broadhurst, R. S. Ellis, D. C. Koo, and A. S. Szalay, Nature **343**, 726 (1990); S. D. Landy, S. A. Shectman, H. Lin *et al.*, Astrophys. J. **456**, L1 (1996); E. Gaztanaga, and C. M. Baugh, Mon. Not. R. Astron. Soc. (in press), astro-ph/9704246 (1997).
[4] C. B. Netterfield, M. J. Devlin, N. Jarosik *et al.*, Astrophys. J. **474**, 47 (1997); E. Wollack, M. J. Devlin, N. Jarosik *et al.*, Astrophys. J. **476**, 440 (1997).
[5] C. L. Bennet *et al.*, Astrophys. J. **464**, L1 (1996).
[6] L. N. da Costa, M. S. Vogeley, M. J. Geller *et al.*, Astrophys. J. **437**, L1 (1994); H. Lin, R. P. Kirshner, S. A. Shectman *et al.*, Astrophys. J. **471**, 617 (1996); C. Park, M. S. Vogeley, M. J. Geller, and J. P. Huchra, Astrophys. J. **431**, 569 (1994); H. Tadros, and G. Efstathiou, Mon. Not. R. Astron. Soc. **282**, 1381 (1996).
[7] H. Bi and L. Z. Fang, Astrophys. J. **466**, 614 (1996); P. Frisch, J. Einasto, M. Einasto *et al.*, Astron. Astrophys. **296**, 611 (1995).
[8] D. Yu. Pogosyan and A. A. Starobinsky, Astrophys. J. **447**, 465 (1995).
[9] C. P. Ma, and E. Bertschinger, Astrophys. J. **455**, 7 (1995); U. Seljak, and M. Zaldarriaga, Astrophys. J. **469**, 437 (1996).
[10] M. White and E. F. Bunn, Astrophys. J. **450**, 477 (1995).
[11] A. Songalia, E. Wampler, and L. L. Cowie, Nature **385**, 137 (1997); D. Schramm and M. Turner, Rev. Mod. Phys. (in press), astro-ph/9706069 (1997).
[12] M. W. Feast and R. M. Catchpole, Mon. Not. R. Astron. Soc. **286**, L1 (1997).

[13] A. S. Szalay, to be published in *Proc. of 18th Texas Symposium on Relativistic Astrophysics*, Eds. A. Olinto, J. Frieman, and D. Schramm, World Scientific Press, (1997).
[14] J. Einasto *et al.*, Mon. Not. R. Astr. Soc. (in press), astro-ph/9704127 (1997); J. Einasto *et al.*, Mon. Not. R. Astr. Soc. (in press), astro-ph/9704129 (1997).
[15] L. A. Kofman, A. D. Linde, and A. A. Starobinsky, Phys. Lett. B **157**, 361 (1985); L. A. Kofman and A. D. Linde, Nucl. Phys. B **282**, 555 (1987); L. A. Kofman and D. Yu. Pogosyan, Phys. Lett. B **214**, 1753 (1988); S. Gottlöber, V. Müller, and A. A. Starobinsky, Phys. Rev. D **43**, 2510 (1991); D. Polarski, and A. A. Starobinsky, Nucl. Phys. B **385**, 623 (1992).
[16] A. A. Starobinsky, JETP Lett. **55**, 489 (1992).

Published in English in the original Russian journal. Edited by Steve Torstveit.

Effect of nonlinear wave mixing on ultrafast modulation of interband light in semiconductor quantum wells

A. Neogi

New Energy Development Organization, FESTA Laboratories, Tsukuba 300-26, Ibaraki, Japan

(Submitted 5 August 1997)
Pis'ma Zh. Éksp. Teor. Fiz. **66**, No. 6, 379–385 (25 September 1997)

We investigate the effect of an induced sum-frequency signal on the transient modulation of interband-resonant probe light by a train of intersubband-resonant coupling light pulses in undoped quantum wells. The origin of the generated sum-frequency signal lies in the asymmetry of the three-level quantum well structure. The modulation characteristics are found to be significantly affected in the presence of a strong sum-frequency signal that builds up proportionately to the input probe field. © *1997 American Institute of Physics.*
[S0021-3640(97)00318-6]

PACS numbers: 78.66.Db, 42.65.Re, 42.65.Hw

Coherent optical effects in semiconductor devices are currently being extensively explored for their application in various information systems associated with the generation, propagation, processing, and detection of ultrashort signals. The investigation of nonlinear optical phenomena in multilevel quantum well structures involving the simultaneous utilization of both interband and intersubband transitions[1–10] have consequently attracted considerable attention. The study of transient properties of the control of light by light in quantum wells provides an insight into its possible application in an optical switch in which the transmission of a highly absorptive medium can be controlled by an additional coupling light field. The transient analyses for a three-level quantum well system reveals that for resonantly interacting fields under ideal conditions the amount of probe absorption by the semiconducting medium acts as the amplitude of a damped harmonic oscillator.[5–8] The ultimate modulation speed of interband (IB) light by intersubband (ISB) light in quantum wells is extremely fast, as it is governed by the intersubband relaxation rate.[1] Higher modulation speed can therefore be expected on application of ultrashort ISB coupling pulses in the femtosecond regime.[6]

In this letter we investigate the modulation process in a three-level asymmetric quantum well system in the presence of an additional interband sum-frequency field[2] generated by the nonlinear interaction of the interband probe and intersubband coupling light fields. Our recent analyses[6,8] reveal that the modulation of a strong interband probe light by a train of coupling light pulses with pulse width and repetition rates comparable or longer than the intersubband lifetimes and interband relaxation rates is most efficient. The interband probe light is modulated by the switching of a train of intersubband-coupling light pulses at a correspondingly high speed and depends critically on the intensities of the coupling and the probe light fields. We investigate the effect of the

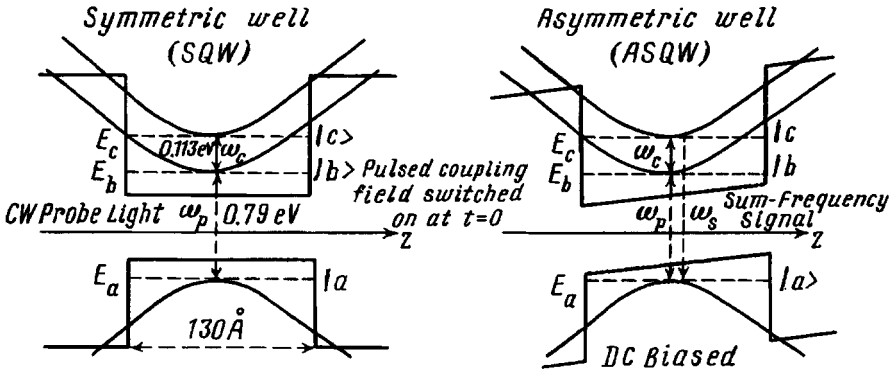

FIG. 1. Schematic drawing for modulation of interband resonant light by intersubband resonant light in undoped quantum wells.

additional induced optical field on the transient absorption of the interband probe field by comparing the modulation process in both symmetric and asymmetric structures.

The density-matrix approach is employed in this study. The steady-state modulation characteristics of the probe light by an intersubband coupling light in an undoped quantum well can be clearly interpreted in terms of excitonic effects, where the system becomes a completely discrete three-energy level system.[1] The interband and intersubband transitions are considered to correspond to two individual oscillators. The interband-related oscillator oscillates at its own frequency due to the resonant probe field in the absence of the coupling light. In the presence of a strong coupling field the intersubband-related oscillator becomes coupled to the interband-related oscillator. The strong coupling between the two oscillators leads to a deviation of the oscillation frequency from their own frequencies and thus to the splitting of a single excitonic peak into two peaks. We consider this transient analysis at the resonance frequency, where the reduction in the absorption of the probe field due to electromagnetically induced transparency by the coupling field is maximum. The three-level quantum well system is shown in Fig. 1. A cw interband probe light $\{F_p \exp(-i\omega_p t)+\text{c.c. at } \omega_p\}$ is resonantly tuned to the first heavy-hole state to first conduction subband transition $|a\rangle-|b\rangle$. The ISB coupling field consists of a train of resonant pulses, $\{[F_c \operatorname{sech}(t/\tau_p)\exp(-i\omega_c t)+\text{c.c.}] \text{ at } \omega_c\}$ tuned to the transition $|b\rangle$ and $|c\rangle$ and is switched on at time $t=0$, when the three-level system is at a steady state in presence of the cw probe field. The pulses are also assumed to be in phase with one another, i.e., coherent. In an asymmetric quantum well structure there is an additional polarization at the sum-frequency field $\omega_s=(\omega_p+\omega_c)$ arising from the finite transition dipole moment (μ_{ca}) between the first heavy-hole state $|a\rangle$ and the second conduction subband state of the three-level system $|c\rangle$. This allows a direct interband transition between the states $|c\rangle$ and $|a\rangle$ which is otherwise forbidden under the interband selection rules in a symmetrical structure where the dipole moment μ_{ca} is taken to be zero. Thus the modulation process in symmetric wells involves two-wave interaction with frequencies ω_p and ω_c, while in asymmetric well it involves the interaction of three distinct waves at ω_p, ω_c and ω_s. This induced sum-frequency signal

$\{F_s(t)\exp(-i\omega_s t)+\text{c.c.}\}$ is expected to modify the modulation characteristics of the interband light.

The generalized equations of motion for both symmetric and asymmetric structures are obtained by incorporating the Rabi frequencies of the interacting fields in the respective system in the 3×3 interaction Hamiltonian matrix and applying the slowly varying wave approximation. The off-diagonal elements of the density matrix satisfy

$$\frac{\partial \rho_{jk}(t)}{\partial t} = -\{i\Delta_{jk}+\Gamma_{jk}\}\rho_{jk}(t) + i[\Omega_{jk}\{\rho_{kk}(t)-\rho_{jj}(t)\}+\Omega_{ji}\rho_{ik}(t)-\Omega_{ik}\rho_{ji}(t)], \quad (1)$$

where Ω_{ji} is the Rabi frequency of the optical field tuned to the states $|j\rangle$ and $|i\rangle$, Ω_c and Ω_p are the Rabi frequencies of the coupling and the probe fields, Γ_{ji} is the dephasing rate between levels j and i, the optical energies coupling the two states are defined as $\hbar\Delta_{jk}=E_j-E_k-\hbar\omega_{jk}$, and $\rho(t)$ has the symmetry property $\rho(t)_{jk}=\rho(t)^*_{kj}$.

The diagonal elements for a closed three-level quantum well system is represented by,

$$\frac{\partial \rho_{jj}(t)}{\partial t} = [(\partial\rho/\partial t)_{\text{relax}}]_{jj} + i[\Omega_{ji}\rho_{ij}(t)-\Omega_{ij}\rho_{ji}(t)+\Omega_{jk}\rho_{kj}(t)-\Omega_{kj}\rho_{jk}(t)], \quad (2)$$

where the relaxation Hamiltonian matrix elements for the states $|a\rangle$, $|b\rangle$, and $|c\rangle$ are taken, respectively as

$$\begin{aligned}
&[(\partial\rho/\partial t)_{\text{relax}}]_{aa} = \rho_{bb}(t)\Gamma_{bb},\\
&[(\partial\rho/\partial t)_{\text{relax}}]_{bb} = -\rho_{bb}(t)\Gamma_{bb}+\rho_{cc}(t)\Gamma_{cc}, \quad (3)\\
&[(\partial\rho/\partial t)_{\text{relax}}]_{cc} = -\rho_{cc}(t)\Gamma_{cc},
\end{aligned}$$

with T_{jj} $(1/\Gamma_{jj})$ being the lifetime of the electrons in state $|j\rangle$. In Eqs. (1) and (2) the indices i, j, and k refer to different subband states $|a\rangle$, $|b\rangle$, and $|c\rangle$. We have assumed that the three-level undoped quantum well is a completely closed system satisfying the condition $\rho_{aa}+\rho_{bb}+\rho_{cc}=1$. In symmetrical quantum wells the electrons are assumed to decay from state $|c\rangle$ to $|b\rangle$ and from $|b\rangle$ to $|a\rangle$, with $|a\rangle$ being taken as the ground state ($\Gamma_{aa}=0$). In case of asymmetric structures there is an additional decay channel direct from state $|c\rangle$ to $|a\rangle$ for the electrons to decay back to the ground state without the intermediate conduction subband state $|\text{b}\rangle$. This leads to reduced interference between the interband and intersubband transitions, which become significant in the case of highly populated conduction subband states.

The analyses of the sum-frequency field generated due to the three wave interaction in an asymmetric well and its effect on the modulation of the probe field involves the transient evolution of the Maxwell–Bloch equations. The transient sum-frequency polarization is deduced from the wave equation under slowly varying envelope approximation as,

$$\frac{\partial F_s(t)}{\partial t} = -\frac{\omega_s}{\epsilon_0\epsilon_1}\,\text{Im}[P_s(t)], \quad (4)$$

where ϵ_0 is the permittivity of free space and ϵ_1 is the dielectric constant of the medium. The absorption of the signal due to internal losses has been neglected. We solve the set of six coupled nonlinear optical Bloch equation obtainable from Eqs. (1) and (2) by the fourth-order Runge–Kutta method in case of the symmetrical quantum well structure, whereas for the asymmetric structure the transient evolution of the generated sum-frequency signal is estimated by solving Eq. (4) simultaneously with Eqs. (1) and (2).

The probe field dresses the initial population of the state $|b\rangle$ and induces a finite polarization due to interband transitions. The electrons are coherently excited by the probe field prior to the switching of the coupling field, i.e., for the time $t<0$, so that the initial conditions for Eqs. (1) and (2) are

$$\rho_{bb}(0)=\frac{2(\Omega_p^2\Gamma_{ba}/\Gamma_{bb})}{\Delta_{ba}^2+\Gamma_{ba}^2+4\Omega_p^2\Gamma_{ba}/\Gamma_{bb}}, \tag{5a}$$

$$\rho_{aa}(0)=1-\rho_{bb}(0)-\rho_{cc}(0), \tag{5b}$$

$$\rho_{ba}(0)=\frac{\Omega_p(\Delta_{ba}+i\Gamma_{ba})\{1-\rho_{bb}(0)\}}{\Delta_{ba}^2+\Gamma_{ba}^2+4\Omega_p^2\Gamma_{ba}/\Gamma_{bb}}, \tag{5c}$$

$$\rho_{cc}(0)=\rho_{cb}(0)=\rho_{ca}(0)=0. \tag{5d}$$

The band-filling factor $\{1-\rho_{bb}(0)\}$ arising due to the accumulation of carriers in the first conduction subband state $|b\rangle$ reduces the availability of vacant sites and reduces absorption in the case of a strong probe field. This factor has therefore been introduced in the steady state transition probability of the interband density matrix element in (5c).

The electronic polarization P arising from an interband probe field and an intersubband coupling field in the presence of the induced sum-frequency field is

$$P(t)=\epsilon_0\chi(t)[F_p(t)+F_c(t)+F_s(t)]\approx[\mu\rho(t)+\rho(t)\mu], \tag{6}$$

where $\chi(t)$ is the complex susceptibility. The linear susceptibility $\chi_{ba}(t)$ of the medium at the probe frequency can be related to the absorption coefficient α through its imaginary part $\mathrm{Im}[\chi_{ba}(t)]$ by assuming that the amplitude and polarization due to the probe field vary slowly over a wavelength or over a period. However the slowly varying envelope approximation approaches the limits of its validity for the case of femtosecond pulses with optical frequencies. It is observed that in the case of a resonant coupling and probe field, when $\Omega_c \gg \Gamma_{ba}$, the dressed susceptibility $\chi_{ba}(t)$ is described by a damped harmonic oscillator with initial amplitude $\rho_{ba}(0)$.

The physical characteristics of the modulation of the probe light due to the coupling pulses are analyzed with parameters appropriate for an actual $In_{0.53}Ga_{0.47}$ As/AlAs quantum well grown on an InP substrate with a well width of 130 Å. Asymmetry is induced in a symmetrical quantum well by the application of a dc electric field of 30 kV/cm perpendicular to the layers. The steady-state perturbation theory predicts very strong quadratic interband sum-frequency nonlinearity with a negative sign at resonant frequencies.[2] Our investigation reveals that the response time of the material, such as the population lifetime or the dephasing time, sets a limit to the length of the coupling light pulses which might be employed for the efficient modulation of the probe light. The

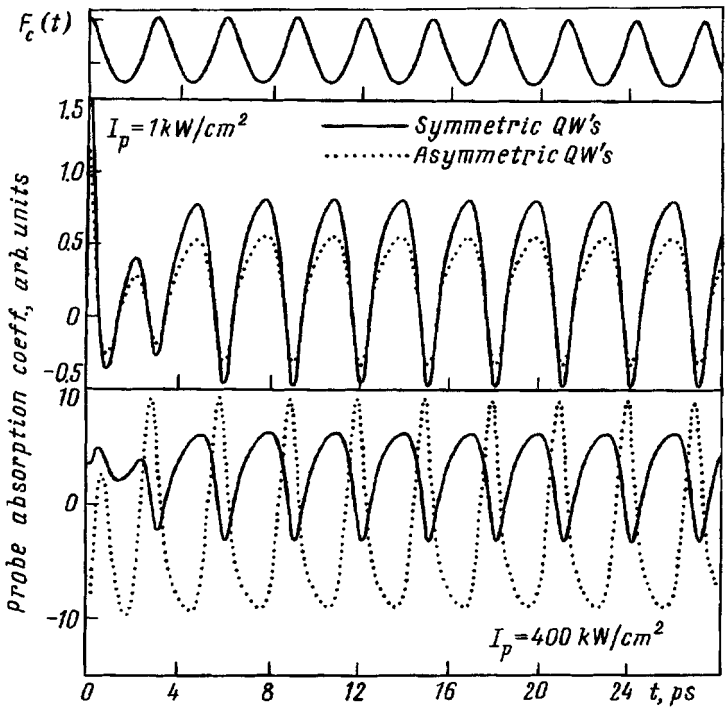

FIG. 2. Comparison of transient interband probe absorption in symmetric and asymmetric wells for $\tau_d > T_{ba}$, T_{cc}; with coupling intensity $I_c = 1.0$ MW/cm^2, $\tau_d = 3.0$ ps, $\tau_p = 1.0$ ps, $T_{cc} = T_{ba} = 1.0$ ps, $T_{bb} = 1.0$ ns, (a) $I_p = 1$ kW/cm^2; (b) $I_p = 400$ kW/cm^2.

relative ratios of the coupling pulse width to the intersubband lifetime T_{cc} is one of the most significant parameters governing the transient modulation characteristics of the IB-resonant probe light in the presence of a coupling field. This is because for comparatively long T_{bb} it is T_{cc} that determines the duration for which the carriers excited by the coupling field from the conduction subband state $|b\rangle$ is retained at state $|c\rangle$ and thereby affects the temporal absorption of the probe light. The carrier density of the well does not affect the modulation process unless the Rabi frequency of the probe light is very much lower than T_{ba}^{-1}. It is found that the sum-frequency response depends on the initial dressing of the intersubband states.[8] The magnitude of the sum-frequency oscillation increases with the probe field strength as the population buildup due to the pumping of carriers increases the electrons available at the state $|c\rangle$ in the presence of the intersubband resonant field and which subsequently decay directly back to the ground state. The increase in probe field also induces a change in phase of the generated sum-frequency oscillations.

In Fig. 2 we have compared the modulation process induced in symmetric and asymmetric structures by a train of symmetric pulses with their widths (τ_p) and repetition rates (τ_d) larger than the phenomenological intersubband lifetime (T_{cc}) and interband relaxation rates (T_{ba}). The transient variation of the optical field amplitude of the cou-

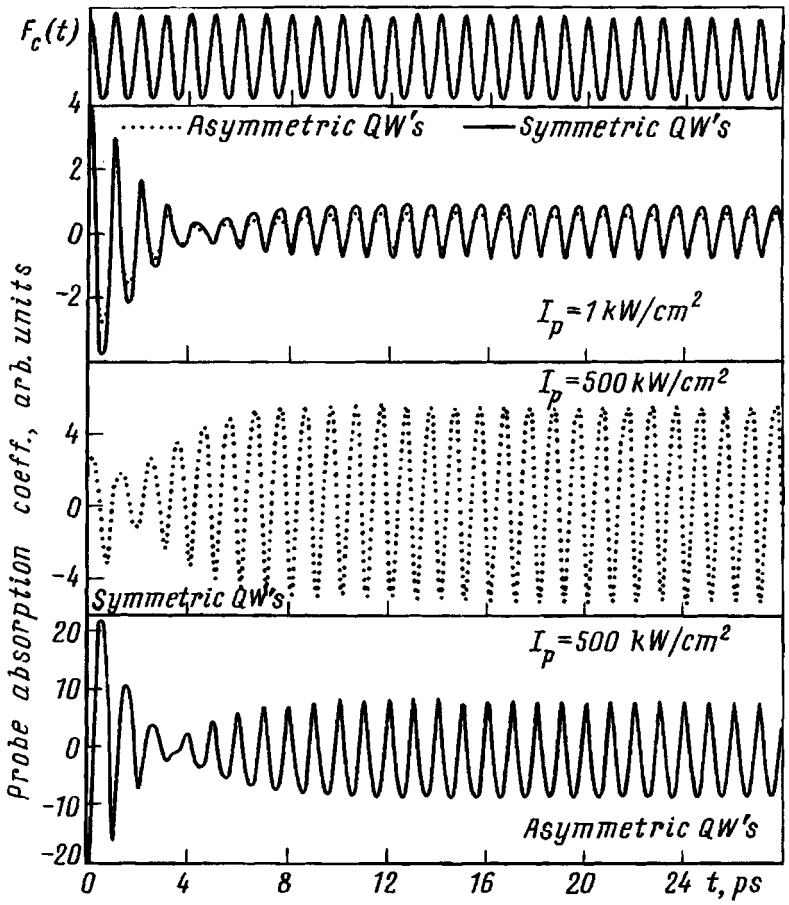

FIG. 3. Comparison of transient interband probe absorption in symmetric and asymmetric wells for $\tau_d < T_{ba}$, T_{cc} with coupling intensity $I_c = 1.0$ MW/cm^2, $\tau_d = 1.0$ ps, $\tau_p = 400$ fs, $T_{cc} = 1.0$ ps, $T_{ba} = 3.0$ ps, $T_{bb} = 1.0$ ns; (a) $I_p = 1$ kW/cm^2, (b) $I_p = 500$ kW/cm^2 without a sum-frequency field; (c) $I_p = 500$ kW/cm^2 in the presence of a sum-frequency field.

pling pulse train is depicted at the top of Figs. 2 and 3. The interband probe absorption coefficient is alternately positive and negative, implying that absorption and emission occur simultaneously. It has been noticed that in case of the modulation of weak probe fields, when the nonlinearity due to the three-wave mixing is weaker, the transient oscillatory features of the interband absorption are very similar to those in symmetric structures (Fig. 2a). There is actually a slight reduction in the probe oscillations due to the asymmetry-related decrease[9] in the interband transition dipole moment μ_{ba}. In the presence of stronger probe fields the dressing of the conduction subband states results in an increase in the initial population of electrons in the conduction subband state $|b\rangle$. This results in a population inversion between the interband states, which leads to stronger oscillatory transient sum-frequency signal arising from the direct transition between the

states $|c\rangle$ and $|a\rangle$. The strength of the induced probe oscillations at higher F_p is also considerably enhanced in case of the asymmetric quantum wells as the transfer of energy from the nonlinear sum-frequency wave oscillates between the two interband fields (Fig. 2b). It can also be observed that in asymmetric wells in the presence of an appreciable sum-frequency field there is a change in the phase of the induced oscillations along with the input probe field strength. Thus an increase in the probe power level induces a change in the phase of the modulated oscillations under the influence of the nonlinear sum-frequency signal field.

In Fig. 3 the effect of repetitive excitation of the coupling light on the probe modulation is shown for pulse delay time τ_d shorter than interband dephasing time scale T_{ba}. As is seen in Fig. 2a, at weaker probe field strengths the transient response is similar for both the symmetric and asymmetric quantum wells. In this case, over time scales lower than T_{ba}, the polarization left in the medium by the first pulse interacts with the second pulse, resulting in the interaction of two pulses separated in time. In case of the modulation of a weak probe field it has been observed that due to a destructive interference effect suppressing the population buildup, the transient oscillatory behavior of the probe field is reduced despite repetitive pulse excitation. Therefore the switching of the coupling field with short delay times τ_d has less effect on the induced interband polarization, on account of the destructive interference effect which reduces the oscillatory absorption characteristics of the weak probe light on time scales shorter than or comparable to T_{ba} (Fig. 3a). It can be further observed from Fig. 3b that if the probe field is appreciably stronger, then in symmetric structures on time scales larger than T_{ba} the transient oscillations build up proportionately to the magnitude of the Rabi frequency after the initial suppression of the induced oscillations at time scales $t<T_{ba}$. This characteristic is found to be reversed in the presence of the sum-frequency field in asymmetric wells (Fig. 3c). The nonlinear sum-frequency field quenches the buildup in the probe oscillation observed in Fig. 3b at time scales longer than T_{ba} after the decay of the stronger initial oscillations during $t<T_{ba}$.

We have analyzed theoretically the influence of transient sum-frequency signal on the interband-resonant probe light modulation by a train of intersubband resonant light in an undoped quantum well. The presence of an additional sum-frequency signal that is adequately strong is expected to enhance the induced oscillations of the interband probe light. The magnitude of the instantaneous response of the medium at the sum frequency depends on the extent of the population inversion between states $|b\rangle$ and $|a\rangle$, which can be controlled by the probe light. The most efficient modulation can be achieved in the presence of strong probe and coupling light fields. In case of modulation of ultrashort light pulses a stable modulation characteristic is achieved at time scales longer than the interband dephasing time (T_{ba}) of the system. Possible applications of the proposed model include the realization of picosecond lasers in the visible and near-infrared regions.

A part of the work was supported by the Japan Society for Promotion of Sciences and was completed within the Femtosecond Technology Project Scheme supported by NEDO.

[1] S. Noda, M. Ohya, Y. Muromoto *et al.*, IEEE J. Quantum Electron. **QE-32**, 448 (1996).
[2] A. Neogi, Y. Takahashi, and H. Kawaguchi, IEEE J. Quantum Electron. **QE-32**, 701 (1996).
[3] D. S. Lee and K. J. Malloy, Phys. Rev. B **54**, 15749 (1996).
[4] V. W. Lee and T. K. Gustafson, Appl. Phys. Lett. **66**, 271 (1995).
[5] I. Brener, P. C. M. Planken, M. C. Nuss *et al.*, J. Opt. Soc. Am. B **11**, 2457 (1994).
[6] A. Neogi, Y. Takahashi, and H. Kawaguchi, ''Analysis of transient interband light modulation by ultrashort pulses in semiconductor quantum wells,'' IEEE J. Quantum Electron. **QE-33** (1997) (in press).
[7] Y. Li and X. Xiao, Opt. Lett. **20**, 1489 (1995).
[8] A. Neogi and H. Kawaguchi, in *Technical Digest of the International Topical Meeting on Microwave Photonics* (MWP 96), Kyoto, Japan, 1996, p. 17.
[9] M. S. C. Luo, S. L. Chuang, P. C. M. Planken *et al.*, IEEE J. Quantum Electron. **QE-30**, 1478 (1994).
[10] A. Neogi, Opt. Commun. **133**, 479 (1997).

Published in English in the original Russian journal. Edited by Steve Torstveit.

Diffraction of the wave packet of a three-level Λ atom in the field of a multifrequency standing light wave

A. S. Pazgalev and Yu. V. Rozhdestvenskiĭ
S. I. Vavilov State Optics Institute 199034 St. Petersburg, Russia

(Submitted 21 July 1997; resubmitted 26 August 1997)
Pis'ma Zh. Éksp. Teor. Fiz. **66**, No. 6, 386–391 (25 September 1997)

The diffraction of the wave packet of a three-level atom in a multifrequency optical radiation field is studied. A new type of coherent beam splitter for atoms that employs the scattering of a wave packet in the field of four standing light waves with different spatial shifts is proposed on this basis. It is shown that this interaction scheme makes it possible to obtain large splittings ($>100\hbar k$) of the wave packet of a three-level Λ atom in momentum space into only two coherent components. In addition, the atoms in these coherent components are in long-lived atomic states, which substantially simplifies the experimental implementation of such a splitter. © *1997 American Institute of Physics.* [S0021-3640(97)00418-0]

PACS numbers: 42.79.Fm, 42.25.Fx, 03.75.Be, 03.75.Dg, 39.20.+q

In recent years atomic interferometry has emerged as a promising method for performing high-precision measurements in the detection of gravitational waves, and it is already being used for checking the fundamental principles of quantum theory, such as the principle of superposition, the possibility of instantaneous collapse of the wave function (Einstein–Podolsky–Rosen paradox), and the Aharonov–Bohm effect.[1]

It is well known that a coherent splitter of atomic wave packets (beam splitter) is the main component of an atomic interferometer.[1] The efficiency of such a splitter is characterized both by the magnitude of the splitting between the components into which the initial wave packet of the atom in momentum space is split and by the number of atoms contained in these coherent components.

At the present time, the beam-splitter based on the optical Kapitsa–Dirac effect has the highest efficiency — the coherent diffraction of a beam of two-level atoms in the field of two spatially-shifted standing light waves.[2,3] In this case, for a definite ratio of the Rabi frequency and the detunings of the standing waves the beam of atoms splits in momentum space into only two coherent components, and the fraction of the atoms contained in these two main peaks is comparable to the initial intensity of the atomic beam and remains practically unchanged as the splitting increases. However, such a splitter also has a fundamental drawback, since the atomic state in which the splitting occurs is a mixture of the lower (ground) and upper (excited) states of the system. This means that the lifetime of the interference state in which the atom enters (and exits) the region of interaction with the field is determined solely by the lifetime $\simeq 10^{-8}$ s of the excited state.

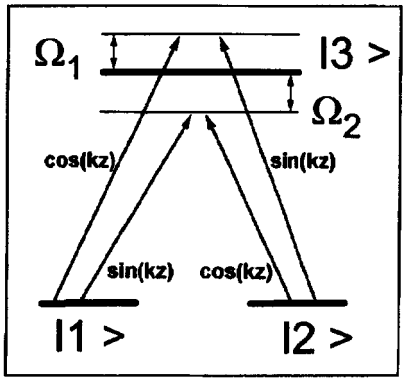

FIG. 1. Scheme of the interaction of a three-level atom with the field of four shifted standing light waves.

In the present letter we propose a new efficient beam splitter for atoms that is based on the optical Kapitsa–Dirac effect for a three-level atom interacting with the field of four spatially-shifted standing waves. We show that the efficiency of the proposed beam splitter equals that of a splitter based on the interaction of a two-level atom with the field of two spatially-shifted standing waves. In addition, for the proposed splitter there is no restriction on the size of the splitting, and the initial state required for unbounded scattering is a superposition of the long-lived lower states of the Λ system. This makes it possible to prepare without difficulty an atom in the appropriate state prior to its interaction with the optical field, and after interacting with the radiation field almost the entire atomic beam is in a long-lived state consisting of a superposition of the lower levels.

Let us consider the scattering of a three-level atom in the field of four standing waves with frequencies ω_m $(m=1,2,3,4)$:

$$\mathbf{E}=E_0[\mathbf{e}_1(\cos(k_1x)\exp(i\omega_1t)+\sin(k_2x)\exp(i\omega_2t)+\mathbf{e}_2(\sin(k_3x)\exp(i\omega_3t) + \cos(k_4x)\exp(i\omega_4t))]+\text{c.c.}, \tag{1}$$

where $\mathbf{e}_{1,2}$ are the polarization vectors and k_m are the wave numbers of the standing waves. It is convenient to represent the field (1) as two pairs of standing waves spatially shifted by $\pi/2$ so that each pair is symmetrically detuned relative to the upper excited level of the system (Fig. 1).

We shall assume that spontaneous relaxation does not occur in the system. In this case the translational dynamics of the wave packet of a three-level Λ atom in the field (1) can be described by a wave function of the form

$$\Psi(x,\xi,t)=\sum_i \tilde{a}_i(x,t)\psi_i(\xi)\exp\left(-\frac{i}{\hbar}E_mt\right), \tag{2}$$

where x is the coordinate of the center of mass of the atom (we are considering only motion along the x axis), ξ represents the coordinates of the internal motions, and E_m are the energies of the levels $(m=1,2,3)$. We underscore that in studying coherent scattering we shall be interested in the change in the momentum distribution of the atomic beam

along the x axis only. We also assume that all atoms, irrespective of their transverse momentum, traverses the interaction region over the same time T_{int}, which is the transit time of the beam of atoms through the interaction region.

Next, we write the Hamiltonian of our system in the form

$$\hat{H}=\hat{H}_0+\hat{V}\,\frac{1}{2M}\,\hat{P}^2, \tag{3}$$

where $\hat{H}$ corresponds to the internal states of the atom, the operator $\hat{V}$ describes the dipole interaction of the atom with the field (1), $(1/2M)\hat{P}^2$ is the kinetic energy operator of the atoms along the x axis, and M is the mass of the atom. Substituting the wave function (2) into the time-dependent Schrödinger equation, we obtain a system of equations for the nonstationary probability amplitudes $a_i(z,t)$ of the states of a three-level atom in the case of an interaction with the field (1):

$$i\frac{da_1}{dt}=-\frac{\hbar}{2M}\nabla^2 a_1+Gn(x,t)a_3, \quad i\frac{da_2}{dt}=-\frac{\hbar}{2M}\nabla^2 a_2+Gn^*(x,t)a_3,$$

$$i\frac{da_3}{dt}=-\frac{\hbar}{2M}\nabla^2 a_3+Gn^*(x,t)a_1+Gn(x,t)a_2, \tag{4}$$

where $n(x,t)=e^{i\Omega t}\cos(kx)+e^{-i\Omega t}\sin(kx)$, G are the Rabi frequencies of the standing waves, and $|\Omega|$ is the modulus of the frequency detuning. In Eq. (4) we also assumed that all the wave numbers of the standing waves are identical and equal to k.

We underscore that we are studying the case of coherent diffraction of an atomic wave packet. For this reason, the width of the spatial distribution of the atomic packet along the x axis must be much larger than the wavelength of the optical radiation ($\Delta x \gg \lambda$) or, equivalently, the width Δp_x of the distribution in momentum space should be much smaller than the momentum of an individual photon ($\Delta p_x \ll \hbar k$).

Switching in Eq. (4) to the momentum representation by means of the transformation

$$a_i(p,t)=\frac{1}{\sqrt{2\pi}}\int a_i(x,t)\exp(-ipx/\hbar)dx, \tag{5}$$

we obtain a system of equations for the nonstationary probability amplitudes $a_i(p,t)$:

$$\begin{aligned}
&ida_1(p)/dt=Rp^2a_1(p)+f(t)a_3(p-1)+g(t)a_3(p+1),\\
&ida_2(p)/dt=Rp^2a_2(p)+f^*(t)a_3(p+1)+g^*(t)a_3(p-1),\\
&ida_3(p)/dt=Rp^2a_3(p)+f^*(t)a_1(p+1)+g^*(t)a_1(p-1)+f(t)a_2(p-1)\\
&\qquad\qquad \times a_2(p+1),
\end{aligned} \tag{6}$$

where $f(t)=G(1-i)[\cos(\Omega t)-\sin(\Omega t)]/2$, $g(t)=G(1+i)[\cos(\Omega t)+\sin(\Omega t)]/2$, and $R=\hbar k^2/(2M)$ is the recoil frequency. In Eq. (6) we also normalized the momentum acquired by an atom to the momentum $\hbar k$ of an individual photon.

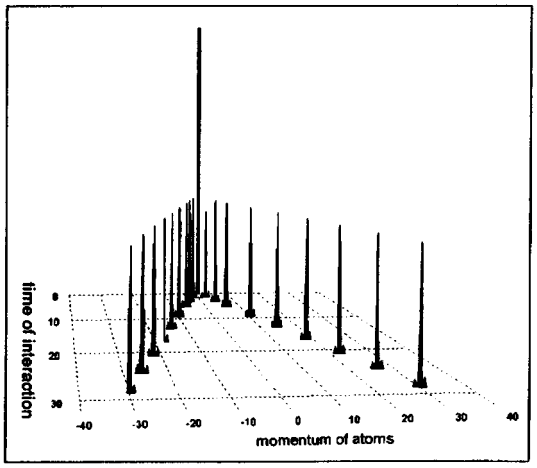

FIG. 2. Temporal evolution of the wave packet of a three-level atom in the field of four shifted standing waves (1) for a special value of the modulus of the frequency detuning $\Omega_{BS}=\sqrt{2/3}G$, where $G=10^7$ Hz. Initially the entire population is equally distributed between the lower states with a momentum distribution width of $0.25\hbar k$. One can see that over the interaction time $T_{\text{int}}=28.9$ (in units of the frequency detuning) a splitting of $60\hbar k$ is achieved mainly in two coherent components with a total intensity of the order of the initial intensity of the atomic beam.

The system of Eq. (6) for the nonstationary probability amplitudes completely determines both the internal and translational dynamics of a three-level Λ atom in the field (1). We underscore that in this case there exists a certain value of the modulus of the frequency detuning $\Omega_{BS}=\sqrt{2/3}G$ for which the atomic beam splits into only two coherent momentum components. A similar condition also holds in the case of the scattering of a two-level atom in the field of two spatially-shifted standing waves, in which case only two main components are present in the wave packet after the interaction.[2,3]

Figure 2 shows the scattering pattern obtained by solving Eq. (2) numerically in momentum space, neglecting the kinetic energy of the atoms and taking the special case of detuning $\Omega_{BS}=\sqrt{2/3}G$, for which the initial momentum distribution is a Gaussian with width $0.25\hbar k$ and the entire initial population is distributed equally between the lower states of the three-level atom. One can see that for the interaction times

$$T_{\text{int}}=(1/2,1,3/2\ldots)\,\pi/\Omega_{BS} \tag{7}$$

the atomic wave packet consists of mainly two coherent components with a total intensity in the peaks of the order of 80% of the initial value. The number of atoms in the coherent components remains unchanged as the interaction time of the atoms with the optical radiation field increases, and for the coherent interaction regime any arbitrarily large splitting between two coherent components of the beam can be obtained.

This can be explained physically by the fact that for our value of the modulus of the detuning of the standing waves the quasipotentials for the states of the three-level atom assume an almost triangular shape, as happened for the case of a two-level atom interacting with the field of two shifted standing waves.[2,3]

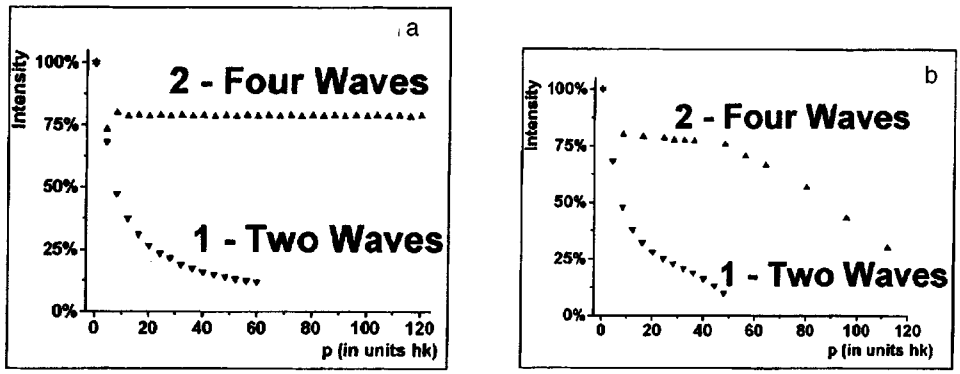

FIG. 3. a) Intensity of the coherent components versus the splitting for a three-level atom interacting with the field of both two (curve *1*) and four (curve *2*) standing light waves for the same values of the parameters as in Fig. 2. Note that for the case of the interaction of a three-level atom with the field of two standing waves the optimal (according to Refs. 4 and 5) detuning $\Delta_{bs}=\sqrt{1/3}G$ was chosen. b) Intensity of the coherent components versus the splitting with the change in the kinetic energy of the atoms taken into account. The recoil frequency $R=1/400G$; all other parameters are the same as in Fig. 2. Curve *1* corresponds to coherent scattering of a three-level atom in two standing waves, and curve *2* corresponds to coherent scattering in four standing waves.

We note that for interaction times $T_{\text{int}}=(N+1/2)\pi/\Omega_{BS}$ the coherent peak for negative momenta consists of atoms in the state *1*, while the coherent peak in the region of positive momenta consists of atoms in the state *2*. Conversely, for times $T_{\text{int}}=N\pi/\Omega_{BS}$ the coherent peak in the region of negative momenta consists of atoms in the state *2* and the other peak, lying in the region of positive momenta, consists of atoms in the state *1*. For interaction times different from (3), two coherent peaks, one of which consists of atoms in the state *1* (or *2*) and the other of atoms in the excited state *3*, are present in the regions of both negative and positive atomic velocities.

We underscore that in our case the character of the coherent scattering depends strongly on the initial state in which the Λ atom enters the region of interaction with the field of the standing waves (1), and an efficient beam splitter in a superposition of the lower (stable) states of a Λ atom (Fig. 1) can be obtained only for an initial state in the form of the superposition

$$a(p)=a_1(p)\pm a_2(p), \tag{8}$$

with $|a_1(p)|=|a_2(p)|$. If only one of the two lower states is populated initially, then after interacting with the field (1) the beam is deflected as a whole, as happened in the case of a two-level atom.[3]

The dependence of the intensity of the coherent components (we take into account the intensities of only the two main components of the scattered beam) on the magnitude of the splitting of the wave packet of a three-level atom accompanying the interaction with the field of both two and four shifted standing waves is shown in Fig. 3a. One can see that the proposed splitter for wave packets is much more efficient than the splitter based on the interaction of a three-level atom with the field of two spatially shifted standing waves. We note that in the latter case several coherent components with com-

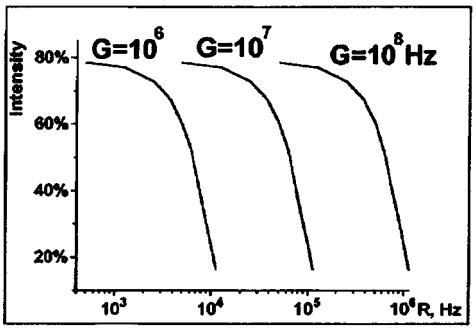

FIG. 4. Total intensity of the two main coherent components as a function of the recoil frequency for splitting equal to $100\hbar k$. The numbers on the curves correspond to different values of the Rabi frequency.

parable intensities are already present in the scattering of a wave packet for a splitting on the scale of $50\hbar k$. This makes it difficult to estimate the efficiency of such a splitter for large splittings. In order for the split peaks to form rapidly, just as in order to obtain a large splitting, it is desirable to employ high saturations of the atomic transitions. However, this results in a large population of the excited state of the system and decreases the coherently scattered part of the atomic population.

Let us examine the effect of recoil on the character of the coherent scattering of the wave packet of a three-level atom accompanying the absorption (or emission) of a photon. It is well known that in the general case of the scattering of atomic wave packets in the field of standing waves, taking the kinetic energy of the atoms into account results in both a limit on the magnitude of the splitting of a wave packet on the velocity scale and to dephasing of coherent components with different momenta. This lowers the overall efficiency of the coherent splitter. The decrease becomes especially noticeable when the splitting is large.

The maximum intensity of the coherent components as a function of the momentum transfer, with allowance for the change in the kinetic energy of the atoms, is shown in Fig. 3b. One can see the for a recoil frequency $R=\hbar k^2/(2M)=1/400$ (in units of the Rabi frequency) the maximum intensity of the coherent components decreases somewhat. However, for the case of the interaction of a three-level atom with the field of four standing waves (curve *2*) the scattering efficiency once again remains high compared with the case of two spatially-shifted standing waves (curve *1*), as was the case when recoil effects were neglected. Once again, these features in the scattering are due to the fact that for our frequency detuning the quasipotential for the states of a three-level atom acquires an almost triangular form. As was noted in Ref. 3, the form of the potential determines the possibility of obtaining a large splitting and preserves the regime in which scattering into only two coherent components occurs, which strongly distinguishes the realization of the Kapitsa–Dirac effect in shifted standing waves from the same effect in the field of in-phase standing waves.

Figure 4 shows the intensity in the two main coherent components versus the recoil energy for a splitting of $48\hbar k$ between these components and different Rabi frequencies

of the standing waves. One can see that as the recoil energy increases, the number of atoms scattered in the two main components decreases. However, even for quite high recoil frequencies (corresponding to elements with a low atomic weight and short-wavelength transitions in the optical region of the spectrum) it is possible to obtain a splitting of $48\hbar k$. After the interaction the wave packet once again has two main components with a total intensity of about 50% of the initial value.

In summary, we have shown that the interaction scheme examined above for a three-level atom interacting with the field of four shifted standing waves (1) produces a splitting of the atomic wave packet into practically only two coherent components consisting of atoms in the lower (stable) states. The magnitude of the splitting between these components is limited only by the interaction time of the atoms with the optical radiation field. This offers the hope that splittings much larger than $100\hbar k$ can be realized experimentally.

We thank the Russian Fund for Fundamental Research for financial support of this work (Grant No. 15500-625-97).

[1] *Optics and Interferometry with Atoms* (special issues), Appl. Phys. **54**, 319 (1992); J. Phys. (Paris) **4**, No. 11 (1994); Quantum Semiclassic. Opt. **8** (1996).
[2] R. Grimm, J. Soding, and Yu. Ovchinnikov, Opt. Lett. **19**, 658 (1994).
[3] S. M. Tan and D. F. Walls, Opt. Commun. **118**, 412 (1995).
[4] K. Johnson, I. D. Paul, A. Chu *et al.*, in *International Conference on Quantum Electronics 1994* (IQEC'94), QTuC4, p. 35.
[5] K. S. Johnson, A. Chu, T. W. Lynn *et al.*, Opt. Lett. **20**, 1310 (1995).

Translated M. E. Alferieff

Anomalous heating of a system of dust particles in a gas-discharge plasma

V. V. Zhakhovskiĭ,[a] V. I. Molotkov,[b] A. P. Nefedov, V. M. Torchinskiĭ, A. G. Khrapak, and V. E. Fortov

Scientific-Research Center for the Thermophysics of Pulsed Actions, Russian Academy of Sciences, 127412 Moscow, Russia

(Submitted 7 August 1997)
Pis'ma Zh. Éksp. Teor. Fiz. **66**, No. 6, 392–397 (25 September 1997)

The coexistence of regions of negatively charged macroparticles with substantially different kinetic temperatures in a highly nonideal dusty plasma in a dc glow discharge has been observed experimentally. An explanation of the observed anomalous heating of the system of dust particles in a gas-discharge plasma is proposed on the basis of a molecular-dynamics model. © *1997 American Institute of Physics.* [S0021-3640(97)00518-5]

PACS numbers: 52.80.−s, 52.50.−b

The interest shown in the properties of dusty plasma is largely due to the recent discovery that ordered structures of charged macroparticles form in different types of laboratory plasmas: in the cathode region of an rf gas discharge,[1–4] in thermal plasmas,[5,6] and in standing striations of a glow discharge.[7,8] Dust crystals possess a number of unique properties: They are optically transparent, the size of the dust particles equals 1–100 μm, and the intersite separation in a crystal equals 100–1000 μm, which makes it possible to study the properties of the crystals in beams of visible light with the unaided eye; the characteristic relaxation times equal fractions of a second, which advantageously distinguishes plasma crystals from colloidal crystals, where these times reach several days; and, the parameters of quasicrystalline structures can be changed simply by changing the gas pressure or the current or power in the discharge. For this reason, dust crystals are an effective tool for investigating the properties of highly nonideal plasmas, the fundamental properties of crystals, and the properties of gas discharges. Interesting experimental results have now been obtained on polymorphic phase transitions between different crystalline structures, the melting of dust crystals, and the propagation of sound waves in plasma crystals. Theoretical investigations of charging of dust particles, the interaction of dust particles with one another and with external fields, and collective effects in highly nonideal dusty plasmas are being actively pursued. A discussion of these questions is contained in recently published reviews.[9–11]

An anomalous increase in the kinetic temperature of macroscopic particles due to their chaotic translational motion has been observed in an investigation of the melting of quasicrystalline plasma structures.[8,9,12,13] Until very recently it was ordinarily assumed that the kinetic temperature of dust particles can be only slightly higher than the temperature of the ionic and neutral components of a gas-discharge plasma $T \approx 300$ K. However, measurements of the velocity distribution function of the dust particles in an rf

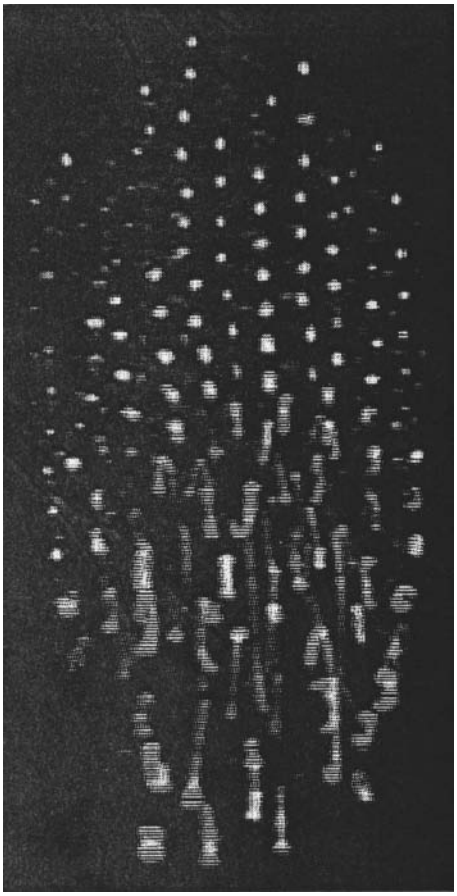

FIG. 1. Video image of a vertical section of a structure consisting of dust particles. Discharge in neon at a pressure of 0.35 torr with a discharge current of 0.5 mA. Frame size — 4.6×9.0 mm.

discharge showed that as the pressure in the discharge decreases or the current increases, changes which are accompanied by a loss of long-range order in a dust crystal, the kinetic temperature of the particles can increase by hundreds[9,12] or even thousands[13] of times.

In the present work we performed experiments which attest to the growth of the kinetic energy of macroparticles in a dusty plasma in a dc glow discharge in neon. We offer below a theoretical interpretation of the results obtained. The experimental arrangement was virtually identical to the one we used previously.[7,8] Quasicrystalline structures formed in standing striations in a low-pressure discharge in a cylindrical glass tube (inner diameter 3 cm) with cold electrodes. Figure 1 shows a video frame showing an image of a structure (cloud) consisting of negatively charged (charge $\sim 10^4 e$), monodisperse (diameter 10.24 ± 0.12 μm) microspheres of melamine formaldehyde ($\rho = 1.5$ g/cm^3). The exposure time was 10^{-2} s. The structure was made visible by illuminating with a probe laser beam in a vertical plane. A characteristic feature of the formation shown is that two states of the subsystem of charged macroparticles coexist: A region with a well-ordered

structure (''plasma crystal'') is seen at the top of the photograph, and extended (up to 1000 μm long) tracks made by oscillating particles can be seen at the bottom. Analysis of successive video images shows that the characteristic displacements of the particles in the top part equal about 100 μm over a time of 0.04 sec, while at the bottom the maximum displacement of the particles over 10^{-2} sec equals about 1000 μm. Therefore the particle velocities in these two regions differ by approximately a factor of 40 and the corresponding kinetic temperatures by more than a factor of 10^3. The maximum kinetic temperature of the particles at the bottom of the cloud reaches 2.4×10^3 eV. We note that the coexistence of regions with strongly different temperatures has not been observed in dusty plasmas in rf discharges.[9,12,13]

Before undertaking a theoretical analysis and a simulation of the observed anomalous heating of a dusty plasma, we shall briefly discuss the main characteristics of the potential trap produced for charged dust particles by the electrostatic fields of the striations and walls of the discharge tube as well as by the force of gravity. Striations in a low-pressure discharge have been studied quite well experimentally.[14,15] The energy losses by electrons in elastic collisions in the positive column of the discharge under the conditions of interest to us are negligibly small, and the electron distribution function is formed by the electric field and inelastic collisions. This can give rise to striations — spatial periodicity of the plasma parameters with a characteristic scale of the order of several centimeters. The electron density, the electron energy distribution, and the electric field are highly nonuniform in the direction along the striations. The electric field is relatively strong at the head of a striation (the maximum value equals about 10–15 V/cm) — a region occupying 25–30% of the length of a striation — and weak (approximately 1 V/cm) outside this region. The maximum electron density is shifted relative to the maximum field strength in the direction of the anode.[15] The electron energy distribution is strongly bimodal,[15] the second maximum, whose center lies near the excitation potential ε_1, being predominant at the head of a striation. On account of the high floating potential of the walls of the discharge tube, the striations are strongly two-dimensional: The center-to-wall potential difference reaches 20–30 V at the head of a striation. Therefore an electrostatic trap is present at the head of each striation. When oriented vertically, such a trap is capable of preventing particles with a sufficiently large charge and small mass from falling to the bottom, and the strong radial field prevents the particles from settling on the wall of the discharge tube. The charge on the dust particles is proportional to the floating potential of the plasma, which in turn is proportional to the local electron energy. For this reason, as a result of the appreciable variation in the floating potential, following from the observed variation of the wall potential in the direction along a striation,[15] the charge on the particles depends on the height. This is possible because the subsystem of dust particles is not closed and can exchange charge and energy with the gas-discharge plasma. It is easy to show that the energy of a dust particle moving along a closed contour may not be conserved. This is the main reason for the anomalous heating of the subsystem of dust particles on account of the energy supplied by an external source.

Let us consider a system of $N\gg 1$ charged dust particles in a glow-discharge plasma. We shall assume that the charge $q_i=q_i(z)$ on the ith particle is a bounded function of the

z coordinate of the particle and that the interparticle interaction is determined by the screened Coulomb force

$$f_{ij}=\frac{q_i(z_i)q_j(z_j)}{r_{ij}^2}D(\mathbf{r}_i,\mathbf{r}_j), \tag{1}$$

where $D(\mathbf{r}_i,\mathbf{r}_j)$ is the screening function. It is easily verified that the interaction (1) is not derivable from a potential (for example, by considering the work performed by a dust particle moving along a closed trajectory in the field of a different, stationary dust particle). In other words, the system of dust particles is not a closed system. Furthermore, the gas exerts on the particles a friction force $f_i=-\beta v_i$, where β is the coefficient of friction.

Experiments and computer simulation show that the system of dust particles can be in a stationary state at some temperature T, but this state is not in equilibrium with the state of the surrounding gas with temperature T_g, and $T\gg T_g$.

As a very simple model of this phenomenon, let us consider one particle with charge $q=q(z)=1+1/(z^2+1)$ moving in the (y,z) plane and in the electric potential $\phi=(y^2+z^2)/2$. Then the vector field of the forces $F_y=-q(z)y$ and $F_z=-q(z)z$ will not be a potential field, because $\nabla\times\mathbf{F}\neq 0$. Furthermore, as calculations show, for almost any initial conditions the kinetic energy of the particle grows with time as $\sim t^2$, on the average, with the exception of cases when the initial velocity is directed in the radial direction. When friction is included in this model, the particle loses all of its energy for any friction coefficient >0. For a larger number of particles (>2) interacting via Coulomb forces, there arise stationary states in which the particles have some average kinetic energy, and a balance is maintained between energy losses due to friction and the energy acquired during motion in a nonpotential force field. Calculations of the dynamics of this system showed the following: 1) There exists a maximum coefficient of friction β_m for which only one stationary state is realized asymptotically; on account of its ordered nature, we shall call this state crystal-like; 2) if $\beta<\beta_m$ then only two stationary states with substantially different kinetic energies and spatial configurations — ordered and disordered (liquid-like) states — are realized in the limit $t\to\infty$. The crystal- and liquid-like phases form depending on the energy of the initial state and cannot coexist in a region of space where $q\neq$ const. As will be shown below, these conclusions remain valid for a more complicated model which reproduces the main features of a real experiment.

We attempted to develop an analytical approach to this problem. Let the test charge q be located at the origin of the coordinate system inside a stationary system of charged dust particles. On account of the stationary character of the problem the charges of the dust particles can be represented in the form $q_i(z_i(t))=\overline{q_i}+\delta q_i(z_i(t))$, where $\overline{q_i}$ is the average charge on the ith dust particle ($\overline{q_i}=\overline{q_j}=q$) and $\delta q_i(t)$ is the fluctuational variation in the charge on the particle. Then the force acting on the test charge can be written as

$$f=q\sum_{i=1}^{N}\frac{\overline{q_i}+\delta q_i(t)}{r_i^2}D(r_i)=\sum_{i=1}^{N}\frac{q^2}{r_i^2}D(r_i)+\sum_{i=1}^{N}\frac{q\,\delta q_i(t)}{r_i^2}D(r_i). \tag{2}$$

As indicated above, the second sum in Eq. (2) is not derivable from a potential, and for this reason it can serve as a source of additional heating, while the first sum of forces is a potential function and does not result in heating of the system of dust particles. On account of the extreme complexity and entanglement of the motion of the dust particles, we shall represent the second sum in Eq. (2) as a random force $R(t)$. We shall assume that $R(t)$ has a Gaussian distribution with $\overline{R(t)}=0$, autocorrelation function $\overline{R(t_1)R(t_2)}=g(t_2-t_1)$, and correlation time $\tau=\int_0^\infty g(t)dt/\overline{R^2}$. Then the ith dust particle is acted on, in addition to the potential force, by a random Langevin force

$$f_i=R(t)-\beta v_i. \tag{3}$$

It should be noted that a similar replacement of the potential part in expression (2) by a random force would require the introduction of a friction correlated with this force in order to compensate the energy fluctuations. Therefore the effect of the potential forces on the heating can be neglected.

The relation between the parameters of the Langevin force (3) and the temperature of the system is well known:[16]

$$k_BT=\overline{R^2}\tau/\beta. \tag{4}$$

To estimate the variance $\overline{R^2}$ of the random force, neglecting screening, we shall use the relation

$$\overline{R^2}\sim q^2\overline{\delta q^2}/\overline{r^4},$$

where $\overline{r}$ is the average interparticle distance and $\overline{\delta q^2}$ is the mean-square fluctuation of the charge. Then

$$k_BT\sim q^2\overline{\delta q^2}\tau/\beta\overline{r^4}. \tag{5}$$

It is easy to see that the mean-square fluctuation $\overline{\delta q^2}$ of the charge on the dust particles depends sharply on the gradient of the function $q(z)$ and the phase state of the system. It is much smaller in the crystal-like phase than in the liquid-like phase, as a result of which, according to Eq. (5), a sharp increase in temperature occurs on melting. Figure 1 can serve as an illustration of this effect.

We performed a molecular-dynamics (MD) simulation of a system of charged dust particles in a glow-discharge plasma. The parameters of the electric fields were chosen to be close to the experimentally measured values.[15] The walls of a cylindrical tube of radius $R_t=15$ mm create at a dust particle the potential $\phi_w=\phi_t(r/R_t)^{3/2}$, where $r^2=x^2+y^2$ and $\phi_t=10+20/(1+((z-z_0)/d_w)^2)$ is the potential (in volts) on the walls of the tube, $z_0=0.8$ mm, and $d_w=4$ mm. The charge on the dust particles was given by the relation $q=R_d\phi_t$. The interaction of the dust particles was determined, according to Eq. (1), for a Debye screening function with a Debye radius $r_d=0.488$ mm. A dust particle was subjected along the z axis to gravity and a lifting potential $\phi_z=14/(1+(z/d_z)^2)$, where $d_z=1$ mm. The buffer gas exerted on a dust particle a friction force and a fluctuating force $\xi(t)$ satisfying the condition $\langle\xi^2\rangle=2\beta T_g/\Delta t$, where Δt is the integration step in time. The coefficient of friction β was determined for neon at a pressure of 0.1 torr and $T_g=300$ K. The method of Ref. 17 was used to integrate the equations of motion. The

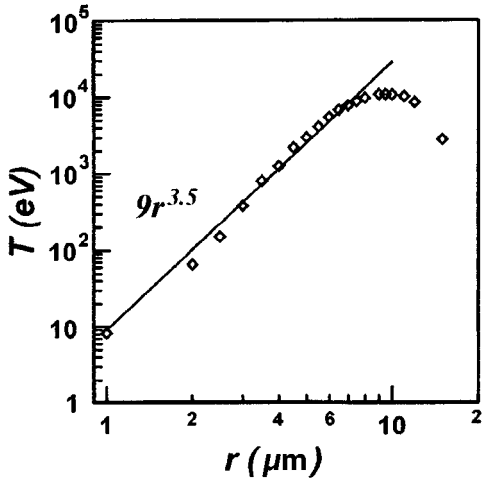

FIG. 2. Kinetic temperature of a system of dust particles versus the particle radius.

number of dust particles varied from 1 to 8000. Figure 2 displays the MD results for the temperature of a system consisting of 500 dust particles as a function of their radius for constant values of the striation parameters described above. It should be noted that on account of the Debye character of the interaction the average distance between the dust particles varied very little (0.55–0.6 mm).

If it is assumed that the charge on a dust particle and the fluctuation of this charge are proportional to the radius of the particle (which is close to what is observed in a MD experiment), $\beta \sim R_d^2$ in the free-molecular regime, and the correlation time $\tau \sim \sqrt{M_d} \sim R_d^{3/2}$, then

$$T \sim R_d^{7/2}. \tag{6}$$

Relation (6) approximates satisfactorily the MD calculation in the region where the dust cloud occupies the entire region of charge exchange on the particles.

In conclusion, we note that our MD simulation of a system of charged dust particles of different size reproduces the experimentally observed parameters: the characteristic size of a structure consisting of particles, the average interparticle distance, and the saturation of the electrostatic trap by particles. Linear structures (chains) consisting of a small number (up to 10) of particles were also reproduced. The model developed showed that, just as in the experiments, anomalous heating of macroparticles occurs. It was found that the heating of a system of dust particles is due to the height dependence of the charges on the particles and also to the variability of the Debye radius in the screening function D in Eq. (1). In our view, these effects are manifested not only in a dc glow discharge but also in an rf plasma on account of the nonuniformity of the electrical field and electron density in the layer at the electrode.

We thank V. S. Filinov for some stimulating discussions. This work was performed under the partial support of the Russian Fund for Fundamental Research (Grant No. 95-02-0645) and INTAS-RFBR (Grant No. 95-1335).

[a)]e-mail: basil@landau.ac.ru
[b)]e-mail: molotkov@hedric.msk.su

[1] J. H. Chu and I. Lin, Phys. Rev. Lett. **72**, 4009 (1994).
[2] H. Thomas, G. E. Morfill, V. Demmel *et al.*, Phys. Rev. Lett. **73**, 652 (1994).
[3] A. Melzer, T. Trottenberg, and A. Piel, Phys. Lett. A **191**, 301 (1994).
[4] Y. Hayashi and K. Tachibana, Jpn. J. Appl. Phys., Part 2 **33**, L804 (1994).
[5] V. E. Fortov, A. P. Nefedov, O. F. Petrov *et al.*, JETP Lett. **63**, 187 (1996).
[6] V. E. Fortov, A. P. Nefedov, O. F. Petrov *et al.*, Phys. Lett. A **219**, 89 (1996).
[7] V. E. Fortov, A. P. Nefedov, V. M. Torchinskiĭ *et al.*, JETP Lett. **64**, 92 (1996).
[8] V. E. Fortov, A. P. Nefedov, V. M. Torchinsky *et al.*, Phys. Lett. A **229**, 317 (1997).
[9] H. M. Thomas and G. E. Morfill, Nature **379**, 806 (1996).
[10] V. N. Tsytovich, Usp. Fiz. Nauk **167**, 57 (1997).
[11] A. P. Nefedov, O. F. Petrov, and V. E. Fortov, Usp. Fiz. Nauk **167**, No. 9 (1997).
[12] J. B. Pieper and J. Goree, Phys. Rev. Lett. **77**, 3137 (1996).
[13] A. Melzer, A. Homann, and A. Piel, Phys. Rev. E **53**, 2757 (1996).
[14] Yu. P. Raĭzer, *Gas Discharge Physics* [in Russian], Nauka, Moscow, 1987.
[15] Yu. B. Golubovskiĭ and S. U. Nisimov, Zh. Tekh. Fiz. **66**(7), 20 (1996) [Tech. Phys. **41**, 645 (1996)].
[16] D. W. Heerman, *Computer Simulation Methods in Theoretical Physics*, Springer-Verlag, New York, 1986.
[17] V. V. Zhakhovskiĭ and S. I. Anisimov, Zh. Éksp. Teor. Fiz. **111**, 1328 (1997) [JETP **84**, 734 (1997)].

Translated by M. E. Alferieff

Generation of mesoscopic magnetic structures by local laser action

A. S. Logginov,[a] A. V. Nikolaev, V. N. Onishchuk, and P. A. Polyakov
M. V. Lomonosov Moscow State University, 119899 Moscow, Russia

(Submitted 22 July 1997)
Pis'ma Zh. Éksp. Teor. Fiz. **66**, No. 6, 398–402 (25 September 1997)

New effects are observed wherein the internal structure of the domain walls in a thin magnetic iron garnet film are modified by the action of focused laser radiation. A single laser pulse with increasing power gives rise to the following: 1) displacement of vertical Bloch lines in a domain wall; 2) generation of a pair of vertical Bloch lines on initially line-free walls; and, 3) an irreversible change in shape of a domain wall and the domain structure as a whole. The mechanism leading to the generation and displacement of Bloch lines is connected with the motion of domain walls which is induced by a local change in the distribution of demagnetizing fields as a result of a heating-induced decrease of the magnetization in the focal spot of the laser radiation. © *1997 American Institute of Physics.* [S0021-3640(97)00618-X]

PACS numbers: 75.70.Kw, 75.50.Gg

The search for new physical mechanisms and materials whose parameters can be changed at the submicron level by optical action is arousing great interest in connection with possible applications in memory devices with optical and thermomagnetic writing of information.

The present letter reports the generation and driving of vertical Bloch lines (VBLs) in domain walls (DWs) of a thin magnetic iron garnet film as a result of the action of focused laser radiation. The VBLs are stable magnetic vortices separating sections of a domain wall with opposite polarity.[1] The Bloch lines are characteristically a fraction of a micron in size and are mesoscopic objects.

The experiment was arranged as follows. The radiation from an LGI-21 pulsed nitrogen laser with wavelength $\lambda \simeq 337$ nm was converted by rhodamine 6 G dye into radiation with wavelength $\lambda \simeq 540$ nm and focused on the sample by an objective lens with a numerical aperture of 0.2. The diameter of the focused beam was equal to approximately 4 μm. The sample consisted of a $\langle 111 \rangle$ iron garnet film with the composition $(BiTm)_3(FeGa)_5O_{12}$ and the following parameters: $4\pi M_s = 173$ G; $H_{col} = 126$ Oe; period of the equilibrium stripe structure 8.5 μm; film thickness 7.5 μm; and, $Q = 3.8$. The duration of the laser pulse was equal to ~ 10 ns and the pulse was nearly Gaussian. The maximum energy of the light pulse re-emitted by the dye and striking the sample was $W_{max} \sim 10^{-6}$ J (with an instability of approximately 15%).

The state of the domain structure was monitored by one-sided dark-field illumination, which made it possible to observe domain walls and the VBLs contained in them.[2]

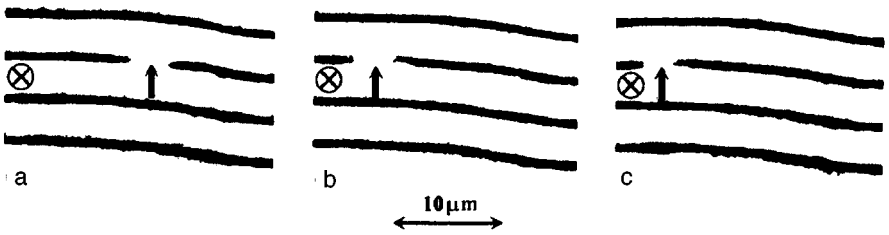

FIG. 1. Displacement of a VBL under the action of laser radiation: a — Initial position; b, c — displacement of a VBL accompanying the successive application of two single laser pulses. The symbol ⊗ shows the location of the focal spot of the laser beam; the arrows mark the VBL. The images were obtained in a one-sided dark field; the contrast is reversed.

In this method the domain walls appear to be light-colored lines against a dark background, and a local decrease or increase in the DW brightness corresponds to Bloch lines (see Fig. 2 below; the VBLs are marked by arrows). In the experiment an LGI-21 laser in a dark-field setup[3] was used to act on the domain structure and as a source of dark-field illumination.

The experiments were performed on a equilibrium stripe domain structure obtained by demagnetizing a sample from a single-domain state in the presence of a constant in-plane magnetic field. This gave a perfect lattice of stripe domains with VBL-free walls.

The following procedure was used. The initial image of the domain walls and vertical Bloch lines was recorded with a video camera, which was connected to a computer, by the method of one-sided dark-field illumination. Next, a single laser pulse with fixed power was generated and the resulting change in the structure of the domain wall was once again checked by dark-field observation. No external magnetic fields were applied.

It was found that three different physical phenomena are observed, depending on the energy W of the laser radiation.

1. Vertical Bloch lines start to move under the influence of a pulse with $W<0.2W_{\max}$ (VBLs which were specially introduced beforehand into the domain walls and located $\sim$10–15 μm from the focal spot). The initial pattern is displayed in Fig. 1a. The arrows mark VBLs; the crosses enclosed in a circle show the spot where the beam was focused. Figures 1b and 1c show the result of the successive action of two individual laser pulses. It should be noted that the motion of the Bloch lines is unstable and the lines do not always move toward the beam. The displacement of VBLs is noted both at the wall closest to the focused beam and on neighboring walls.

2. When the energy increases up to $W\simeq 0.2W_{\max}$, a single laser pulse gives generates a pair of vertical Bloch lines on initially VBL-free walls. Figure 2 shows typical images obtained after the action of a pulse. The location of the focal spot of the laser beam is marked by a cross enclosed in a circle. As one can see, regions of altered contrast are formed in the walls. These regions correspond to pairs of VBLs. With respect to their image in a one-sided dark field and with respect to the dynamic response to an in-plane

field pulse and a bias field pulse they are identical to the lines generated in a DW by the standard method — the motion of a wall with a velocity higher than a critical value.[1] Convergence of the generated pairs (for example, with the aid of in-plane field pulses along the wall) results in their annihilation. Hence it follows that the pairs are not twisted.[1]

The generation of VBLs is of a statistical character and occurs with probability increasing from ~ 0.1 for $W \simeq 0.2 W_{\max}$ up to ~ 0.9 for $W \simeq 0.24 W_{\max}$. The location of a pair on a domain wall as well as the distance between the constituent individual Bloch lines in the wall can vary from pulse to pulse, other parameters being fixed.

3. As the energy increases further, $W > 0.25 W_{\max}$, in addition to generation of VBLs an irreversible modification of the domain structure is observed to occur next to the focal spot of the laser beam and consists of a bending of the DW. A local disequilibrium of the array of stripe domains as well as an appreciable pinning of the wall at this location attest to the appearance of a defect in the magnetic film. The formation of a defect is most likely due to local heating of the sample by the laser radiation.

In our opinion, the heating action of a light pulse, and not some photomagnetic effects (observed as a direct influence of the electromagnetic field of a light wave on the magnetic system of the sample), is the physical reason for both the generation effects described above and the driving of the VBL.

To check this conjecture and to determine the mechanism leading to the generation of Bloch lines, the dynamics of a domain structure after the application of a laser pulse was studied by means of high-speed photography[4] in real-time. The LGI-21 laser radiation power corresponded to the conditions for generation of Bloch lines. A semiconductor injection laser with wavelength $\lambda \simeq 670$ nm was used as the source of illumination for the high-speed photography. The domain structure was illuminated by the semiconductor laser radiation in a direct-illumination optical geometry (using the Faraday effect) with crossed polarizers at fixed moments in time following the generation of a pulse from the LGI-21 laser. The semiconductor laser pulse had a duration of the order of 30 ns. This made it possible to obtain the instantaneous configuration of the domain structure perturbed by the focused light pulse and to follow the evolution of this perturbation in time. As one can see in the photographs presented in Fig. 3, a dark region appears at the location of the focal spot of the laser beam after the beam is applied. The bending grows most rapidly during the first 50 ns after the LGI-21 pulse, being mostly formed by 100 ns (Fig. 3b). It subsequently evolves slowly (Figs. 3c and d) and relaxes to the initial state within 1500–2000 ns simultaneously with the disappearance of the dark region.

The experimental results can be explained on the basis of the following qualitative model. The dark region recorded in the photographs corresponds to a section of the sample with decreased Faraday rotation. The decrease in the Faraday rotation is caused by a large local decrease of the saturation magnetization of the film (and possibly also by a transition into a paramagnetic phase) on account of the laser heating. The change in the magnetization of a local section during heating and subsequent cooling changes substantially the distribution of the demagnetizing fields in this region. This change gives rise to a displacement of nearby domain walls. As is well known, when the velocity of a moving wall exceeds a critical value, a horizontal Bloch line (HBL), breaking through to the

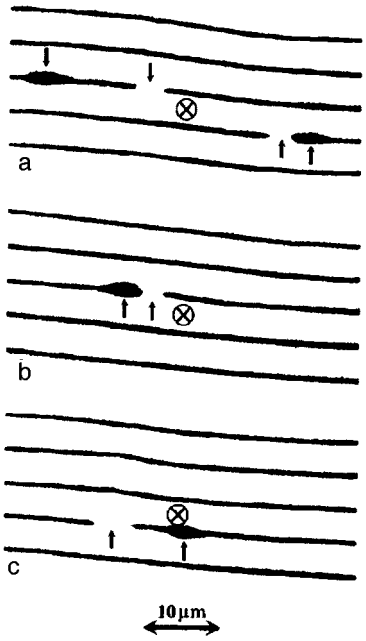

FIG. 2. Typical images of Bloch lines generated in domain walls by the action of a laser pulse. The symbol ⊗ shows the location of the focal spot of the laser beam; the VBLs are marked by arrows. The photographs were obtained in a one-sided dark field; the contrast is reversed.

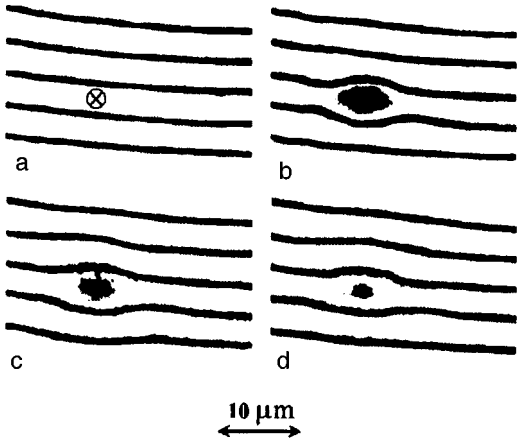

FIG. 3. Instantaneous dynamic configurations of a domain structure at different moments in time after the application of a focused LGI-21 laser pulse. The images were obtained (a) before the pulse (the symbol ⊗ shows the location of the focal spot of the laser beam) and at delays of (b) 100 ns, (c) 300 ns, and (d) 1000 ns after the action of the pulse.

surface of the magnetic film with the formation of a pair of VBLs, is generated in the wall.[1] If the velocity of the DW is lower than the critical value, this can result in driving of the Bloch lines.

One can see from the experimental results obtained with high-speed photography that the velocity of the wall is highest during the first several tens of nanoseconds after the application of the LGI-21 pulse, i.e., during the heating of the magnetic film. An estimate shows that the DW velocity can reach 15–20 m/s. This approximately corresponds to the critical velocity of a wall, as measured for the given sample in the case of a DW moving in a uniform pulsed bias field, which was $\sim$30 m/s. Therefore in the case of the motion of a wall after the laser pulse it can be expected that HBL loops will be generated in the wall and will break through, resulting in the formation of VBLs.

The process of generation of Bloch lines described above demonstrates that a submicron-size magnetic bit of information (in the form of a VBL) can in principle be written optically with a laser beam focused into a region of substantial size. In contrast to the standard thermomagnetic writing technique,[5] in which a bit of information is a domain and the size of the domain is determined mainly by the diameter of the focused laser beam (which requires special methods to decrease the size of the recorded domain to fractions of a micron[6]), in our case the size of a bit is determined by its physical nature as a mesoscopic object inside a domain wall and not by the characteristic size of the writing instrument.

This work was performed with the support of the Russian Fund for Fundamental Research under Grant No. 97-02-17788.

[a)]e-mail: asl@osc.phys.msu.su

---

[1] A. P. Malozemoff and J. C. Slonczewski, *Magnetic Domain Walls in Bubble Materials*, Academic Press, New York, 1979 [Russian translation, Mir, Moscow, 1982].
[2] A. Thiaville, J. Ben Youssef, Y. Nakatani *et al.*, J. Appl. Phys. **69**, 6090 (1991).
[3] A. S. Logginov, A. V. Nikolaev, and V. V. Dobrovitski, IEEE Trans. Magn. **29**, 2590 (1993).
[4] L. P. Ivanov, A. S. Logginov, and G. A. Nepokoĭchitskiĭ, Zh. Éksp. Teor. Fiz. **84**, 1006 (1983) [Sov. Phys. JETP **57**, 583 (1983)].
[5] M. Marsuripur, *The Physical Principles of Magneto-Optical Recording*, Cambridge University Press, New York, 1995.
[6] T. Suzuki, MRS Bull. **21**, 42 (1996).

Translated by M. E. Alferieff

Hall resistance anomalies induced by a radiation field

E. N. Bulgakov
Kirensky Institute of Physics, 660036 Krasnoyarsk, Russia

A. F. Sadreev[a)]
Krasnoyarsk State Technical University, 660036 Krasnoyarsk, Russia

(Submitted 11 August 1997)
Pis'ma Zh. Éksp. Teor. Fiz. **66**, No. 6, 403–408 (25 September 1997)

A study is made of the four-terminal Hall junction under the influence of a radiation field. The frequency of the radiation field is tuned to a transition between the energy of a bound state below a conduction subband and the Fermi energy of the incident electrons. Radiation-field-induced resonant dips of the Hall resistance are exhibited at low magnetic fields. © *1997 American Institute of Physics.* [S0021-3640(97)00718-4]

PACS numbers: 72.20.My, 73.20.Dx

For several decades the transport of electrons in structures of low dimensionality and complicated geometry has been the focus of extensive theoretical and experimental study. Electrons can be confined to very narrow regions fabricated on an interface of an AlGaAs/GaAs heterostructure. Since the electrons in such regions can have high mobilities in the two dimensions available to them, such systems are called two-dimensional electron gases (2DEGs). The study of electronic transport properties of 2DEGs is of great current interest not only from the standpoint of the basic quantum effects involved but also for potential engineering applications. An idealized sample becomes an electron waveguide, wherein the quantum transport properties are solely determined by the geometry of the structure and the wavelike nature of the electrons. A remarkable manifestation of the successful achievement of quantum ballistic transport through a semiconductor nanostructure is the observation of quantized steps on the conductance through a narrow structure as the number of one-dimensional channels is successively varied,[1,2] the quenching of the Hall effect, and the last plateau and the negative bend resistance in the cross geometry.[3–5]

Ford *et al.*[5] presented a systematic investigation of the influence of cross geometry on the Hall effect. They fabricated various differently shaped cross sections based on GaAs–$Al_xGa_{1-x}As$, which demonstrated that near zero magnetic field the Hall resistance can be quenched, enhanced over its classical value, or even negative. This effect has been considered in detail theoretically by Schult *et al.*[6] and Amemiya and Kawamura.[7] The aim of the present article is to demonstrate similar effects induced by a radiation field which is assumed to be resonant with the energy of a transition between a bound state of the cross section and the Fermi energy of the incident electron state. The radiation field mixes the localized bound state to the propagating wave functions and changes the quantum mechanical interference within the cross section. Therefore the application of a

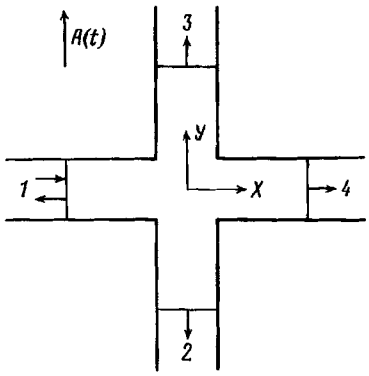

FIG. 1. Schematic representation of a four-terminal Hall junction. A static magnetic field is applied normal to the plane of the junction. The input and output wave functions are shown by arrows. The solutions are to be matched across the boundaries shown by fine lines.

radiation field to a Hall junction is similar to a variation of the geometry of the junction.

The bound states in a four-terminal junction of narrow wires have been found independently by Schult *et al.*[6] and Peeters[8] (see also Refs. 9 and 10) and those in quantum wires with circular bends have been found by Exner and Šeba[11] (see also Refs. 12–14). For a stationary energy-conserving process of electron transmission through a 2D structure, only quasibound states with energies within the conduction subbands are important.[6,7] In particular, it was shown that the quasibound states in a Hall junction result in resonant dips of the resistance in high magnetic fields.

Although the bound states below the lowest subband threshold do not participate in the steady-state transmission, the possibility of observing of them, at least in principle, was shown by Berggren and Ji in the case of two intersecting electron waveguides with finite electrodes.[15] In that case the bound states can be probed by resonant tunneling through the electrodes below the subband. However, it is possible to include the bound states directly in the electron transmission through a Hall junction with infinite electrodes by applying a radiation field, provided that matrix elements between the bound state and propagating states are not equal to zero. Let E_0 be the energy of the bound state below the subband transmission energies, which for zero external magnetic field are equal to $E(k)=(\hbar^2/2m^*d^2)(k^2+\pi^2n^2)$, where d is the width of the electrodes, n is the number of the subband, and k is the wave number of incident electron. At a perturbation frequency $\hbar\omega=E(k)-E_0$ one can expect resonant anomalies in the electron transmission through a Hall junction.

Theoretically, the simplest device is the four-terminal junction (Fig. 1), for which the steady-state transport was studied in Refs. 6, 7, and 9. That junction is a combining element of the Hall structures. The Schrödinger equation for an electron of mass m^* subjected to a magnetic field B applied normal to the junction and to a radiation field $\mathbf{A}_1(t)$ directed in the plane of the junction (Fig. 1) can be written as follows

$$i\hbar\frac{\partial\psi(\mathbf{r},t)}{\partial t}=\frac{\hbar^2}{2m}\left(i\nabla+\frac{e}{\hbar c}(\mathbf{A}_0(\mathbf{r})+\mathbf{A}_1\cos\omega t)\right)^2\psi(\mathbf{r},t). \tag{1}$$

Here we use the gauge $\mathbf{A}_0(\mathbf{r})=(-By,0,0)$. The radiation field is considered in the long-wavelength approximation, in which the wavelength of the radiation field is much greater than the size of the junction. We use the following procedure of dimensionless transformations:

$$t\to\hbar t/2md^2,\quad \mathbf{r}\to\mathbf{r}/d,\quad \epsilon=2md^2E/\hbar^2,$$

$$\omega\to 2md^2\omega/\hbar,\quad \mathbf{a}=2\pi d\mathbf{A}_1/\phi_0,\quad \tilde{B}=2\pi d^2B/\phi_0, \tag{2}$$

where $\phi_0=ch/e$ is the magnetic flux quantum.

Since inside the Hall junction the processes of absorption/emission of photons give rise to satellite channels of transmission at quasi-energies $E+n\hbar\omega$, we write the wave function of the electrodes as[17,18]

$$\phi(\mathbf{r},t)=\sum_n \exp[-i(E+\hbar n\omega)t]\phi_{E+\hbar n\omega}(\mathbf{r}). \tag{3}$$

Substituting (3) into (1) with a gauge transformation of the wave function,

$$\psi(\mathbf{r},t)=\exp\left(ie\frac{\mathbf{A}_1\cdot\mathbf{r}}{\hbar c}\cos\omega t\right)\phi(\mathbf{r},t),$$

and using the dimensionless variables (2), we obtain the following equation for the satellite functions $\phi_{\epsilon+n\omega}(\mathbf{r})=\phi_n(\mathbf{r})$:

$$(\epsilon+n\omega)\phi_n=(i\nabla+\mathbf{a}_0(\mathbf{r}))^2\phi_n+\frac{i\omega}{2}(\mathbf{a}\cdot\mathbf{r})(\phi_{n+1}-\phi_{n-1}), \tag{4}$$

where $\mathbf{a}_0(\mathbf{r})=(-\tilde{B}y,0,0)$. In order to simplify the solutions inside the electrodes we assume that the perturbation is weak and not in resonance with transitions between subbands for a fixed energy of the incident electron in the electrodes. That allows us to neglect the last term in (4) and write the solution inside electrodes 1 and 4 as

$$(1,4);\quad \chi_\epsilon(\mathbf{r},t)=e^{i(kx-\epsilon t)}f_k(y), \tag{5}$$

where $f_k(y)$ satisfies the equation

$$\epsilon f_k(y)=-\frac{d^2}{dy^2}f_k(y)+(k+\tilde{B}y)^2f_k(y). \tag{6}$$

In electrodes 2 and 3 it is convenient to use the Truscott transformation[19]

$$\phi(\mathbf{r},t)=\varphi(x,t)\exp\left[-\frac{i}{2}a^2t+\frac{2ika}{\omega}\sin\omega t+iy(k-a\cos\omega t)-\frac{ia^2}{4\omega}\sin 2\omega t\right]$$

and the following gauge for the magnetic field: $\mathbf{a}_0(\mathbf{r})=(0,\tilde{B}x,0)$. We then have

$$(2,3);\quad i\frac{\partial}{\partial t}\varphi(x,t)=\left[-\frac{\partial^2}{\partial x^2}+(k-\tilde{B}x)^2+2\tilde{B}ax\cos\omega t\right]\varphi(x,t). \tag{7}$$

Further we consider weak perturbations $\tilde{B}ad \ll 1$, for which the effect of the time-dependent term in (7) can be neglected. Actually, in computer calculations this restriction can be relaxed considerably. In that case Eq. (7) transforms to a form which is similar to Eq. (6). Therefore, in electrodes 2 and 3 one can write approximate solutions in the same form as in electrodes 1 and 4, except for the phase

$$\tilde{\chi}_\epsilon(\mathbf{r},t)=\exp\left\{-i\left[\tilde{B}xy+\epsilon t-\frac{2ak}{\omega}\sin\,\omega t-y(k-a\,\cos\,\omega t)\right]\right\}f_{-k}(x). \tag{8}$$

Also, we have neglected the a^2 terms in (8).

Inside the Hall junction, with boundaries in each electrode (shown by fine lines in Fig. 1), is the scattering region, in which there are two bound states with energies ϵ_0 and ϵ_1, with $\epsilon_0<\pi^2$ and $\pi^2<\epsilon_1<4\pi^2$ (Ref. 6). The positions of the boundaries in the electrodes are chosen so that the contribution of evanescent modes at the boundaries in computer simulations is negligible.

Since we have assumed that the radiation field is resonant to transitions between the ground bound state and a propagating state, for small perturbations we can restrict ourselves to only two satellite states in Eq. (4), with the following equations for them:

$$-(i\nabla+\mathbf{a}(\mathbf{r}))^2\phi_0+\epsilon\phi_0=-\frac{i}{2}(\mathbf{a}\cdot\mathbf{r})\phi_{-1},$$

$$-(i\nabla+\mathbf{a}(\mathbf{r}))^2\phi_{-1}+(\epsilon-\omega)\phi_{-1}=\frac{i}{2}(\mathbf{a}\cdot\mathbf{r})\phi_0, \tag{9}$$

where the functions ϕ_0 and ϕ_{-1} correspond to the propagating and the bound states, respectively. In order to obtain a complete solution of the scattering problem in the Hall junction, the solutions of equations (9) are matched with propagating modes in each respective electrode.[6] The electrode 1 in which electron is incident we denote as In(1), while the electrodes in which electron is outgoing we denote as Out:

$$\text{In}(1)=(\chi_\epsilon,0);\quad \text{Out}(1,4)=(\chi_\epsilon,\chi_{\epsilon-\omega});\quad \text{Out}(2,3)=(\tilde{\chi}_\epsilon,\tilde{\chi}_{\epsilon-\omega}).$$

These boundary conditions for the solutions of equations (9) can be expressed as Neumann boundary conditions for numerical solution of Eqs. (9) with the help of the MatLab PDE Toolbox.

Results of the calculations are given in Figs. 2 and 3. In Fig. 2 the transmission probabilities from the input electrode 1 to all the other electrodes 2–4 are shown as functions of the incident electron energy in the presence of a radiation field with the frequency $\omega\approx\epsilon(k,\tilde{B})-\epsilon_0$. Also for comparison the transmission probabilities for the steady-state case are shown in Fig. 2. From this figure one can see that in the vicinity of exact resonance the radiation field induces significant anomalies in the electron transmission. In particular, the transmission probability to the left electrode can exceed the transmission probability to the right electrode. As a result, the Hall resistance becomes negative in the vicinity of the resonance. The total Hall resistance[18] in terms of $\hbar/e^2$, viz.,

$$R_H=\frac{2(T_R-T_L)}{(2T_F+T_R+T_L)^2+(T_R-T_L)^2} \tag{10}$$

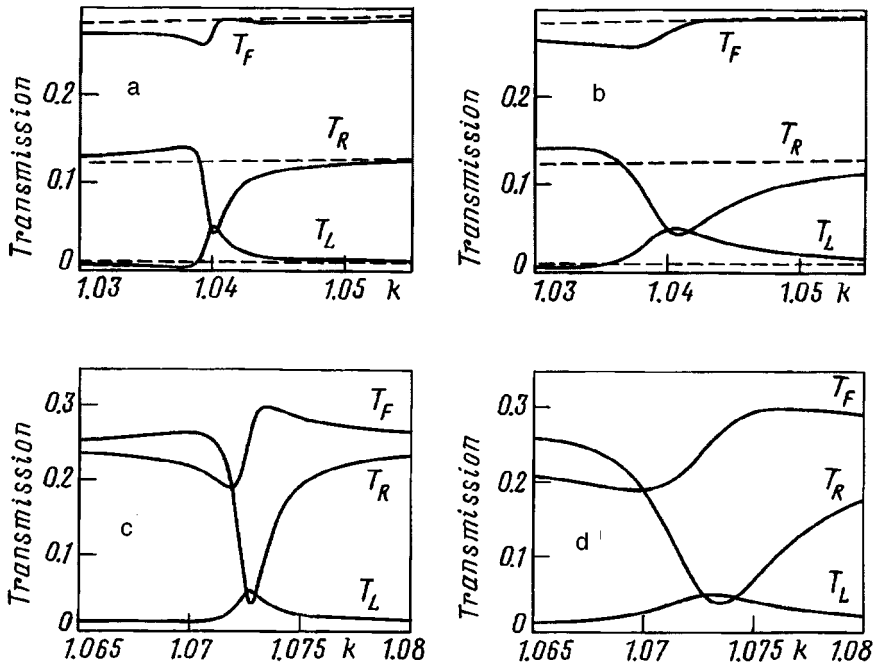

FIG. 2. The energy (wave number) dependence of the transmission probabilities in the Hall junction. T_F, T_R, and T_L are the probabilities of transmission from the first electrode to the fourth, second, and third electrodes, respectively (see Fig. 1). The steady-state case for zero radiation field is shown by dashed lines. (a) $\widetilde{B}=1.0$, $a=0.05$; (b) $\widetilde{B}=1.0$, $a=0.1$; (c) $\widetilde{B}=2.0$, $a=0.05$; (d) $\widetilde{B}=2.0$, $a=0.1$.

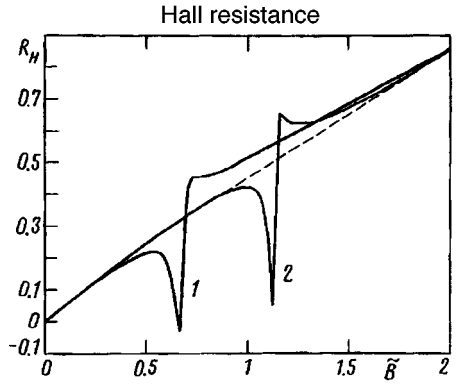

FIG. 3. The magnetic-field dependence of the Hall resistance (formula (10)) for different values of the Fermi energies $\epsilon_F=\pi^2+k_F^2$. Curve *1* corresponds to $k_F=1.04$, and curve *2* to $k_F=1.06$. The frequency and amplitude of the radiation field are $\omega=4.3$ and $a=0.05$, respectively. The dashed curve corresponds to the steady-state case $a=0$.

is shown in Fig. 3 as a function of applied magnetic field $\widetilde{B}$. Since the frequency of the radiation field and the Fermi energy of the incident electron are fixed, only the external magnetic field, by slightly varying the electron energy, can fulfill condition of resonance at a specific value $\widetilde{B}$. Therefore the field dependence of the Hall resistance under the influence of a radiation field has a resonant dip at the corresponding values of the magnetic field. This phenomenon is distinctly demonstrated in Fig. 3, where for two values of the Fermi energy of the incident electron one can see two corresponding resonant quenchings of the Hall resistance.

Hall resistance anomalies in the form of negative resistance have previously been observed theoretically and experimentally by special construction of the Hall junctions.[6,7,20,5] The present study gives another possibility for observing this phenomenon, by applying a resonant radiation field without changing the geometry of the Hall junction. Note that in contrast to the steady-state quenching of the Hall resistance,[6,7] the radiation-field-induced anomalies take place at low values of the external magnetic field (Fig. 3).

A. F. S. acknowledges Pavel Exner and Petr Šeba for valuable explanations of bound states in 2DEG systems. This work was supported by the INTAS-RFBR Grant 95-IN-RU-657 and RFFI Grant 97-02-16305.

[a)]e-mail: zeos@zeos.krascience.rssi.ru

---

[1] B. J. van Wees, H. van Houten, C. W. J. Beenakker *et al.*, Phys. Rev. **60**, 848 (1988).
[2] D. A. Wrahamn, T. J. Thornton, R. Newbury *et al.*, J. Phys. C **21**, L209 (1988).
[3] M. L. Roukes, A. Sherer, S. J. Allen *et al.*, Phys. Rev. Lett. **59**, 3011 (1987).
[4] Y. Takagaki, K. Gamo, S. Namba *et al.*, Solid State Commun. **68**, 1051 (1988).
[5] C. J. B. Ford, S. Washburn, M. Büttiker *et al.*, Phys. Rev. Lett. **62**, 2724 (1989).
[6] R. L. Schult, D. G. Ravenhall, and H. W. Wyld, Phys. Rev. B **39**, 5476 (1989).
[7] K. Amemiya and K. Kawamura, J. Phys. Soc. Jpn. **63**, 3087 (1994).
[8] F. M. Peeters, Superlattices Microstruct. **6**, 217 (1989).
[9] Y. Avishai and Y. B. Band, Phys. Rev. Lett. **62**, 2527 (1989).
[10] K.-F. Berggren, Ç. Besev, and Z.-L. Ji, Phys. Scr. T**42**, 141 (1992).
[11] P. Exner and P. Šeba, J. Math. Phys. **30**, 2574 (1989) and references therein.
[12] C. S. Lent, Appl. Phys. Lett. **56**, 2554 (1990).
[13] F. Sols and M. Macucci, Phys. Rev. B **41**, 11887 (1990).
[14] H. Wu, D. W. L. Sprung, and J. Martorell, Phys. Rev. B **45**, 11960 (1992).
[15] K.-F. Berggren and Z.-L. Ji, Phys. Rev. B **43**, 4760 (1991).
[16] E. N. Bulgakov and A. F. Sadreev, Phys. Rev. B **52**, 11938 (1995).
[17] E. N. Bulgakov and A. F. Sadreev, Phys. Low-Dim. Struct. **1/2**, 33 (1977).
[18] M. Büttiker, Phys. Rev. Lett. **57**, 317 (1986).
[19] W. S. Truscott, Phys. Rev. Lett. **70**, 1900 (1993).
[20] G. Kirczenow and E. Castaño, Phys. Rev. B **43**, 7343 (1991).

Published in English in the original Russian journal. Edited by Steve Torstveit.

Nonlinear Faraday effect near the fundamental absorption edge in the ferromagnetic semiconductor $CdCr_2Se_4$

L. L. Golik[a)] and Z. É. Kun'kova
Institute of Radio Engineering and Electronics, Russian Academy of Sciences, 141120 Fryazino, Moscow District, Russia

(Submitted 31 July 1997)
Pis'ma Zh. Éksp. Teor. Fiz. **66**, No. 6, 409–413 (25 September 1997)

A sharp increase of the Faraday rotation with increasing incident radiation power is observed in a band near the fundamental absorption edge of the ferromagnetic semiconductor $CdCr_2Se_4$. The magnitude of the effect is a nonmonotonic function of the radiation intensity. The effect is explained by narrowing of an excitonic resonance as a result of screening of the internal electric fields by photoexcited carriers. [S0021-3640(97)00818-9]

PACS numbers: 75.50.Dd, 78.20.Ls

A large change in the magnitude of the Faraday rotation (FR) with increasing incident radiation power has been observed in the ferromagnetic semiconductor $CdCr_2Se_4$ subjected to pulsed neodymium laser radiation ($\lambda = 1060$ nm).[1] The maximum change in the FR angle was equal to 1.6×10^4 deg/cm at $T = 75$ K as the radiation power density P increased from 3 to 300 kW/cm^2. This is greater than the nonlinear Faraday effect observed in the semimagnetic semiconductor $Cd_{1-x}Mn_xTe$ at gigawatt power densities and picosecond pulse durations.[2–4] The spectral dependence and nature of the nonlinear Faraday effect in $CdCr_2Se_4$ remain unknown. In the present work we investigated the spectral dependence of the nonlinear FR in $CdCr_2Se_4$ near the fundamental absorption edge. It was found that the FR in a band associated with the resonance at the absorption edge increases rapidly with increasing radiation power.

The investigations were conducted on $CdCr_2Se_4$ wafers with dimensions of $\simeq 1.5\times 2$ mm $\times 12$ μm thick, obtained by grinding and polishing single crystals. A pulsed tunable laser working on F^2 color centers in LiF was used as the radiation source. The laser was excited by the second harmonic of the neodymium laser. The tuning range of the laser was 830–1030 nm, the peak lasing power at the maximum of the tuning curve was equal to 25 kW, the pulse duration was equal to 8 ns, and the pulse repetition frequency was equal to 10 s^{-1}. The laser beam, attenuated by neutral filters, was focused to a spot 1 mm in diameter on the surface of a sample in a vacuum cryostat. The FR measurements were performed on an automated apparatus with direct readout of the rotation angle of the analyzer. An FÉK-29KPU photocell served as the radiation detector; the signal from the photocell at the moment corresponding to the maximum intensity of the radiation pulse was recorded with an S1-122/4 stroboscopic oscillograph. The long-wavelength limit of the tuning range of the laser and the strong heat-induced red shift of the experimental FR band determined the lower limit of the temperature range accessible

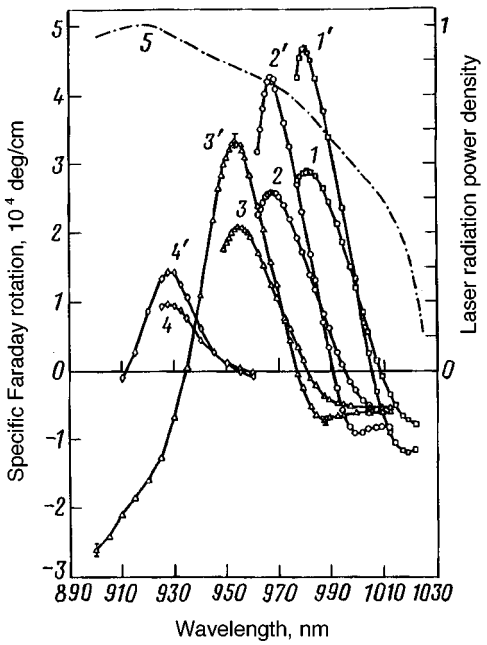

FIG. 1. Spectral dependences of the specific Faraday rotation measured in $CdCr_2Se_4$ at low (*1–4*) and high (*1′–4′*) incident radiation intensities; $T=110$ K (curves *1,1′*), 117 K (*2,2′*), 125 K (*3,3′*), and 135 K (*4,4′*); curve *5* is spectral dependence of the radiation power of the laser employed (in relative units).

for investigation. The investigations were performed in the temperature interval $T=110-135$ K, which includes the ferromagnetic transition temperature $T_c=130$ K, in a magnetic field $H=4.8$ kOe, which saturates the sample in the ferromagnetic phase.

Figure 1 shows the spectral dependences $F(\lambda)$ of the specific FR measured at different temperatures T for low (*1–4*) and high (*1′–4′*) intensities of the radiation incident on the sample. The figure also shows the spectral dependence of the radiation power $P(\lambda)$ of the laser employed (dot-dash curve). The intensity level referred to as low (with a power at the maximum of the $P(\lambda)$ curve $P_{\max}=15$ kW/cm^2) was determined by the sensitivity of the photodetector and was already in the region of nonlinearity of the Faraday effect. The radiation power density incident on the sample at each wavelength was approximately 30 times higher for the curves *1′–4′* ($P_{\max}=470$ kW/cm^2). The onset of a rapid increase in the fundamental absorption limited the measurements of $F(\lambda)$ at low radiation intensity on the short-wavelength side. The error in the FR measurements, which varied over the spectrum, is shown for three wavelengths on the curve *3′* in Fig. 1.

As the radiation power in the experimental temperature range increases, the FR at the maximum of the positive peak in the curves $F(\lambda)$ increases strongly (approximately by 60%). The maximum increase in FR is observed at $T=110$ K and equals 1.8×10^4 deg/cm. The magnitudes of the FR at the maxima of the positive peaks ($F_{\max}$) on the curves *1′–4′* are approximately double the value of $F_{\max}$ for the linear Faraday effect in

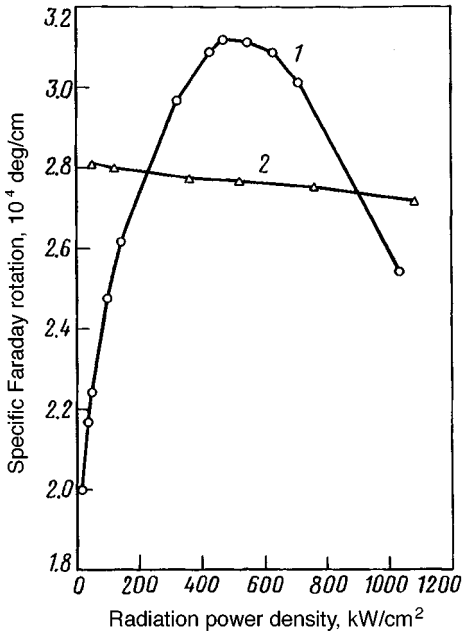

FIG. 2. Absolute magnitude of the specific Faraday rotation measured at $T=125$ K versus the power density of the incident radiation: $\lambda=957$ nm (curve *1*) and 900 nm (curve *2*).

this sample at the same values of T. A faint peak (curves $1'-3'$) appears on the long-wavelength wing of the dispersion structure, and the long-wavelength negative FR increases. We note that for some, apparently the most perfect, $CdCr_2Se_4$ crystals a negative FR peak was observed at $T=77$ K in measurements performed using an incandescent lamp.[5] No changes were observed in the spectral position of the maximum of the positive FR peak as a function of the radiation intensity.

The character of the dependence of the FR on the power P of the incident radiation changes with wavelength. Figure 2 displays the functions $F(P)$ for $\lambda=957$ and 900 nm at $T=125$ K. The wavelength 957 nm is close to the maximum positive FR peak. It is well known that resonance transitions near the absorption edge are responsible for the FR at this wavelength,[5] and shorter-wavelength transitions with $\lambda_0\simeq 680$ and 800 nm make the main contribution to the FR at the wavelength 900 nm, which falls in the fundamental absorption region.[6] The power dependences $F(P)$ at the maxima of the positive FR peaks for two other temperatures are qualitatively close to curve *1* in Fig. 2.

It follows from the data presented that in $CdCr_2Se_4$ single crystals a strong nonlinear Faraday effect is observed in the FR band due to resonance at the absorption edge. The power dependence of the FR is very weak at energies beyond the absorption edge. The character of the change in FR with increasing radiation power and the relative magnitude of the effect do not change as the temperature passes through T_c and then decreases. Therefore the nonlinear Faraday effect is not due to the onset of magnetic ordering. As is well known, the spectral dependence of the FR is determined by the difference

$n_+(\lambda)-n_-(\lambda)$ of the refractive indices in right- and left-circularly polarized light. The spectral dependence of the FR angle which we observed corresponds to the dispersion $n_{+,-}(\lambda)$ due to resonance absorption and exchange splitting of the resonance level. The increase in the maximum value of the FR angle with increasing light intensity could be due to narrowing and intensification of the resonance in absorption as well as an increase in the splitting of the energy level. Since no appreciable change of the spectral position of the maxima on the curves $F(\lambda)$ occurs with increasing radiation intensity (Fig. 1), the observed changes in the FR band must be attributed to the narrowing and intensification of the resonance in absorption.

The optical nonlinearities in absorption near the fundamental absorption edge are ordinarily attributed to the renormalization of the band gap and broadening of the excitonic bands.[7] The decrease observed in the magnitude of FR in $Cd_{1-x}Mn_xTe$ under irradiation with photons whose energy is much lower than the band gap is due to the dynamic Stark effect as well as two-photon absorption, which changes the populations and increases the magnetization on account of the $s-d$ exchange interaction.[3] There is no general agreement concerning the nature of the transitions that are responsible for the FR band studied in $CdCr_2Se_4$, but there are grounds for believing that they are due to excitons. This is indicated by the attenuation and broadening of the resonances in absorption and FR, observed with increasing In concentration in $CdCr_2Se_4$,[8] as is typical for excitons. On the basis of the excitonic nature of the FR band studied, it should be expected that as the intensity of the incident radiation increases, the band should broaden and not narrow, as is observed experimentally for a large range of intensities. The narrowing of the resonances could be due to the existence of internal electric fields (impurity fluctuation potential and a surface field) and screening of these fields. Apparently, the relative weakness of the resonance in absorption and its large half-width $\simeq 20$ meV are due to these fields and also to the formation of impurity excitonic complexes and exciton–phonon and exciton–magnon interactions. As excitons dissociate, thus increasing the free charge-carrier density, these fields are screened and the excitonic bands in the absorption and FR spectra narrow. As the radiation power increases further, the screening of the electron–hole interaction starts to dominate, which is manifested as a decrease in the FR at high radiation intensities.

We shall present some estimates that substantiate this mechanism of the nonlinear FR. The lifetime of nonequilibrium charge carriers in the experimental material can be long as a result of the spatial separation of the carriers that occurs in the field of the fluctuation potential. This apparently explains the relaxation time $\tau > 10^{-6}$ s of the nonlinear FR observed in Ref. 1. Assuming that the lifetime of the nonequilibrium charge carriers is longer than the radiation pulse duration ($\sim 10^{-8}$ s), for a peak power density of 500 kW/cm^2 (corresponding to the maximum on the $F(P)$ curve), a value of the absorption coefficient $\alpha \simeq 10^3$ cm^{-1} near the maximum of the FR,[5] and a quantum yield of 1, we estimate the nonequilibrium charge carrier density produced by a single pulse up to the time of measurement to be $N_e \simeq 10^{18}$ cm^{-3}. Assuming that screening of the electron–hole interaction first appears at this density, the relation $N_e \simeq (3\pi^2 a_{ex}^3)^{-1}$, where a_{ex} is the Bohr radius of the exciton,[9] yields $a_{ex} \simeq 3 \times 10^{-7}$ cm, which at a dielectric constant $\epsilon = 10$ corresponds to a reduced exciton mass $m_{ex} \simeq 0.2 m_0$ and an exciton binding energy $E_{ex} \simeq 30$ meV. The value obtained for E_{ex} is consistent with the observed[5]

wavelength dependences $\alpha(\lambda)$ near the absorption edge of $CdCr_2Se_4$.

For low intensity ($P_{max}=15$ kW/cm^2) the nonequilibrium charge carrier density and the corresponding Debye screening length L_D can be estimated as 3×10^{16} cm^{-3} and 1×10^{-6} cm. Since for our material the real defect density is $N_t\simeq10^{17}$ cm^{-3}, we obtain the following relation between the screening length, the distance between the impurities determining the fluctuation potential, and the exciton radius: $a_{ex}\simeq3\times10^{-7}$ cm $<L_D\simeq1\times10^{-6}$ cm $\leqslant(N_t)^{-1/3}\simeq2\times10^{-6}$ cm. As the radiation intensity increases, L_D decreases. Therefore the photoexcited charge carriers screen the internal electric fields first and then the electron–hole interaction.

We thank T. G. Aminov and G. G. Shabunina for providing the $CdCr_2Se_4$ single crystals and V. E. Pakseev for assisting in the construction of the experimental apparatus.

[a)]e-mail: llg197@ire216.msk.su

[1] V. G. Veselago, S. G. Rudov, and M. A. Chernikov, JETP Lett. **40**, 940 (1984).
[2] J. Frey, R. Frey, C. Flytzanis, and R. Triboulet, Opt. Commun. **84**, 76 (1991).
[3] J. Frey, R. Frey, and C. Flytzanis, Phys. Rev. B **45**, 4056 (1992).
[4] S. Huggonard-Bruyere, C. Buss, R. Frey, and C. Flytzanis, Appl. Phys. Lett. **66**, 2043 (1995).
[5] L. L. Golik, Z. É. Kun'kova, T. G. Aminov *et al.*, Fiz. Tverd. Tela (Leningrad) **22,** 877 (1980) [Sov. Phys. Solid State **22**, 512 (1980)].
[6] L. L. Golik, S. M. Grigorovich, M. I. Elinson *et al.*, Fiz. Tverd. Tela (Leningrad) **19,** 629 (1977) [Sov. Phys. Solid State **19**, 365 (1977)].
[7] H. Haug and S. Schmitt-Rink, J. Opt. Soc. Am. B **2**, 1135 (1985).
[8] L. L. Golik, Z. É. Kun'kova, V. E. Pakseev *et al.*, Fiz. Tverd. Tela (Leningrad) **26,** 3081 (1984) [Sov. Phys. Solid State **26**, 1856 (1984)].
[9] K. Seeger, *Semiconductor Physics*, Springer-Verlag, New York, 1973 [Russian translation, Mir, Moscow, 1977].

Translated by M. E. Alferieff

Anomalous orientation of ferroelectric liquid crystal films in an electric field

P. O. Andreeva, V. K. Dolganov,[a)] and K. P. Meletov
Institute of Solid-State Physics, 142432 Chernogolovka, Moscow District, Russia

(Submitted 5 August 1997)
Pis'ma Zh. Éksp. Teor. Fiz. **66**, No. 6, 414–418 (25 September 1997)

An anomalous orientation of ferroelectric liquid crystals in an electric field is observed. The tilt planes of the molecules are oriented in a direction parallel to the electric field. The anomalous orientation is observed in freely suspended films above the smectic-C*–smectic-A bulk phase transition temperature. The effect is explained by the appearance of giant flexoelectric polarization, 10^4 times greater than that in bulk liquid-crystal samples, in the film. © *1997 American Institute of Physics.* [S0021-3640(97)00918-3]

PACS numbers: 61.30.Gd, 77.84.Nh

Ferroelectric liquid crystals (Sm-C*) have a layered structure, each layer consisting of a two-dimensional liquid with the long axes of the chiral molecules tilted with respect to the normal to the smectic layers.[1,2] The spontaneous polarization $\mathbf{P}_0$ in a smectic layer is perpendicular to the tilt plane of the molecules ($\mathbf{P}_0$ is parallel to the vector $(\mathbf{z}\times\mathbf{n})$, where $\mathbf{z}$ is the normal to the smectic plane and $\mathbf{n}$ is the director, i.e., the direction of predominant orientation of the long axes of the molecules). The chirality of the molecules causes the tilt plane of the molecules (and, correspondingly, the spontaneous polarization) in neighboring smectic layers to rotate, as a result of which there is no macroscopic polarization in samples which are large compared to the helical pitch. If the sample is smaller in the direction normal to the smectic layer than the helical pitch or if an electric field strong enough to untwist the helix is applied to the crystal, then a ferroelectric liquid crystal has a macroscopic spontaneous polarization $\mathbf{P}_0$. The presence of a spontaneous polarization $\mathbf{P}_0$, the possibility of flexoelectric liquid crystals to be oriented in weak electric fields, and numerous technical applications in this connection arouse great interest in investigations of ferroelectric liquid-crystal structures. We underscore once again that in an electric field the polar axis of the ferroelectric liquid crystal should be oriented in the direction of the field and the tilt plane of the molecules in the smectic layers should be oriented perpendicular to the field. This follows from the symmetry of a ferroelectric liquid crystal and has been confirmed in many experiments.

In the present work it was observed that an abrupt change in the direction of orientation of the molecules occurs in freely suspended films above the temperature of the Sm-C*–Sm-A bulk phase transition. If an electric field orients a ferroelectric film at low temperatures in the same manner as in a bulk sample, then at high temperatures the orientation changes by 90°: The tilt planes of the molecules become oriented in the direction of the field. We attribute the reorientation of the structure to the onset in the film

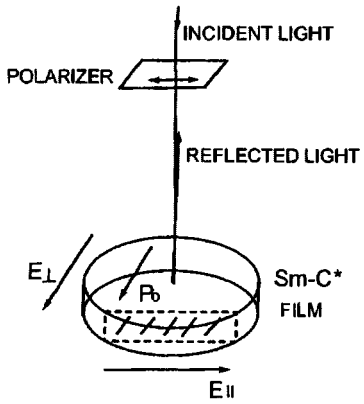

FIG. 1. Relative arrangement of a ferroelectric film and the optical part of the apparatus. The orientation of the molecules in the film is shown for the case when the film is in the low-temperature region of the Sm-C* phase and an electric field $E_\perp$ is applied to it. $\mathbf{P}_0$ — ferroelectric polarization vector.

of an anomalously high flexoelectric polarization $\mathbf{P}_f$, directed perpendicular to the spontaneous ferroelectric polarization $\mathbf{P}_0$.

The measurements were performed in the ferroelectric liquid crystal *n*-nonyloxybenzylidene-n'-amino-2-methylbutylcinnamate (NOBAMBC), in a bulk sample of which the following sequence of phase transitions occurs: Sm-H* (76 °C)–Sm-C* (91 °C)–Sm-A (116 °C)–I (isotropic liquid). The Sm-C*–Sm-A transition is a second-order phase transition. Some measurements were performed on the flexoelectric liquid crystal *n*-decyloxybenzylidene-n'-amino-2-methylbutylcinnamate (DOMAMBC), which forms the same liquid-crystal phases as does NOBAMBC. The films were placed in a 6-mm opening in a glass plate. The planes of the smectic layers in freely suspended films are parallel to the film surface. Optical reflection from the films was measured in the ''backward'' geometry (Fig. 1). An electric field (3 V/cm) could be applied to the film in two mutually perpendicular directions. The thickness of the films (for $N>12$ smectic layers) was determined from the spectral dependence of the optical reflection in the Sm-A phase,[3]

$$I(\lambda)=\frac{(n^2-1)^2\sin^2(2\pi nNd/\lambda)}{4n^2+(n^2-1)^2\sin^2(2\pi nNd/\lambda)}, \tag{1}$$

where d is the interplanar distance ($d\approx 3.2$ nm in the Sm-A phase of NOBAMBC) and $n=1.48$ ($\lambda=630$ nm) is the index of refraction. The spectral reflection curve for thin films is virtually thickness-independent:

$$I(\lambda)\approx N^2d^2\pi^2(n^2-1)^2/\lambda^2. \tag{2}$$

The number of smectic layers in this case was determined from the relative intensity of the reflections for films with a different number of layers $I(N)\sim N^2$. Films with the required thickness were prepared by layer-by-layer thinning by heating above the temperature of the liquid crystal — isotropic phase bulk phase transition.[4–6]

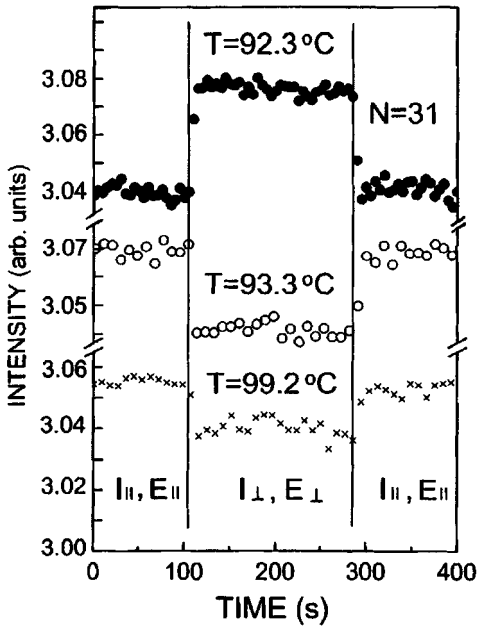

FIG. 2. Optical reflection intensity ($I_\perp$, $I_\parallel$) for a ferroelectric film ($N=31$) in an electric field applied parallel ($E_\parallel$) and perpendicular ($E_\perp$) to the direction of polarization of the light ($\lambda=630$ nm).

The transition into the Sm-A phase in freely suspended films is shifted to higher temperatures with respect to the transition in the bulk sample.[7–9] In the present work we measured the optical reflection ($I_\parallel$, $I_\perp$) for electric fields oriented parallel ($E_\parallel$) and perpendicular ($E_\perp$) to the plane of polarization of the light in the Sm-C* temperature range and at the transition to the Sm-A phase. This method enabled us to detect an intensity difference of $\sim 10^{-3}$ when the direction of the electric field was switched. The in-plane optical anisotropy is due to the tilting of the long axes of the molecules in Sm-C*. The refractive index $n_0=n_\perp$ in a direction perpendicular to the tilt plane of the molecules is virtually temperature-independent (n_0 is the ordinary index of refraction). The refractive index for the extraordinary ray, $n_e>n_0$, depends on the tilt angle θ of the molecules. Measurement of the reflection for two polarizations is a simple and direct method for determining both the film orientation and the temperature dependence of n_e as well as the polar angle θ in the ferroelectric phase (θ is the order parameter for the Sm-C*–Sm-A phase transition). If the angle θ is not constant in the film, then the intensity of the optical reflection for thin films is determined by the mean-square tilt angle $\overline{\theta^2}/N$ of the molecules (the averaging is over the smectic layers of the film).

The change occurring in the intensity of reflection from the film when the direction of the electric field is switched is qualitatively different at low and high temperatures (Fig. 2, $N=31$). For $T<92.8$ °C we have $I_\perp>I_\parallel$, in agreement with the conventional ideas about the direction of the spontaneous polarization in Sm-C*: For $\mathbf{P}_0$ oriented in the direction of the electric field, the larger value of the refractive index n_e and, accordingly,

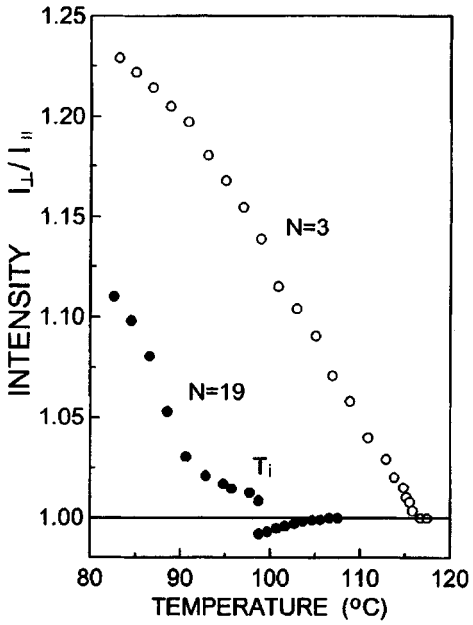

FIG. 3. Temperature dependences of the relative optical reflection intensities $I_\perp / I_\parallel$ for films 3 and 19 smectic layers thick ($\lambda = 630$ nm).

the larger value of the reflection coefficient $I_\perp$ correspond to a direction perpendicular to the field (the tilt plane of the molecules in Sm-C*). At $T_i \approx 92.8$ °C an abrupt change in the reflection intensities occurs for both polarizations: The intensity $I_\parallel$ becomes equal to $I_\perp$, the value at temperatures $T < T_i$, while $I_\perp$ decreases to the value of $I_\parallel$ at temperatures $T < T_i$. Above this temperature and up to the transition to the Sm-A phase the reflection intensity decreases when the field is switched $E_\parallel \rightarrow E_\perp$. This means that the tilt plane of the molecules is oriented in the direction of the field. Figure 3 displays the temperature dependence of the relative reflection intensity $I_\perp / I_\parallel$ for films with $N = 19$ and $N = 3$. The temperature T_i above which anomalous orientation of the films was observed depends on the film thickness — the higher the temperature, the thinner the film: For films with 12 smectic layers $T_i \approx 104$ °C and for thick films T_i lies close to the temperature of the bulk phase transition ($T_i - T_c \approx 0.3$ °C for $N = 50$). We did not observe anomalous orientation in ultrathin films ($N = 3$, Fig. 3).

It should be underscored that the observed effect is qualitatively different from the reorientation of the direction of the spontaneous polarization by 180°, which has been observed previously in ferroelectric liquid crystals.[10,11] That reorientation is not specific to thin films and is observed in both films and bulk samples; in addition, the tilt plane of the molecules remains perpendicular to the direction of spontaneous polarization and the electric field. In our case, however, the structure rotates by 90° with respect to the external field.

The decrease of the absolute value $|I_\perp / I_\parallel - 1|$ with increasing temperature (Fig. 3)

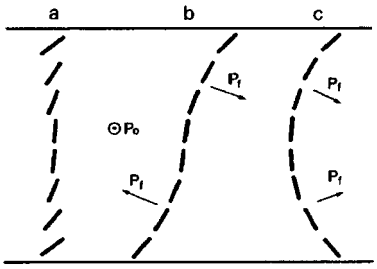

FIG. 4. Orientation of the molecules in a smectic ferroelectric liquid crystal film: *S*-like orientation of the director (a, b), *C*-like orientation of the director (c). $\mathbf{P}_0$ — spontaneous ferroelectric polarization, $\mathbf{P}_f$ — flexoelectric polarization.

characterizes the variation of the tilt angle of the molecules with temperature. For $T=82$ °C the angle θ determined from our data equals 28° for a film with $N=3$ and 21° for $N=19$. A jump in the reflection intensity ($N=19$) occurs at a molecular tilt angle $\theta\approx 6°$. The dependence of θ on the film thickness is related with the surface ordering of the smectic layers.[7–9,12] Surface ordering is strongest above the bulk phase transition temperature. In this temperature range the angle θ depends strongly on the distance of the smectic layer from the surface.[7–9] In our opinion, the variation of the angle θ in the smectic layers could be responsible for the anomalous orientation of the film. Figures 4a and 4b show schematically the orientation of the molecules in the smectic layers of a ferroelectric liquid crystal film. The bending of the director should give rise to a flexoelectric polarization $\mathbf{P}_f$ in the tilt plane of the molecules:[1]

$$\mathbf{P}_f = e_1\mathbf{n}(\nabla\cdot\mathbf{n}) + e_3(\nabla\times\mathbf{n})\times\mathbf{n}. \tag{3}$$

Let us compare the spontaneous polarization $\mathbf{P}_0$ and the flexoelectric polarization $\mathbf{P}_f$, induced by bending of the director $\mathbf{n}$, in the temperature range where a transition to anomalous orientation occurs ($N=19$, $\theta\approx 6°$). The ferroelectric polarization $\mathbf{P}_0$ with $\theta=6°$ is of the order of 1×10^{-5} C/m^2 for substances of the NOBAMBC type.[13] In liquid crystals the flexoelectric constants e_1 and e_3 are typically of the order of 10^{-10}–10^{-12} C/m.[2,14] To estimate $\mathbf{P}_f$ we assume the value $\epsilon_3=10^{-11}$ C/m. For the case when the tilt angles of the molecules in the surface layer and at the center of the film differ by $\Delta\theta=0.2$ rad we obtain $\mathbf{P}_f\approx 7\times 10^{-5}$ C/m^2.

These estimates show that a flexoelectric polarization $\mathbf{P}_f$ appreciably greater in magnitude than the spontaneous ferroelectric polarization $\mathbf{P}_0$ can arise in a plane perpendicular to $\mathbf{P}_0$. As a result of the much larger bending of the director in a film, the polarization $\mathbf{P}_f$ is 10^4 times greater than the flexoelectric polarization in bulk liquid crystal samples.

In the case of *S*-shaped bending of the director (Fig. 4b) the direction of $\mathbf{P}_f$ is different at the top and bottom of the film. For a film which is not too thin, the tilt angle of the molecules at the center of the film can become quite small (or zero) above the bulk phase transition temperature. In this case the top and bottom of the film can be oriented independently, and a transition to a *C*-like orientation of the director (Fig. 4c) with

flexoelectric polarizations directed in the same direction becomes possible. For $\mathbf{P}_f > \mathbf{P}_0$ the C orientation is favored in an electric field, and the $S \rightarrow C$ transition leads to a 90-degree reorientation of the tilt plane of the molecules.

We also observed anomalous orientation in a ferroelectric liquid crystal DOBAMBC. The nonuniform orientational structure of the films that is associated with stabilization of the tilt surface of the molecules and the proximity of the phase transition to the Sm-A, nematic, or isotropic phase is typical for liquid-crystal films. Anomalous reorientation of the structures (caused by transitions of the type $S \rightarrow C$) can be expected to occur in this connection in a wide class of liquid-crystal substances.

We thank E. I. Kats and V. I. Marchenko for helpful discussions. This work was performed with the support the Russian Fund for Fundamental Research (Grant No. 95-02-05343), the State Science and Technology Program ''Statistical Physics,'' and INTAS (Grant No. 94-4078).

[a)]e-mail: dolganov@issp.ac.ru

[1] P.-G. de Gennes, *The Physics of Liquid Crystals*, Clarendon Press, Oxford, 1974 [Russian translation, Mir, Moscow, 1977].
[2] S. A. Pikin, *Structural Transformations in Liquid Crystals* [in Russian], Nauka, Moscow, 1981.
[3] M. Born and E. Wolf, *Principles of Optics*, Pergamon Press, New York, 1964 [Russian translation, Nauka, Moscow, 1970].
[4] T. Stoebe, P. Mach, and C. C. Huang, Phys. Rev. Lett. **74**, 1384 (1994).
[5] E. I. Demikhov, V. K. Dolganov, and K. P. Meletov, Phys. Rev. E **52**, R1285 (1995).
[6] V. K. Dolganov, E. I. Demikhov, R. Fouret, and C. Gors, Phys. Lett. A **220**, 242 (1996).
[7] S. Heinekamp, R. A. Pelcovits, E. Fontes *et al.*, Phys. Rev. Lett. **52**, 1017 (1984).
[8] S. M. Amador and P. S. Pershan, Phys. Rev. A **41**, 4226 (1990).
[9] Ch. Bahr, C. Booth, D. Fliegner, and J. W. Goodby, Phys. Rev. E **52**, 4612 (1995).
[10] N. Mikami, R. Higuchi, T. Sakurai *et al.*, Jpn. J. Appl. Phys., Part 1 **25**, 833 (1986).
[11] Ch. Bahr, C. Booth, D. Fliegner, and J. W. Goodby, Europhys. Lett. **34**, 507 (1996).
[12] V. K. Dolganov, E. I. Demikhov, R. Fouret, and C. Gors, Zh. Eksp. Teor. Fiz. **111,** 949 (1997) [JETP **84**, 522 (1997)].
[13] B. I. Ostravskiĭ, A. Z. Rabinovich, A. S. Sonin *et al.*, JETP Lett. **25**, 70 (1977).
[14] L. M. Blinov, *Electro-Optical and Magneto-Optical Properties of Liquid Crystals*, Wiley, New York, 1983 [Russian original, Nauka, Moscow, 1978].

Translated by M. E. Alferieff

Observation of the atomic structure of a crystal without a high-resolution electron microscope

V. L. Indenbom
Institute of Crystallography, Russian Academy of Sciences, 117333 Moscow, Russia

(Submitted 20 August 1997)
Pis'ma Zh. Éksp. Teor. Fiz. **66**, No. 6, 419–422 (25 September 1997)

It is demonstrated for the example of tetragonal tungsten bronze that it is possible, as was indicated in a previous paper [V. L. Indenbom and S. B. Tochilin, JETP Lett. **65**, 252 (1995)], to resolve to within 0.2–0.3 Å the atomic columns along which electrons are channeled. The –Nb–O–Nb– columns are represented by 1*S* Bloch waves with a half-width of the order of 0.1 Å and the –W–O–W– columns are represented by 2*S* Bloch waves, which give aureoles with diameters of the order of 1 Å. A chemical analysis of the sample is performed on the basis of the brightness of the peaks in the Patterson map. © *1997 American Institute of Physics.* [S0021-3640(97)01018-9]

PACS numbers: 61.66.Dk

In Ref. 1 it was stated that the atomic structure of a crystal can be observed *in situ* with a Rayleigh point resolution of 0.2–0.3 Å, while the best high-resolution electron microscope in the world, JEOL-JEM-ARM 1250, located in Stuttgart, gives a resolution of 1.0–1.1 Å. An example is given below of an implementation of a method demonstrated at the International School of Electronic Spectroscopy in Halle in September 1995. Special care is taken to eliminate spurious peaks which do not correspond to atomic columns.

The investigation was conducted on the tetragonal tungsten bronze TTB (W, Nb, O) sample investigated in detail in Ref. 2. A Patterson map (Fig. 1) was constructed from the dynamic electron diffraction pattern of TTB by means of a two-dimensional Fourier transform.[1] The images of –Nb–O–Nb– and –W–O–W– chains differ sharply in this map. The 1*S* waves channel along chains of the first type, and 1*S* and 2*S* waves, which are surrounded by aureoles[3] with a diameter of about 3 Å, channel along chains of the second type.

Besides W ($Z=74$) and Nb ($Z=41$), the –W–O–W– and –Nb–O–Nb– columns contain oxygen O ($Z=16$). The projected potential increases to $Z=90$ and $Z=56$, respectively, and the parameter ρ decreases from 0.19 Å for W to 0.13 Å for –W–O–W– and from 0.27 Å for Nb to 0.21 Å for –Nb–O–Nb–. In accordance with Eq. (6) of Ref. 1, conditions are created for ψ_{1S} and ψ_{2S} waves to arise in the case of –W–O–W– chains; this is observed experimentally as ψ_{2S} aureoles (Fig. 2). The estimates obtained for ρ (neglecting the variation of the screening radius along a chain) make it possible to construct tables of the main quantities appearing in the experiment (Table I).

Four –Nb–O–Nb– chains surround one –W–O–W– chain and five –Nb–O–Nb–

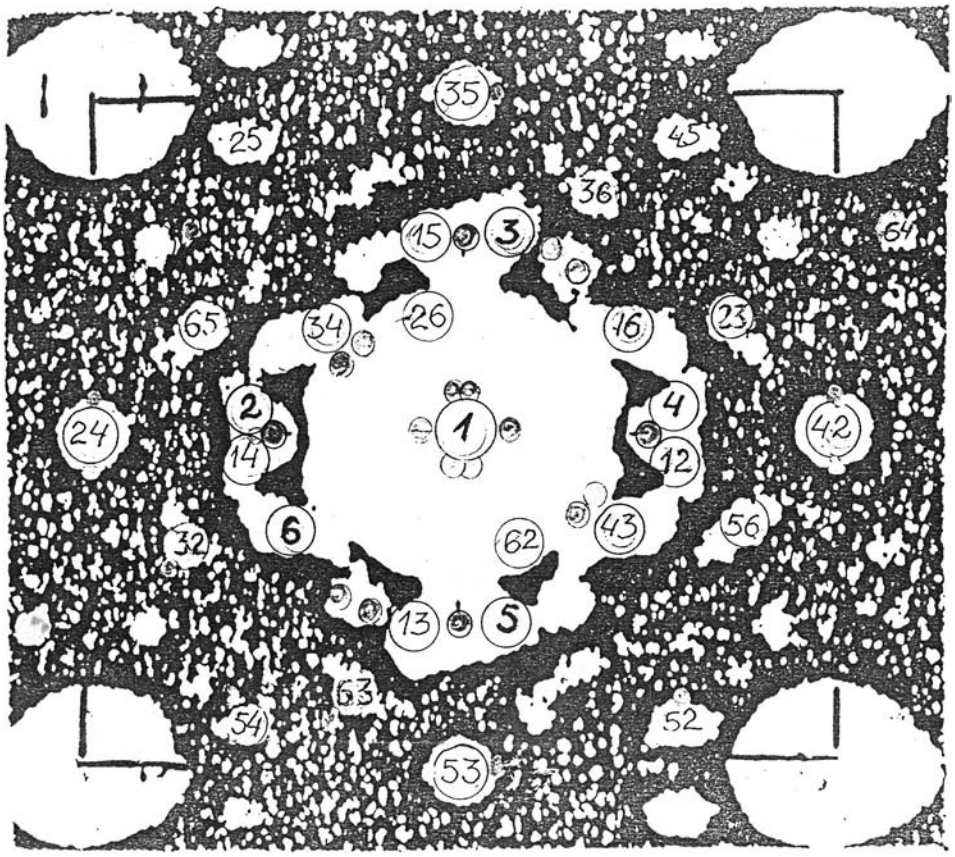

FIG. 1. Patterson map for tetragonal tungsten bronze.

chains surround the other –W–O–W– chain along circles with a diameter of about 4 Å and give spots which are less bright, since the atomic numbers Z for W and Nb are 74 and 41, respectively, and to a first approximation the intensity of the image is proportional to Z^2 (an accurate estimate is given in Ref. 1). These nine –Nb–O–Nb– chains, multiplying according to general rules, give 64 spurious chains, which can be eliminated by Burger's rule.[4] Therefore a chemical analysis of the sample can be performed by comparing the brightness of the spots in the Patterson map. Oxygen ($Z=16$) is almost unnoticeable against the background formed by the heavy chains. In Fig. 3 the circles mark four oxygen peaks, forming a 4×4 Å cross, and some uninterpreted peaks at distances of 0.5 and 0.3 Å. It can be assumed that the oxygen structure of TTB is formed by 4×4 Å crosses not only around the –W–O–W– chains but also around the –Nb–O–Nb– chains, not counting the oxygen in the W–O–W and –Nb–O–Nb– chains. Then the (2W, 9Nb) structure, i.e., 11 heavy chains, contains only $11\times5=55$ oxygen atoms. The distance between the –Nb–O–Nb– chains equals approximately 1 Å.

Besides the –Nb–O–Nb– chains, revealed in the Patterson map by the (W, Nb)

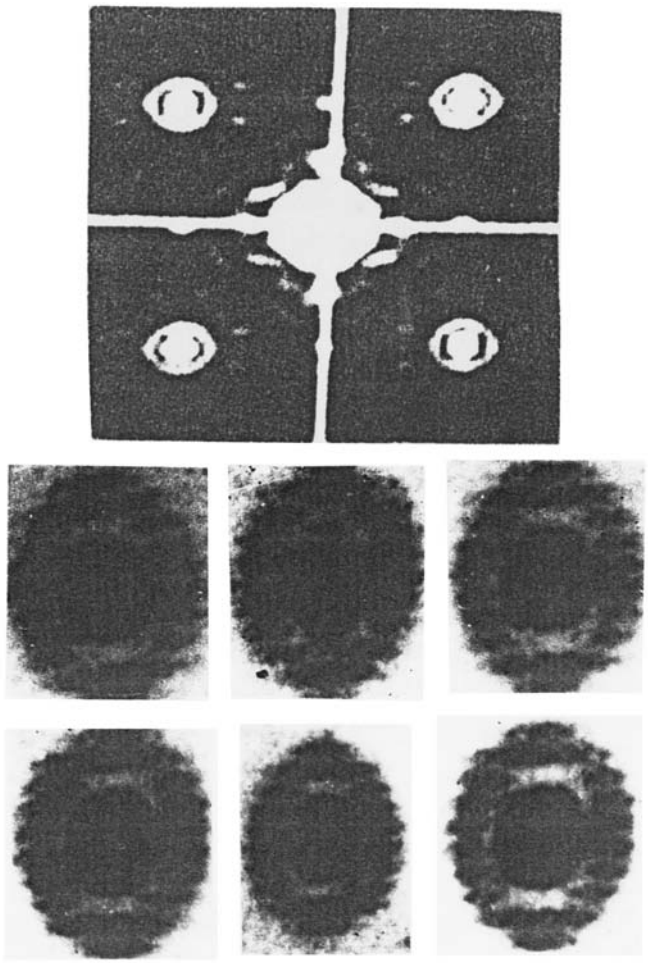

FIG. 2. Aureoles around –W–O–W– chains.

peaks, spurious peaks are also seen in this map. We attempted to eliminate the spurious peaks by Burger's method,[4] but this method is less effective for crystals than for a separate group of atoms. To avoid misunderstandings, we note that in the interpretation of an atomic structure the question is not one of distinguishing overlapping atomic images, which in Patterson's method is a very difficult problem,[4] but rather distinguishing the images of sharp peaks of width 0.1 Å and less which arise in the electron density at the exit from the foil transilluminated in the electron diffraction camera under electron channeling conditions. We shall simplify the main results,[1] using the well-known expression for the Bohr radius for the wave function of hydrogen,

$$\alpha_0 = h^2/m_o e^2 = 0.59 \text{ Å}, \tag{1}$$

TABLE I.

	W–O–W chain	Nb–O–Nb chain
ρ	0.13 Å	0.21 Å
Half-width of the intensity of the electron peak $\lvert\psi_{1S}\rvert^2$ at the exit from the foil 0.346ρ	0.045 Å	0.072 Å
Diameter of ψ_{2S} aureole approximately 10ρ	1.3 Å	–
Half-width of electron diffraction spot 2ρ	0.26 Å	0.42 Å
Rayleigh point resolution 2.6ρ	0.34 Å	1.0 Å *

*The last estimate is apparently exaggerated: No overlapping of the images of Nb–O–Nb chains is noticeable in the Patterson map. Moreover, intermediate chains, displaced by 0.5 Å, and separate regular intensity spots (dumbbell type) at a distance of 0.3 Å are seen, in complete agreement with the theoretical estimates discussed at the International Electron Microscopy School in Halle, Germany in 1995 and at the author's lectures in Stuttgart and Berlin in February 1996 and at the University of Antwerp in September 1996.

where m_0 and e are the electron mass and charge. From Eq. (1) above and Eq. (4) of Ref. 1 it follows that

$$\rho = 1.13 Z^{2/3} d/(1 + eH/m_0 c^2),$$

where H is the accelerating voltage of the microscope and d is the distance between the heavy atoms in a chain. In our case $H = 200$ keV and $d = 3.97$ Å. Hence it follows that $\rho = 0.13$ Å for –W–O–W– chains and $\rho = 0.16$ Å for –Nb–O–Nb– chains. The spot width in a Patterson map equals 2ρ, i.e., 0.26 and 0.32 Å, respectively, not counting the aforementioned aureoles of diameter 1.3 Å in the first case.

According to Ref. 1, the brightness of the peaks in a Patterson map is determined by the quantities $Z_i Z_s$. This makes it possible to perform a chemical analysis of the sample using Table II. The (W, O) intensity approaches that of (Nb, Nb) and can account the 4×4 Å cross of peaks in the X, Y planes. In this case it can be assumed that the same oxygen crosses surround all heavy chains, so that the unit cell contains two W, nine Nb, and fifty-five O.

At the end of the present investigation it became apparent that it is possible to obtain a resolution of the order of 10^{-3} Å and that the atomic structure can be analyzed with a discrepancy factor R of the order of 5–6%. This corresponds to a transition from electron diffraction analysis to electronic crystallography and to a resolution which is two orders

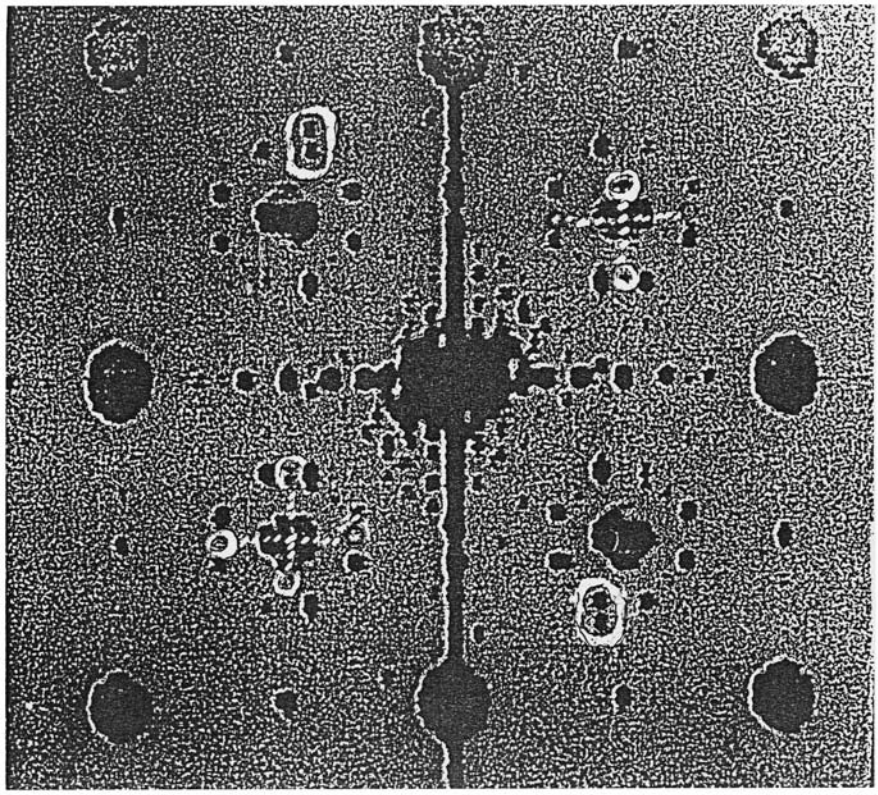

FIG. 3. Oxygen peaks and unidentified atoms (marked by circles) with distances 0.5 Å and 0.3 Å.

of magnitude higher than that of the best electron microscopes. Such a resolution has been possible only in x-ray diffraction crystallographic analysis, but here it is impossible to observe atomic structure *in situ*.

I am deeply grateful to V. V. Klechkovskaya, Margaret Sundberg, Monica Lundberg, and V. V. Volkov for fruitful discussions of the results. I am also grateful to the Universities of Oxford, Stuttgart, and Antwerp, the Institute of Metal Physics Research at the Max Planck Institute (Stuttgart), the Institute of Crystallography of the Russian Acad-

TABLE II. Brightness of peaks in the Patterson map.

Peaks	Brightness
(W, W)	$Z_W Z_W = 74^2 = 5476$
(Nb, Nb)	$Z_{Nb} Z_{Nb} = 41^2 = 1681$
(W, Nb)	$Z_W Z_{Nb} = 74 \times 41 = 3034$
(W, O)	$Z_W Z_O = 74 \times 16 = 1184$

emy of Sciences, and the Institute of Microstructure Physics (Halle) for their interest in this work. This work was performed under the Russian Fund for Fundamental Research Grant No. 96-03-32772a.

[1] V. L. Indenbom and S. B. Tochilin, JETP Lett. **62**, 268 (1995).
[2] M. Sundberg and M. Lundberg, Chem. Scr. **28**, 7780 (1988).
[3] V. L. Indenbom and S. B. Tochilin, Zh. Éksp. Teor. Fiz. **98**, 1402 (1990) [Sov. Phys. JETP **71**, 782 (1990)].
[4] B. K. Vaĭnshteĭn, *Modern Crystallography* [in Russian], Nauka, Moscow, 1981.

Translated by M. E. Alferieff

Multiply-charged magnetoexcitons in low-dimensional structures

A. O. Govorov and A. V. Chaplik[a)]
Institute of Semiconductor Physics, Russian Academy of Sciences, 630090 Novosibirsk, Russia

(Submitted 25 August 1997)
Pis'ma Zh. Éksp. Teor. Fiz. **66**, No. 6, 423–427 (25 September 1997)

The frequencies and intensities of absorption lines of a ''hole + N electrons'' complex in a magnetic field are found. The motion of all particles is assumed to be two-dimensional, and the electron and hole quantum wells are assumed to be spatially separated. It is shown how Kohn's theorem can be extended to the case of a system with a finite total mass. The energy of a N-electron complex in a quantum ring oscillates as a function of the magnetic flux with a period that depends on N and the ratio of the masses. © *1997 American Institute of Physics.* [S0021-3640(97)01118-3]

PACS numbers: 71.35.Ji

Charged excitons (''hole + two electrons'' or ''electron + two holes'' complexes) were recently discovered experimentally in quantum wells (QWs).[1] An interesting idea, making it possible in principle to realize a multiply-charged exciton, i.e., a bound state of a hole and $N>2$ electrons, was recently proposed by Yudson.[2] In the structure proposed (see Fig. 1) the distance d from the metal electrode to the electron QW is much less than the distance l to the hole QW. Then the Coulomb repulsion of the electrons is suppressed more strongly by the image forces in the metal than is the attraction of the electrons to the hole, and for a sufficiently small ratio d/l the system ''hole + N electrons'' can be stable for N appreciably greater than 1. The conditions of equilibrium for $N=3, 4$ in the case of classical mechanics were found in Ref. 2.

In the present letter we calculate the energy spectrum and infrared absorption of a multiply charged exciton in crossed electric and magnetic fields using the basic parameter of the problem $d/l \ll 1$.

1. The electron–hole potential interaction energy has the form

$$U(\mathbf{r}_h,\mathbf{r}_i)=(e^2/\epsilon)[-1/\sqrt{(\mathbf{r}_h-\mathbf{r}_i)^2+(l-d)^2}+1/\sqrt{(\mathbf{r}_h-\mathbf{r}_i)^2+(l+d)^2}],$$

where ϵ is the dielectric constant of the medium and $\mathbf{r}_h$ and $\mathbf{r}_i$ are, respectively, the electron and hole coordinates in the plane of the structure. It is easy to see that for $d \ll l$ the important values of $|\mathbf{r}_h-\mathbf{r}_i|$ are also much less than l and therefore $U(\mathbf{r}_h,\mathbf{r}_i)$ can be expanded up to quadratic terms. This gives the Hamiltonian of the system (in the presence of a magnetic field $\mathbf{B}$ directed along the z axis and an electric field $\mathbf{F}$ along the y

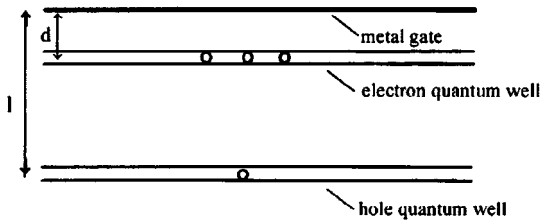

FIG. 1. Transverse cross section of a system with spatially separated electron and hole quantum wells near a metal gate.

axis) in which the electron–hole interaction is quadratic. We note that the electron–electron interaction can be arbitrary. Let us make a change of variables to permit separation of some electron degrees of freedom:

$$\mathbf{R}_c=\sum_{i=1}^{N}\frac{\mathbf{r}_i}{N},\quad \mathbf{R}_1=\frac{\mathbf{r}_1-\mathbf{r}_2}{\sqrt{1\cdot 2}},$$

$$\mathbf{R}_2=\frac{\mathbf{r}_1+\mathbf{r}_2-2\mathbf{r}_3}{\sqrt{2\cdot 3}},\quad \ldots,\quad \mathbf{R}_{N-1}=\frac{\mathbf{r}_1+\mathbf{r}_2+\ldots-(N-1)\mathbf{r}_N}{\sqrt{(N-1)N}}. \tag{1}$$

Then the Hamiltonian decomposes into a part $\hat{H}_1(\mathbf{r}_h,\mathbf{R}_c)$ that depends only on $\mathbf{r}_h$ and $\mathbf{R}_c$ and a part $\hat{H}_2(\mathbf{R}_1,..,\mathbf{R}_{N-1})$ that describes the motion of electrons relative to one another. We shall be interested only in the part

$$\hat{H}_1(\mathbf{r}_h,\mathbf{R}_c)=\frac{\hat{\mathbf{P}}_c^2}{2m_1}+\frac{\hat{\mathbf{P}}_h^2}{2m_2}+\frac{k}{2}(\mathbf{r}_h-\mathbf{R}_c)^2-e_1\mathbf{F}\cdot\mathbf{R}_c-e_2\mathbf{F}\cdot\mathbf{r}_h\,. \tag{2}$$

Here $m_1=Nm_e^*$ and $m_2=m_h^*$, where $m_{e(h)}^*$ are the electron (hole) effective masses. The generalized momenta are given by $\hat{\mathbf{P}}_c=-i\partial/\partial\mathbf{R}_c-(e_1/c)\mathbf{A}_c$ and $\hat{\mathbf{P}}_h=-i\partial/\partial\mathbf{r}_h-(e_2/c)\mathbf{A}_h$, where $\mathbf{A}_{c(h)}$ is the vector potential, the charges $e_1=-N|e|$ and $e_2=|e|$, and $\hbar\equiv 1$. Thus the problem reduces to the motion of two particles with masses $m_{1(2)}$ and charges $e_{1(2)}$, which interact according to the law $k(\mathbf{r}_h-\mathbf{R}_c)^2/2$, where $k=6N(de^2/\epsilon l^4)$. We can see that the system possesses characteristic modes in which the electrons move as a whole relative to the hole. In the absence of external fields this motion corresponds to frequency

$$\omega_0^2=\frac{k}{\mu}=\frac{6de^2}{\epsilon m_e^* l^4}\left(1+N\frac{m_e^*}{m_h^*}\right), \tag{3}$$

where $1/\mu=1/m_1+1/m_2$. Equation (3) expresses another generalization of Kohn's theorem:[3–5] The frequency of a collective mode corresponds to the motion of the center of masses of electrons in a parabolic potential, but in the present case ω_0 depends on the number of particles for purely kinematic reasons. In the limit $m_h^*\to\infty$ we arrive at the previous result for a quantum dot.[4,5]

We now consider the situation in crossed fields. To simplify the equations, we shall denote the coordinates of the centers of mass of the electrons as (x_1,y_1) and the coordinates of the hole as (x_2,y_2). The total momentum of the system in a magnetic field is given by $\hat{\mathbf{P}}=-i\boldsymbol{\nabla}_1-i\boldsymbol{\nabla}_2-e_1\mathbf{A}_1/c-e_2\mathbf{A}_2/c+[\mathbf{B}\cdot(e_1\mathbf{r}_1+e_2\mathbf{r}_2)]$. We shall employ the Landau gauge for the vector potential: $\mathbf{A}_i=(-By_i,0)$, where $i=1,2$. In this gauge the x component of the total momentum P_x is conserved, and x_1 and x_2 appear in the Hamiltonian only in the combination $x_1-x_2=x$. After separating out the factor $\exp(iP_xX)$ in the total wave function, where $X=(m_1x_1+m_2x_2)/M$ and $M=m_1+m_2$, we obtain

$$\hat{H}_1(x,y_1,y_2)=\frac{\hat{p}_x^2}{2\mu}+\frac{\hat{p}_{y1}^2}{2m_1}+\frac{\hat{p}_{y2}^2}{2m_2}+\hat{p}_x(\omega_1y_1-\omega_2y_2)+\frac{m_1}{2}\left(\omega_1y_1+\frac{P_x}{M}\right)^2$$
$$+\frac{m_2}{2}\left(\omega_2y_2+\frac{P_x}{M}\right)^2+\frac{k}{2}[x^2+(y_1-y_2)^2]-e_1y_1F-e_2y_2F, \tag{4}$$

where $\omega_i=e_iB/m_ic$ $(i=1,2)$ and the operator $\hat{p}_x=-i\partial/\partial x$. It is now convenient to treat $\hat{p}_x$ as a generalized coordinate and $\hat{x}=i\partial/\partial p_x$ as a generalized momentum. In this representation $\hat{H}_1(p_x,y_1,y_2)$ corresponds to a three-dimensional anisotropic oscillator with the kinetic energy operator

$$\hat{T}=-\frac{1}{2m_1}\frac{\partial^2}{\partial y_1^2}-\frac{1}{2m_2}\frac{\partial^2}{\partial y_2^2}-\frac{k}{2}\frac{\partial^2}{\partial p_x^2} \tag{5}$$

and the potential energy operator

$$W=\frac{p_x^2}{2\mu}+p_x(\omega_1y_1-\omega_2y_2)+\frac{m_1}{2}\left(\omega_1y_1+\frac{P_x}{M}\right)^2+\frac{m_2}{2}\left(\omega_2y_2+\frac{P_x}{M}\right)^2+\frac{k}{2}(y_1-y_2)^2$$
$$-e_1y_1F-e_2y_2F. \tag{6}$$

The linear terms can be removed by shifting with respect to p_x, y_1, and y_2, which gives

$$W=\frac{p_x^2}{2\mu}+p_x(\omega_1y_1-\omega_2y_2)+\frac{m_1\omega_1^2}{2}y_1^2+\frac{m_2\omega_2^2}{2}y_2^2+\frac{k}{2}(y_1-y_2)^2$$
$$+\frac{cF}{B}P_x-\frac{Mc^2}{2}\frac{F^2}{B^2}. \tag{7}$$

The last two terms in Eq. (7) have the same form as for a separate particle in crossed fields: They describe the drift of the entire complex with the velocity $\partial E/\partial P_x=cF/B$. The oscillatory part of the energy is found by diagonalizing $\hat{T}+W$. As a result the energy has the form

$$E_{n_1,n_2,n_3}(P_x)=\sum_{j=1,2,3}\Omega_j\left(\frac{1}{2}+n_j\right)+\frac{cF}{B}P_x-\frac{Mc^2}{2}\frac{F^2}{B^2}. \tag{8}$$

The three characteristic frequencies in Eq. (8) are determined by the equation

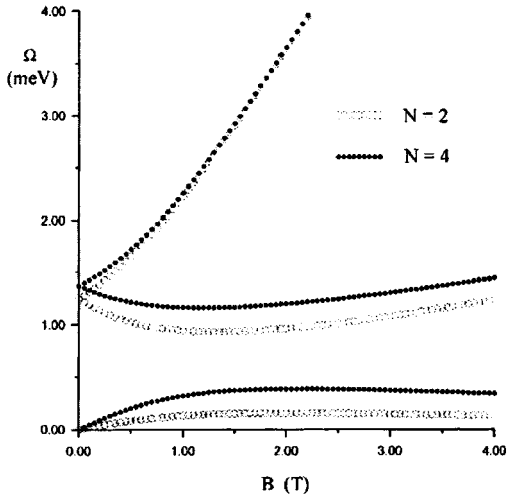

FIG. 2. Exciton excitation energies $\Omega_{1,2,3}$ as a function of the magnetic field for GaAs quantum wells; $N=2,4$, heavy hole and electron masses $m_h^*=0.5\ m_0$, $m_e^*=0.07\ m_0$; system parameters $d=200$ Å, $l=600$ Å.

$$\left(\frac{k}{\mu}-\Omega^2\right)\left[\frac{m_1m_2}{k}(\Omega^2-\omega_1^2)(\Omega^2-\omega_2^2)-m_1(\Omega^2-\omega_1^2)-m_2(\Omega^2-\omega_2^2)\right]$$
$$+\Omega^2(m_1\omega_2^2+m_2\omega_1^2)-M\omega_1^2\omega_2^2-k(\omega_1-\omega_2)^2=0. \tag{9}$$

The roots of the equation (9) which are cubic in Ω^2 have a physically clear asymptotic behavior. In weak magnetic fields

$$\Omega_{1,2}=\omega_0\pm\frac{1}{2}\left|\omega_1\frac{m_2}{M}+\omega_2\frac{m_1}{M}\right|, \quad \Omega_3=\frac{|e_1+e_2|B}{cM}. \tag{10}$$

The third mode corresponds to a cyclotron motion of a charged exciton with total mass $M=m_h^*+Nm_e^*$. For a neutral exciton $e_1+e_2=0$ the frequency Ω_3 vanishes for any B; a neutral exciton moves freely. The existence of the mode Ω_3 distinguishes our case from a parabolic quantum dot, where the spectrum is exhausted by the frequencies $\Omega_{1,2}$ $(M\to\infty)$.[4,5]

As B increases, anticrossing of the two lower branches Ω_2 and Ω_3 occurs. As $B\to\infty$ the frequencies $\Omega_{1,2}$ approach the cyclotron frequencies $|\omega_{1(2)}|=|e|B/cm_{e(h)}^*$ and Ω_3 $\propto 1/B$. The numerical solutions of Eq. (9) for excitons with $N=2$, 4 in GaAs quantum wells are presented in Fig. 2. For an exciton based on a heavy hole in GaAs the characteristic frequency $\omega_0\simeq 1.2$ meV for the parameters $N=2$, $d=200$ Å, and $l=600$ Å.

2. It is not difficult to calculate the intensities of the IR absorption lines for a multiply charged magnetoexciton. In weak ($|\omega_{1,2}|\ll\omega_0$) magnetic fields the line intensities are given by the formulas

$$I_1\simeq I_2\propto\frac{(m_1e_2-m_2e_1)^2}{M}, \quad I_3\propto\frac{(e_1+e_2)^2}{M}. \tag{11}$$

In strong magnetic fields I_1, $I_2 \to$ const, and $I_3 \propto 1/B^2$.

3. In a previous work,[6] one of us showed that the binding energy of a neutral exciton in a one-dimensional quantum ring contains a contribution due to electron-to-hole tunneling along the ring. This contribution oscillates with a universal period Φ_0 as a function of the flux threading the ring. Calculations similar to those of Ref. 6 for a $N+1$-particle complex show that the period of the oscillatory part of the energy is

$$\Phi_0^* = \Phi_0 \frac{m_h^* + N m_e^*}{N(m_h^* + m_e^*)}. \tag{12}$$

For $m_h^* \gg N m_e^*$ the period becomes Φ_0/N, as should be the case for coherent tunneling of N particles. At the same time, the motion of the complex as a whole along the ring makes the contribution

$$E_J = \frac{1}{MR_r^2}\left(J - \frac{Q\Phi}{hc}\right)^2, \quad J = 0, \pm 1, \pm 2, .., \tag{13}$$

to the energy, where $Q = e_1 + e_2 = -(N-1)|e|$ is the total charge, Φ is the magnetic flux, and R_r is the radius of the ring. Therefore the persistent current as a function of Φ oscillates with a period of $\Phi_0/(N-1)$.

The results of Sec. 3 for a one-dimensional ring are exact and do not involve a parabolic approximation of the interaction.

We thank Yu. A. Bychkov and É. I. Rashba for a helpful discussion. This work was sponsored by INTAS (Grant No. 94-1172) and the program ''Solid-State Nanostructures.''

[a)]e-mail: Chaplik@isp.nsc.ru

---

[1] A. J. Shields *et al.*, in *High Magnetic Fields in the Physics of Semiconductors*, edited by G. Landwehr and W. Ossau, World Scientific, Singapore, 1997, Vol. 2, p. 737.
[2] V. I. Yudson, Phys. Rev. Lett. **77**, 1564 (1996).
[3] L. Brey, N. Johnson, and B. Halperin, Phys. Rev. B **40**, 10 647 (1989).
[4] A. O. Govorov and A. V. Chaplik, JETP Lett. **52**, 31 (1990).
[5] P. A. Maksym and T. Chakraborty, Phys. Rev. Lett. **65**, 108 (1990).
[6] A. V. Chaplik, JETP Lett. **62**, 900 (1995).

Translated by M. E. Alferieff

Skyrmion mass and a new kind of cyclotron resonance for the 2D electron gas

S. V. Iordanskii
L. D. Landau Institute of Theoretical Physics, Russian Academy of Sciences, 142432 Chernogolovka, Moscow Region, Russia

(Submitted 25 August 1997)
Pis'ma Zh. Éksp. Teor. Fiz. **66**, No. 6, 428–431 (25 September 1997)

The skyrmionic mass is calculated using a gradient expansion method. A special cyclotron resonance is predicted, with a frequency determined by the exchange energy. The possibility of an extra bound electron is discussed. © *1997 American Institute of Physics.* [S0021-3640(97)01218-8]

PACS numbers: 12.39.Dc, 71.10.Ca, 76.40.+b

The skyrmion energy and charge for 2D electron systems at high magnetic fields were calculated in Refs. 1–4 and in Refs. 5 and 6. The difference in the expressions for the energy in those studies stems from the fact that the kinetic energy was treated as a constant cyclotron energy in Refs. 2–4 and as a differential operator in Refs. 5 and 6. For experimental investigations of the existence of skyrmions it is useful to find specific properties which can be checked by physical measurements. I discuss here the problem of the skyrmion motion as a whole, which is not directly connected with its internal energy. For the calculations I shall use the approach developed in Refs. 6 and 7.

This approach is based upon the transformation $\psi = U\chi$ of the electron spinors ψ to new spinors χ by means of a nonsingular rotation matrix $U(\mathbf{r})$. In this manner one gets a Hartree–Fock equation for the spinor χ. For the extremely simple case of local exchange, considered in this paper, it takes the form

$$i\frac{\partial \chi}{\partial t} = \frac{1}{2m}(-i\nabla_k - A_{0k} + \Omega_k^l \sigma_l)^2 \chi - \gamma \sigma_z \chi + \Omega_t^l \sigma_l \chi.$$

Here σ_l are Pauli matrices and $-iU^+ \partial_k U = \Omega_k^l \sigma_l$, with

$$\vec{\Omega}^z = \frac{1}{2}(\nabla\alpha + \cos\beta \nabla\alpha),$$

$$\vec{\Omega}^x = \frac{1}{2}(\sin\beta \cos\alpha \nabla\alpha - \sin\alpha \nabla\beta), \tag{1}$$

$$\vec{\Omega}^y = \frac{1}{2}(\sin\beta \sin\alpha \nabla\alpha + \cos\alpha \nabla\beta),$$

and γ is the exchange constant. We assume that the Euler angles are α, β, α, with two equal angles to avoid the singularity in Ω^l for a nontrivial degree of mappings Q, and suppose that $\cos\beta = -1$ at the singular point of $\alpha(\mathbf{r})$ (Refs. 6 and 7). This equation for

the electrons in the field of rotation matrix U is fully equivalent to the unrotated Hartree–Fock equation with $\Omega^l=0$ but with a nonuniform exchange term $-\gamma\mathbf{n}(\mathbf{r})\boldsymbol{\sigma}$. Here $\mathbf{n}(\mathbf{r})$ is the unit vector in the direction of the mean spin. We use the system of units with $\hbar=B=l_B=1$, where B is the external magnetic field, l_B is the magnetic length.

We shall assume that the rotation matrix which adjust the spin direction to a given mean spin direction at any point of the 2D plane depends on the position of the skyrmion center $U=U(\mathbf{r}-\mathbf{X})$ and calculate the proper term in the skyrmion action due to the time dependence of $\mathbf{X}(t)$. For the calculation we need to find the electron action for the ground state in the field of the matrix U. In the proper electron Hamiltonian we have the additional perturbation term[6,7]

$$H_1=iU^+\nabla U\mathbf{X}_t=-\vec{\Omega}^l\sigma_l\mathbf{X}_t\,.$$

In order to find the proper term in the skyrmionic action we must perform perturbation theory calculations in H_1.

Due to the isotropy of the system there is no linear term in $\mathbf{X}_t$, and we must find the second-order term in the action $S=i\ \mathrm{Tr}\ \ln G$ where G is the electronic Green function. The second-order term in the action is

$$\delta S=\frac{i}{2}\ \mathrm{Tr}\ H_1G_0H_1G_0\,, \tag{2}$$

where G_0 is the unperturbed Green function for the Hartree–Fock equation with $\Omega^l=0$

$$G_0(\mathbf{r},\mathbf{r}',t-t')=\sum_{s,p}\int\frac{d\omega}{2\pi}e^{i\omega(t'-t)}g_s(\omega)\Phi_{s,p}(\mathbf{r})\Phi^+_{s,p}(\mathbf{r}')\,. \tag{3}$$

Here $\Phi_{s,p}$ are normalized Landau wave functions in the Landau gauge and the summation is over all s and p. The matrices $g_s(\omega)$ correspond to the complete filling of the lowest spin sublevel for $s=0$,

$$g_0(\omega)=\frac{1+\sigma_z}{2}\,\frac{1}{\omega-\omega_c/2+\gamma-i\delta}+\frac{1-\sigma_z}{2}\,\frac{1}{\omega-\omega_c/2-\gamma+i\delta}, \tag{4}$$

while all the other states are empty,

$$g_s(\omega)=\frac{1}{\omega-\omega_c(s+1/2)+\gamma\sigma_z+i\delta}, \tag{5}$$

where $\delta\to(+0)$.

The main term in (2), with no derivatives of Ω^l and $\mathbf{X}_t$, corresponds only to $s=0$. Also, only the cross terms are important, with poles in ω above and below the real axis:

$$\delta S=\frac{1}{2}\int\mathrm{Tr}(\vec{\Omega}^l\mathbf{X}_t\sigma_l)g_0(\omega)(\vec{\Omega}^{l'}\mathbf{X}_t\sigma_{l'})g_0(\omega)e^{i\delta\omega}\frac{d\omega}{2\pi}\,\frac{d^2r}{2\pi}dt. \tag{6}$$

Here we perform the integration over intermediate space coordinates and the summation over p. It is easy to see that only the terms with $l=l'\neq z$ give a nonzero contribution. Using the isotropy and performing simple integration over ω, we get

$$\delta S=\frac{1}{2\gamma}\sum_{l\neq z}\int\frac{(\Omega_x^l)^2+(\Omega_y^l)^2}{2}\dot{X}^2\frac{d^2r}{2\pi}dt=\int\frac{\dot{X}^2}{16\gamma}\left(\frac{\partial n_i}{\partial r_k}\right)^2\frac{d^2r}{2\pi}dt. \tag{7}$$

Here we use the expressions (1) for Ω^l and introduce the unit vector

$$\mathbf{n}=(\cos\beta,\sin\beta\cos\alpha,\sin\beta\sin\alpha).$$

It is known that for the state with minimal skyrmion energy for the given degree of mapping Q the value of the space integral[8] is

$$\frac{1}{2}\int\left(\frac{\partial n_i}{\partial r_k}\right)^2 d^2r=4\pi|Q|.$$

Therefore the kinetic energy term in the Lagrangian is $E_{\rm kin}=m\dot{X}^2/2$, where $m_s=|Q|/2\gamma$ or in ordinary units,

$$m_s=eB|Q|/2c\gamma,$$

where B is the external magnetic field. As has been obtained in a number of papers (see, e.g., Refs. 3–5) the skyrmion has a charge eQ. For a charged skyrmion there are also terms linear in $\mathbf{X}_t$ in the Lagrangian, corresponding to the product of the skyrmion current and the vector-potential of the external magnetic field $\mathbf{B}$, namely $Q\mathbf{X}_t\mathbf{A}_0$. This term can also be calculated by differentiation of the proper additional phase of the wave function obtained by translation of the skyrmion charge eQ. Therefore the full Lagrangian for the motion of the skyrmion as a whole is (in ordinary units)

$$L=\frac{m_s\dot{X}^2}{2}+\frac{e}{c}Q\dot{\mathbf{X}}\cdot\mathbf{A}_0.$$

The Hamiltonian momentum conjugate to $\mathbf{X}$ is $P_i=\partial L/\partial\dot{X}_i$ which can be considered as a quantum operator with the usual commutation relations $[P_iX_i]=i\hbar$. Therefore one has the cyclotron energy for the motion of the skyrmion as a whole

$$\hbar\omega_s=eB/m_sc=2\gamma.$$

The minimal energy of such motion is

$$\hbar\omega_s/2=\gamma$$

and must be added to the internal energy of the skyrmion. In experiments with a sufficient number of charged skyrmions one should observe a cyclotron resonance at a frequency determined by the exchange energy per electron:

$$\omega_s=\frac{1}{\hbar}2\gamma=\frac{e^2}{\hbar l_B}\sqrt{2\pi},$$

where $l_B=\sqrt{c\hbar/eB}$. The final expression is obtained from the expression for the exchange energy for a completely filled Landau level.

The preceding considerations have some important consequences. The thermodynamic energy of a system with a given chemical potential is the quantum average $\langle H-\mu N\rangle$, where H is the Hamiltonian, $\mu=\hbar\omega_c/2$ is the chemical potential, and N is the particle number. The change of the total thermodynamic energy due to the formation of

the charged skyrmion is $E_{\rm tot}=E_{\rm int}+\gamma$, where $E_{\rm int}$ is the internal energy of the skyrmion, not including that due to its motion as a whole in the external magnetic field. If one puts an extra electron in the skyrmion core, its energy will consist of two main parts. One part is the increase in the exchange energy γ because the added electron must have the reverse spin direction, according to Pauli principle (all lower states are filled). The other part is the negative Coulomb energy due to the electron interaction with the skyrmion charge, $\sim -e^2Q/L_c$, where L_c is the skyrmion core size. All other terms in the electron energy are comparatively small $\sim 1/L_c^2$ and can be neglected for a large size of the core. The added electron make the total skyrmion–electron complex neutral. Therefore there is no correction to its energy connected with the motion of the complex as a whole in the external magnetic field. The lowest energy of the complex is $E_{\rm compl}=E_{\rm int}+\gamma -{\rm const}\cdot e^2Q/L_c$, which is lower than the energy of the charged skyrmion for positive Q and $\mu=\hbar\omega_c/2$. One sees that a skyrmion with a large core size and positive charge must bind an electron and become neutral. The spin of this electron is reversed with respect to the direction of the average spin in the middle of the core, i.e., it coincides with the direction of the mean spin at large distances from the core. The results of Refs. 5 and 6 give a negative thermodynamic energy $E_{\rm int}$ because of the strong reduction of the kinetic energy by $-\hbar\omega_c/2$ for $\mu=\hbar\omega_c/2$. Therefore such neutral skyrmions must be spontaneously created.

The calculations reported here use the assumption of a large size of the skyrmion core; otherwise the perturbation theory in Ω_l is invalid. A large core size requires a small enough g factor (see, e.g., Ref. 6). The conclusions of this study must be numerically checked using the actual values of the g factor and magnetic field.

The research described in this publication was made possible in part by award RP1-273 of the US CRDF for the countries of the FSU. It was also supported by INTAS Grant 95-1/Ru-675.

[1] S. Sondhi, A. Kahlrede, S. Kivelson, and E. Rezayi, Phys. Rev. B **47**, 16418 (1993).
[2] H. Fertig, L. Brey, R. Cote, and A. MacDonald, Phys. Rev. B **50**, 11018 (1994).
[3] K. Moon, H. Mori, Kun Yang *et al.*, Phys. Rev. B **51**, 5138 (1995).
[4] Yu. Bychkov, T. Maniv, and I. Vagner, Phys. Rev. B **53**, 10148 (1995).
[5] S. Iordanskii and S. Plyasunov, JETP Lett. **65**, 259 (1997).
[6] S. Iordanskii and S. Plyasunov, Zh. Éksp. Teor. Fiz. **112**, in press (1997) [JETP **85**, in press (1997)]; cond-mat/9706236 (1997).
[7] S. Iordanskii, JETP Lett. **66**, 188 (1997).
[8] A. Belavin and A. Polyakov, JETP Lett. **22**, 114 (1975).

Published in English in the original Russian journal. Edited by Steve Torstveit.

New approach to the theory of spinodal decomposition

I. Ya. Erukhimovich and E. V. Prostomolotova
Department of Physics, Moscow State University, 119899 Moscow, Russia;
Institute of Heteroorganic Compounds, Russian Academy of Sciences, Moscow, Russia

(Submitted 4 August 1997; resubmitted 19 August 1997)
Pis'ma Zh. Éksp. Teor. Fiz. **66**, No. 6, 432–437 (25 September 1997)

A new approach to the study of spinodal decomposition for a scalar field is proposed. The approach is based on treating this process as a relaxation of the one-time correlation function $G(\mathbf{q},\mathbf{t})=\int d\mathbf{r}\langle\phi(0,t)\phi(\mathbf{r},t)\rangle\exp(i\mathbf{q}\cdot\mathbf{r})$, which plays the role of an independent dynamical object (a unique two-point order parameter). The dynamical equation for $G(q,t)$ (the Langevin equation in correlation-function space) is solved exactly in the one-loop approximation, which is the zeroth approximation in the approach proposed. This makes it possible to trace the asymptotic behavior of $G(q,t)$ at long and intermediate times t (from the moment of onset of the spinodal decomposition). The values obtained for the power-law growth exponents for the height and position of the peak in $G(q,t)$ at the intermediate stage is in satisfactory agreement with the data obtained by a number of authors through numerical simulation of the corresponding stochastic equations describing the relaxation of the local order parameter. © *1997 American Institute of Physics.* [S0021-3640(97)01318-2]

PACS numbers: 64.75.+g, 81.30.−t

The question of spinodal decomposition, i.e., the dynamics of phase ordering of systems described by the Landau Hamiltonian beyond the limit of stability of their spatially uniform single-phase state (which we refer to below simply as disordered), arises in many physical applications. The free energy of such systems can be written as a functional integral

$$F=-T\ \ln\frac{\int\delta\varphi\ \exp(-\Phi(\{\varphi(\mathbf{r}\},T)/T)}{\int\delta\varphi\ \exp\left(-\int d\mathbf{x}\varphi(\mathbf{x})\hat{\Gamma}_0\varphi(\mathbf{x})/2\right)}. \tag{1}$$

Here the functional

$$\Phi(\{\varphi(\mathbf{r})\},T)=T\left(\frac{\int d\mathbf{x}\varphi(\mathbf{x})\hat{\Gamma}\varphi(\mathbf{x})}{2}+\int d\mathbf{x}\left(\frac{\alpha\varphi^3}{3!}+\frac{\beta\varphi^4}{4!}\right)\right) \tag{2}$$

is the free energy of the system with a prescribed (generally speaking, nonequilibrium and spatially nonuniform) distribution $\{\varphi(\mathbf{r})\}$ of local values of the order parameter, which, in what follows, we assume for simplicity to be a scalar. The integral operators

$\hat{\Gamma}_0\varphi(\mathbf{x})=\int d\mathbf{x}'\Gamma_0(\mathbf{x}-\mathbf{x}')\varphi(\mathbf{x}')$ and $\hat{\Gamma}\varphi(\mathbf{x})=\int d\mathbf{x}'\Gamma(\mathbf{x}-\mathbf{x}')\varphi(\mathbf{x}')$ are defined by their kernels, which in the Fourier representation have the form

$$\Gamma(q)=\int d\mathbf{x}\Gamma(\mathbf{x})\exp(i\mathbf{q}\cdot\mathbf{x})=\tau+Q^2,\quad \Gamma_0(q)=\tau_0+Q^2,\quad Q^2=a^2q^2, \tag{3}$$

where α, $\beta>0$ and $a^2>0$ are phenomenological constants, and the dimensionless temperature τ characterizes the closeness of the system to the region of instability of its disordered state, which lies in the range $\tau<0$.

The standard formulation of the problem of spinodal decomposition, dating back to Refs. 1–3, consists of the following. The system is initially characterized by some $\tau=\tau_0>0$ and a distribution $\varphi_0(\mathbf{r})$, which is a random function of the coordinates. At this moment the temperature drops abruptly to a negative value $\tau=\tau_1<0$, and the subsequent evolution of the distribution of the order parameter is assumed to satisfy the phenomenological Langevin equation (also called the Landau–Khalatnikov equation[4])

$$\partial\varphi(\mathbf{r},t)/\partial t=-\lambda X(\mathbf{r},t),\quad X=\delta\Phi(\{\varphi(\mathbf{r},t)\},T)/\delta\varphi(\mathbf{r},t), \tag{4}$$

which reflects the idea that the relaxation rate of the order parameter and the corresponding thermodynamic force, defined in accordance with the general approach as a functional derivative of the free energy (2) with respect to the local value of this order parameter, are linearly related. The kinetic coefficient λ is assumed to be free of singularities at $\tau=0$. Confining attention to the first few (quadratic) terms in the expansion of the free energy (2) with respect to φ in the linear-response approximation, assuming the relaxation to be diffusional, and switching to the Fourier transforms, one can rewrite Eq. (4) in the form[1–4]

$$\partial\varphi_{\mathbf{q}}(t)/\partial t=-q^2\lambda(\tau+a^2q^2)\varphi_{\mathbf{q}}(t). \tag{5}$$

As follows from Eq. (5), for $\tau<0$ all initial waves of nonuniformity of the order parameter with wave numbers in the interval $0<Q=qa<\sqrt{|\tau|}$ grow exponentially. This results in the destruction (decomposition) of the disordered state.

The expression for the one-time correlation function

$$G(\mathbf{q},t)=\int d\mathbf{r}\langle\phi(0,t)\phi(\mathbf{r},t)\rangle\exp(i\mathbf{q}\cdot\mathbf{r}) \tag{6}$$

of a system undergoing spinodal decomposition gives a more complete and definite idea about spinodal decomposition. To derive this expression correctly, Eqs. (4) and (5) must be supplemented by a term describing the presence of random forces whose correlation function at different points is related with the value of λ by the fluctuation-dissipation theorem.[5] The simple calculations performed in Ref. 6 lead to the expression

$$G_{\text{Cook}}(\mathbf{q},t)=g(Q)+(G_0(Q)-g(Q))\exp(-2q^2\lambda t/g(Q)), \tag{7}$$

where the averaging is performed over all random realizations (time series) of the external forces and initial conditions and $G_0(Q)=\Gamma_0^{-1}(Q)$ and $g(Q)=\Gamma^{-1}(Q)$ are the correlation functions, calculated by Eqs. (3) in the random-phase approximation, of the

initial and final states, respectively (for $\tau<0$ the correlation function $g(q)$ is physically meaningless).

At long times the thermodynamic force $\delta\Phi(\{\varphi(\mathbf{r},t)\},T)/\delta\varphi(\mathbf{r},t)$ appearing in Eq. (4) becomes a nonlinear function of the order parameter $\varphi(\mathbf{r},t)$. In this case, in contrast to the strict phenomenological linear-response theory, the Langevin equation (4) becomes a nontrivial and constructive method of obtaining a phenomenological description of nonlinear relaxation near a critical point. The procedure for solving this nonlinear and stochastic equation (after a random force is added to its right-hand side) and then averaging for the purpose of obtaining the correlation function (6) has still not been finally worked out, despite a number of constructive attempts based on an approximate decoupling of the two-point correlation functions,[3,7,8] scaling arguments[9–11] concerning the form of the correlation function $G(\mathbf{q},t)$, and analogies with the results of exactly solvable one-dimensional models[12,13] (see also the review in Ref. 14 and the literature cited therein as well as the results[15–21] obtained by solving this equation numerically). Even the question of the existence of scaling for $G(\mathbf{q},t)$ is controversial.[22,23] However, it has been adequately established that the correlation function (6) as a function of q possesses a peak at $q=q_*(t)$ and that at long times both the position $q_*(t)$ and height $I(t)=G(q_*(t),t)$ of this peak exhibit power-law asymptotic behavior:

$$Q_*\sim t^{-\alpha}, \quad I\sim t^{\beta}. \tag{8}$$

In the standard approach described, besides the difficulties indicated, we encounter an important conceptual problem as well. The trouble is that substituting the free energy (2) into the Langevin dynamical equation (4) itself signifies that correlations between local values of the order parameter at different points are neglected, which is entirely natural in the mean-field approximation. However, in the presence of large fluctuations, which are characteristic for the spinodal decomposition phenomenon under study, the possibility of neglecting such correlations is very problematic.

An alternative approach, which to some extent would be free of the shortcomings indicated above, is to study the nonlinear equation governing the relaxation of the correlation function itself instead of solving the nonlinear stochastic equation (4) for the order parameter and then averaging the parameter. Thus far, however, the possibilities of this alternative approach have not been investigated. In the present letter we propose a phenomenological derivation and an analysis of a nonlinear equation describing the relaxation of the correlation function.

Let us represent the free energy (1) in the form

$$F=\min\ \Omega(\{\overline{\Phi}(\mathbf{r})\}, \quad \{G(\mathbf{x}_1,\mathbf{x}_2)\},$$

where the functional $\Omega(\{\overline{\Phi}(\mathbf{r})\}, \{G(\mathbf{x}_1,\mathbf{x}_2)\})$ is the free energy of the system with prescribed (generally speaking, nonequilibrium and spatially nonuniform) distributions of the average values of the order parameter $\{\overline{\Phi}(\mathbf{r})\}$ and the pair correlation function $\{G(\mathbf{x}_1,\mathbf{x}_2)\}$. The so-called second Legendre transformation enables writing the function Ω in the following explicit form:[24–27]

$$\Omega/T=\int\{(\Gamma(\mathbf{x}_1-\mathbf{x}_2)-G^{-1}(\mathbf{x}_1,\mathbf{x}_2))G(\mathbf{x}_1,\mathbf{x}_2)-(\ln G(\mathbf{x}_1,\mathbf{x}_2)$$

$$-\ln g(\mathbf{x}_1,\mathbf{x}_2))d\mathbf{x}_1d\mathbf{x}_2/2\}-\sigma(\{\overline{\Phi(\mathbf{r})}\},\{G(\mathbf{x}_1,\mathbf{x}_2)\})+\int\overline{\Phi(\mathbf{x}_1)}$$

$$\times\Gamma(\mathbf{x}_1-\mathbf{x}_2)\overline{\Phi(\mathbf{x}_2)}d\mathbf{x}_1d\mathbf{x}_2/2-\int h(\mathbf{x})\overline{\Phi(\mathbf{x})}d\mathbf{x}, \tag{9}$$

where the functional $\sigma(\{\overline{\Phi(\mathbf{r})}\},\ \{G(\mathbf{x}_1,\mathbf{x}_2)\})$ is the generating function of all 2-irreducible skeleton diagrams appearing in the expansion of the free energy (2) in powers of the coupling constants α and β. The general procedure for calculating this generating function is well known.[24–28]

In the case of spinodal decomposition the average value of the order parameter over volumes which are large compared with the characteristic scale $l\sim 2\pi/q_*$ of the nonuniformities that arise but small compared with the size L of the entire system remains small as long as $l\ll L$, which is actually the only condition under which one can talk about spinodal decomposition. In other words, the order parameter determined by such large-scale averaging, in contrast to the standard approach, vanishes identically in the thermodynamic limit, so that the correlation function $G(q,t)$ is the only dynamical variable characterizing the departure of the system from equilibrium during spinodal decomposition. Therefore it is natural to write the phenomenological equation describing the relaxation of $G(q,t)$, once it is regarded as a kind of order parameter, in the form of the corresponding Langevin equation

$$\partial G(q,t)/\partial t=-\Lambda(q)X(q), \tag{10a}$$

$$X(q)=\delta\Omega(0,\{G(P,t)\})/\delta G(q,t)=\frac{\Gamma(q)-G^{-1}(q)-\Sigma(q,\{G(q,t)\})}{2}. \tag{10b}$$

Indeed, the relaxation equation (10a) simply states that the relaxation rate of our new order parameter and the corresponding thermodynamic force, which, in accordance with the general approach, is defined in Eq. (10b) as a functional derivative of the free energy (9) with respect to $G(q)$, are assumed to be linearly related. The explicit form of this derivative is written out in Eq. (10b), where the mass operator Σ is the generating function of all 1-irreducible two-pole diagrams (the free energy parts) and itself is a functional of $\{G(q,t)\}$.

We underscore that the arguments presented above are not a derivation of Eq. (10a) from Eq. (4). The two equations are *equally* justified (and equally approximate) phenomenological Langevin equations for *different* order parameters.

A remarkable property of Eq. (10a) is that even its zeroth approximation, in which we assume that $\Sigma(q)\equiv 0$ and to which the present letter is limited, is nonlinear:

$$\frac{\partial G(q)}{\partial t}=\frac{\Lambda(q)}{2}(G^{-1}(q)-\Gamma(q)). \tag{11}$$

We shall determine the form of the new kinetic coefficient $\Lambda(q)$ from the correspondence principle, which requires that the rate of change of the correlation function at short times

$$\left.\frac{\partial G(q)}{\partial t}\right|_{t\to 0}=\frac{\Lambda(q)}{2}(G^{-1}(q,t)-\Gamma(q))|_{t\to 0}=\frac{\Lambda(q)}{2}(\Gamma_0(q)-\Gamma(q)) \tag{12}$$

reproduce the result of the linear-response theory

$$\left.\frac{\partial G_{\text{linear}}(q)}{\partial t}\right|_{t\to 0}=-2q^2\lambda\Gamma(q)(\Gamma_0^{-1}(q)-\Gamma^{-1}(q)), \tag{13}$$

which follows from Eq. (7). Hence $\Lambda=4q^2\lambda G_0$, and the final equation describing the relaxation of the correlation function during spinodal decomposition under all of the assumptions made above has the form

$$\partial G(q)/\partial t=2q^2\lambda(G^{-1}(q)-\Gamma(q))/\Gamma_0(q). \tag{14}$$

Integrating Eq. (14) and renormalizing the time $\lambda t\to\tilde{t}$ yields the following nonlinear equation for $G(q,t)$ in implicit form:

$$g(G-G_0)+g^2\ \ln\left(1-\frac{G-G_0}{g-G_0}\right)=-2q^2G_0\,\tilde{t}. \tag{15}$$

A remarkable difference of the solution of Eq. (15) from Cook's result (7) is that for $\tau<0$ and a prescribed value $g<0$ the observed value of the correlation function $G(q,t)$ at long times grows linearly,

$$\frac{G}{q^2\tilde{t}}\ \to 2\ \frac{G_0}{|g|},$$

and not exponentially. Therefore the proposed approach does indeed make it possible to go well beyond the linear approximation.[6] On the other hand, all quantities appearing in the dynamical equation (15) refer to the same value of the wave number q. This enables us to call it a nonlinear generalization of the dynamic random-phase approximation.

A more detailed comparison of the behavior of the function $G(q,t)$ determined by Eq. (15) and that of Cook's function (7) for different values of the supercooling τ is presented in Figs. 1 and 2, where the height I and position q_m of the peaks of the two functions are displayed as functions of time. To facilitate comparison, they are constructed in the reduced variables $q_m=q/\sqrt{|\tau|}$, $t=\tilde{t}\,\tau^2/2$. In both cases the intermediate (power-law) and final asymptotic time dependences of the indicated quantities are well distinguished. For example, in the approximation which we propose here $I\sim t^{0.36}$ and $q_m\sim t^{-\alpha}$ on the intermediate section and $I\sim t$ and $q_m\to 0.5$ at long times. For Cook's function one has $\alpha=0.25$, in our approximation $\alpha\approx 0.15$, and the values obtained for α in Refs. 14–21 by numerical analysis of the stochastic equation (4) lie in the interval 0.2–0.3. For the approximation studied in the present letter these values of the exponents of the intermediate asymptotic laws are quite satisfactory. Conversely, the manifestly unphysical stopping of relaxation of q_m at long times is an obvious artifact of this approximation. However, it is interesting that a) the time at which this nonphysical asymptotic behavior is reached, as one can see in Figs. 1 and 2, is much longer than the time at which Cook's correlation function starts to diverge exponentially (and the linear

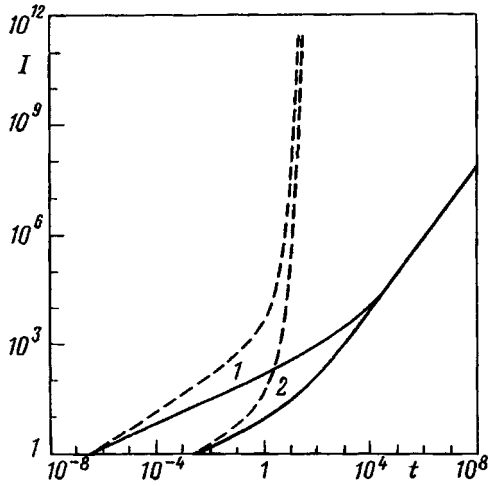

FIG. 1. Height I of the peaks of the function $G(q,t)$ determined by Eq. (15) (solid lines) and Cook's function (7) (dashed lines) versus the reduced time $t=\tilde{t}\,\tau^2/2$ for $\tau=-0.1$ (curves *1*) and $\tau=-0.001$ (curves *2*).

approximation ceases to be applicable) and b) the stopping of the relaxation of q_m (pinning) in time does indeed occur in some numerical simulations[18] and physica experiments.[29]

In summary, we have shown that the approach proposed in the present letter to the theory of spinodal decomposition on the basis of a direct analysis of the correlation function as an independent dynamical variable is indeed quite constructive in the zeroth approximation. It can be expected that refinement of this approach, incorporating the

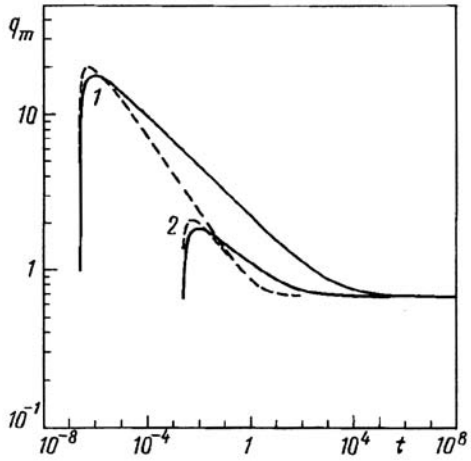

FIG. 2. Height of the reduced maximum $q_m=q/\sqrt{|\tau|}$ of the function $G(q_m,t)$ (15) (solid lines) and Cook's function (7) (dashed lines) versus time for $\tau=-0.1$ (curves *1*) and $\tau=-0.001$ (curves *2*).

intercoupling of the relaxational processes for different values of the wave numbers by taking account explicitly of the nontrivial self-energy parts appearing in Eq. (10b), will make it possible to eliminate this shortcoming of the zeroth approximation and will give an even better description of spinodal decomposition.

[1] J. W. Cahn and J. E. Hilliard, J. Chem. Phys. **28** 258 (1958).
[2] J. W. Cahn, Acta Metall. **9**, 795 (1961).
[3] Yu. I. Ustinovshchikov, *Precipitation of a Second Phase in Solid Solutions* [in Russian], Nauka, Moscow, 1988.
[4] E. M. Lifshitz and L. P. Pitaevskiĭ, *Physical Kinetics*, Pergamon Press, New York, 1981 [Russian original, Nauka, Moscow, 1979, Sec. 101, p. 528].
[5] L. D. Landau and E. M. Lifshitz, *Statistical Physics*, Pergamon Press, New York [Russian original, Nauka, Moscow, 1076, Part 1, p. 584].
[6] H. E. Cook, Acta Metall. **18**, 297 (1970).
[7] J. S. Langer, M. Baron, and H. D. Miller, Phys. Rev. A **11**, 1417 (1975).
[8] C. Billotet and K. Binder, Physica A **103**, 99 (1980).
[9] A. J. Bray, Phys. Rev. Lett. **62**, 2841 (1989).
[10] A. J. Bray and A. D. Rutenberg, Phys. Rev. E **49**, R27 (1995).
[11] A. D. Rutenberg and A. J. Bray, Phys. Rev. E **51**, 5499 (1995).
[12] A. J. Bray, B. Derrida, and C. Godreche, Europhys. Lett. **27**, 175 (1994).
[13] A. J. Bray and B. Derrida, Phys. Rev. E **51**, R1633 (1995).
[14] A. J. Bray, Adv. Phys. **43**, 357 (1994).
[15] M. A. Kotnis and M. Muthukumar, Macromolecules **25**, 1716 (1992).
[16] E. K. Hobbie, B. J. Bauer, and C. C. Han, Phys. Rev. Lett. **72**, 1830 (1994).
[17] F. J. Alexander, D. A. Huse, and S. Janovsky, Phys. Rev. B **50**, 663 (1994).
[18] S. C. Glotzer, M. F. Gyure, F. Sciortino *et al.*, Phys. Rev. E **49**, 247 (1994).
[19] G. Brown and A. Chakrabarti, J. Chem. Phys. **98**, 2451 (1993).
[20] H. Tanaka and T. Sigehuzi, Phys. Rev. E **75**, 874 (1995).
[21] C. Sagui, A. M. Somoza, and R. C. Desai, Phys. Rev. E **50**, 4865 (1994).
[22] A. Coniglio and M. Zannetti, Europhys. Lett. **10**, 575 (1996).
[23] C. Castellano and M. Zannetti, Phys. Rev. Lett. **77**, 2742 (1996).
[24] C. J. de Dominicis, Math. Phys. **3**, 983 (1962).
[25] C. J. de Dominicis and P. C. Martin, J. Math. Phys. **5**, 14, 31 (1964).
[26] V. S. Vasil'ev, *Functional Methods in the Quantum Theory of Fields and Statistics* [in Russian], Izd. LGU, Leningrad, 1976, p. 296.
[27] A. V. Dobrynin and Ya. Erukhimovich, J. Phys. II France **1**, 1991.
[28] A. Z. Patashinskiĭ and V. L. Pokrovskiĭ, *Fluctuation Theory of Phase Transitions*, Pergamon Press, New York [Russian original, Nauka, Moscow, 1982, p. 381].
[29] D. Katzen and S. Reich, Europhys. Lett. **21**, 55 (1993).

Translated by M. E. Alferieff

ERRATA

Erratum: On the possibility of measuring the degree of transverse polarization of a proton beam by means of elastic *pe* scattering [JETP Lett. 65, No. 2, 131–136 (25 January 1997)]

I. V. Glavanakov, Yu. F. Krechetov, G. M. Radutskiĭ, and A. N. Tabachenko
Scientific-Research Institute of Nuclear Physics, 634050 Tomsk, Russia
Pis'ma Zh. Eksp. Teor. Fiz. **66**, No. 6, 438 (25 September 1997)

[S0021-3640(97)01418-7]

PACS numbers: 12.20.Ds, 13.60.Fz, 99.10.+g

There is a misprint in the formula for $A_{NN}\Sigma$ on page 132. The correct formula is

$$A_{NN}\Sigma = 4\frac{Mm}{t}G_E(t)(\varphi_1 - \varphi_3).$$

All the calculations were performed with the correct formula.

Translated by M. E. Alferieff

